# Differential effects of organic versus inorganic selenium species on *BRCA1*-mutated and non-mutated breast cancer cell lines

A thesis

submitted in partial fulfilment

of the requirements for the degree

of

**Masters of Science (Research) in Biological Sciences**

at

**The University of Waikato**

by

**Yi-An (Annie) Ko**


THE UNIVERSITY OF
WAIKATO
*Te Whare Wānanga o Waikato*

2016

# Abstract

Selenium (Se) is an important trace element required for maintaining human health. Small amounts of Se has a chemoprotective effect to protect cells from oxidative damage, but higher dosages can introduce damage to DNA, and trigger apoptosis. The effect of Se is dependent on the dosage and chemical form of Se. Previous studies suggest inorganic Se in the form of selenite is more potent than the organic Se form, methylseleninic acid (MSA). The damaging effect of Se has been utilised to combine with chemotherapy drugs to synergistically kill cancer cells. Interestingly, more recent studies suggest that supranutritional dosage of Se can kill tumorous cells while leaving the normal healthy cells unharmed. *BRCA1* is a tumour-suppressor gene which functions in sensing and repairing DNA damage. Mutations in *BRCA1* are highly associated with breast cancer. Previous epidemiological studies suggest that a patient with *BRCA1* mutations appears to be more sensitive to Se supplements.

The first objective of this research is to evaluate the interaction of Se dose and chemical form in *BRCA1*-mutated and non-mutated breast cancer cells *in vitro*. We applied Se (MSA and selenite) to two commercially-available *BRCA1* and two non-*BRCA1* mutated breast cancer cell lines. We hypothesised that breast cancer cells with a *BRCA1* mutation are more sensitive to DNA damage and death from Se treatment, especially with the inorganic form. Se sensitivity was measured by examining DNA damage and cell viability with the comet assay and the colorimetric MTT assay,

respectively. Based on the results from the first objective, the second aim was to examine the combined effect of Se with the chemotherapy drug, cisplatin, and evaluate the synergistic anti-tumour effect on the breast cancer cell lines. The viability after drug exposure was measured with MTT assay. Lastly, we also validated a new technique called Long run real-time PCR (Lord-qPCR) for quantifying DNA damage based on the amplification efficiency in real-time PCR. Se genotoxicity was again tested with this method and the results were compared to the conventional comet assay.

Comparison of the comet assays between two *BRCA1*-mutated breast cell lines (MDA-MB-231 and Sum149pt) and two non-*BRCA1*-mutated breast cancer cell lines (MCF-7 and MDA-MB-231) showed significantly ($p=0.01$) greater DNA damage in the cells with *BRCA1* mutation for each Se compound. The $IC_{50}$ values for selenite and MSA, obtained with the MTT assay, were lower in *BRCA1*-mutated cells than the non-*BRCA1*-mutated cells. The outcome of the combined treatment with a physiological level of cisplatin and selenite/MSA did not show any synergistic cell inhibition on either *BRCA1*-mutated or non-mutated breast cancer cell lines. Interestingly, cisplatin at the physiological level, appeared to be less potent than 2 μM of Se treatment. Lastly, Lord-qPCR in comparison to the comet assay is indeed much less labour-intensive. The Se genotoxicity results from Lord-PCR followed the overall trend demonstrated in the comet assay. Surprisingly, DNA lesions predicted from mitochondrial DNA appear to be insignificantly greater than nuclear DNA. However, one drawback of the Lord-qPCR is that the reproducibility is much lower than comet assay, and may therefore require further optimisation.

# Acknowledgments

Several people have provided valuable input towards this research thesis. First, I would like to thank my supervisor Dr Linda Peters, who has led me through my master's degree with valuable technical instructions and very helpful recommendations throughout the research period; your patience and ambition in research was very encouraging for me. I would also like to express thanks to my second supervisor, Dr Michael Jameson, with helpful discussion and guidance in my research year. In addition, Kirsty Mayall, thank you for demonstrating the tissue culture techniques. My sincere thanks to Dr Greg Jacobson and Steve Evans with many technical and mental support especially the selfless help in Lord-qPCR methodology that you two developed. Thanks to Sari Karppinen for providing assistance in proof-reading. Lastly, I would like to thank all my lab colleagues in the Laboratory of Molecular Genetics who have supported me with a careful and delightful working environment.

Great thanks to my family and boyfriend who have supported and strengthened me throughout my masters. Thank you for always believing in my will; the encouragement has got me through all the hard times. I will not be able to complete this thesis without the great support from you all.

I am grateful for the financial support of Waikato Research Masters Scholarship and Waikato Graduate Women Educational Trust. Thanks to the student travel award received from NZSO to attend and present at that conference.

# Table of Contents

**Abstract** ..... **ii**

**Acknowledgments** ..... **iv**

**Table of Contents** ..... **v**

**Lists of Tables** ..... **ix**

**List of Figures** ..... **xi**

**List of Equations** ..... **xiv**

**List of Abbreviations** ..... **xv**

**Chapter 1: Introduction and Literature Review** ..... **1**

1.1 Introduction ..... 1

1.2 Dietary source and geographical distribution of Se ..... 3

1.3 Se metabolism ..... 4

1.3.1 Selenoprotein synthesis ..... 6

1.4 Se function in healthy cells ..... 7

1.5 Effect of Se supplementation and cancer ..... 8

1.6 Breast cancer ..... 10

1.6.1 Major mutations in breast cancer ..... 10

1.6.2 Breast cancer cell line classification ..... 13

1.6.3 Common chemotherapy drugs in breast cancer ..... 16

1.7 Se and breast cancer ..... 17

1.7.1 Chemoprotective effect of Se on breast cancer ..... 17

1.7.1.1 Epidemiology studies on chemoprotective effect of Se ..... 18

1.7.1.2 *In vitro* studies on chemoprotective effect of Se ... 20
1.7.2 Therapeutic effect of Se on breast cancer ..... 20
1.7.2.1 *In vitro* studies on therapeutic effect of Se ..... 21
1.7.2.2 *In vivo* studies on therapeutic effect of Se ..... 24
1.8 Mechanisms of anticancer effects of Se ..... 26
1.8.1 Anti-oxidant and DNA repair ..... 27
1.8.2 Apoptosis ..... 29
1.8.3 Inhibition of cancer invasion and metastasis ..... 33
1.9 Differential efficacy of different Se compounds ..... 34
1.10 Pro-oxidant effect of Se ..... 37
1.11 Focus of present research ..... 38

**Chapter 2: Material and Methods ..... 40**
2.1 Breast cancer cells ..... 40
2.2 Reviving of *in vitro* cancer cells ..... 41
2.3 Cell culturing ..... 41
2.4 Sub-culturing cells ..... 42
2.5 Measuring cell concentration using a Haemocytometer ..... 43
*2.6* Cell viability counts with Trypan blue ..... 44
2.7 Freezing cultured cells ..... 44
2.8 Growth assay of cultured breast cancer cells ..... 45
2.9 DNA extraction from cultured breast cancer cells ..... 46
2.10 Testing for mycoplasma contamination using PCR ..... 47
2.11 Confirmation of DNA mutation in the cultured breast cancer cell lines ..... 52
2.12 Comet assays for testing DNA damage from Se ..... 54

2.13 MTT assay for testing Se cytotoxicity.....59
2.13.1 Determining cell concentration.....59
2.13.2 MTT assay with Se .....60
2.13.2.1 Se incubation.....61
2.13.2.2 MTT assay.....63
2.14 Lord-qPCR for DNA damage analysis.....64
2.15 Primer validation .....72
2.16 Confirmation of mRNA expression using LORD-qPCR primers .....74
2.16.1 RNA extraction from cultured cells.....74
2.16.2 cDNA construction .....75
2.16.3 Amplification of the *p53* gene.....77
2.17 Combined treatment of cisplatin and Se .....77

**Chapter 3: Experimental Results.....81**
3.1 Mammalian Cell Culture.....81
3.2 Growth assay.....81
3.3 Mycoplasma contamination PCR test .....82
3.4 Validation of the reported mutations in the cell lines .....84
3.5 Comet assay.....90
3.6 Lord-qPCR.....92
3.6.1 Preparation of DNA template .....93
3.6.2 Primer validation using standard PCR and DNA sequencing.....93
3.6.3 Lord-qPCR.....97
3.6.4 p53 expression in MDA-MB-436 breast cancer cell line ..

..... 101

3.6.5 Validate result with another primer ..... 105

3.7 Se toxicity with MTT assay ..... 108

3.7.1 Formazan test ..... 108

3.7.2 Se cytotoxicity ..... 109

3.8 Cisplatin and Se combined therapy .....112

**Chapter 4: Discussion .....115**

4.1 Validation of Breast Cancer Cell Lines. .....115

4.2 Differential genotoxicity and cytotoxicity of selenite and MSA towards *in vitro* breast cancer cell lines .....115

4.3 Combined therapy of cisplatin and Se ..... 120

4.3.1 No synergism between cisplatin and Se..... 121

4.3.2 Potential chemotherapy drugs with Se ..... 125

4.3.3 Unexpected high sensitivity of MDA-MB-231 from MSA .

..... 127

4.4 Lord-qPCR vs. comet assay..... 129

4.5 Future research ..... 133

**References..... 136**

**Appendix One: Recipes for experimental solutions ..... 146**

**Appendix Two: Melt curve from Lord-qPCR ..... 151**

**Appendix Three: Electropherogram of sequenced top PCR band Figure 28..... 153**

**Appendix Four: Raw data for experimental results..... 155**

# Lists of Tables

**Table 1**, Recommended Se dietary allowances from the USA Department of Health and Human Services ..... 4

**Table 2**, Summary of the four breast cancer cell lines ..... 15

**Table 3,** Association between serum Se concentration with the breast cancer risks in GPx1 TT variant carriers ..... 19

**Table 4**, Summary of the breast cancer cell lines used in this study with Genbank Accession number from NCBI. ..... 41

**Table 5**, 24-well plate arrangement for growth control ..... 45

**Table 6,** Primer sets for mycoplasma detection. ..... 48

**Table 7**, Composition of PCR reaction mixture for mycoplasma detection. ..... 50

**Table 8**, Cycling conditions of PCR for mycoplasma detection ..... 51

**Table 9**, PCR primers designed to detect mutations in the breast cancer cell lines. ..... 53

**Table 11**, PCR cycling conditions to amplify positions with desired mutations. ..... 53

**Table 12**, Sample layout for comet assay on a 24-well plate. ..... 55

**Table 13**, Formula to make up Se media with MEM media for MDA-MB-436, MDA-MB-231, and MCF-7 cell lines. ..... 56

**Table 14**, Formula to make up Se media with Ham's F12 media for Sum149pt cell line. ..... 57

**Table 15**, MTT assay arrangement on a 96-well plate. ..... 61

**Table 16**, Formula to make up Se media with their corresponding Se

concentrations for MDA-MB-231, MDA-MB-436, and MCF-7 cell lines..... 62

**Table 17**, Formula of Se media with their corresponding Se concentrations for Sum149pt cell line. ..... 63

**Table 18**, Formula of Lord-qPCR master mix. ..... 67

**Table 19**, Formula of Lord-qPCR set up. ..... 67

**Table 20**, Lord-qPCR primers used to amplify *H. sapiens* mitochondrial or genomic DNA. ..... 69

**Table 21**, Cycling conditions for Lord-qPCR ..... 70

**Table 22,** PCR composition for validating primers used in Lord-qPCR.... 73

**Table 23,** Cycling condition of PCR for Lord-qPCR primer validation. ..... 74

**Table 24**, Formula of reverse transcription reaction..... 76

**Table 25**, PCR cycling condition for confirming expression of p53 mRNA transcript in cancer cell lines..... 77

**Table 26**, Layout of 96 well plate for combined treatment between Se and cisplatin..... 78

**Table 27**, Composition of combined drug mixture for MTT assay in triplicates ..... 80

**Table 28**, Summary of $IC_{50}$ deduced from **Figure 34**.....110

# List of Figures

**Figure 1**, Appearance of Se ..... 2

**Figure 2**, Chemical structure of MSA (left) and sodium selenite (right). ..... 3

**Figure 3**, Se metabolic pathway. ..... 5

**Figure 4**, Structural differences between cysteine (Cys) and selenocysteine (Sec) ..... 6

**Figure 5**, Schematic diagram to show incorporation of codon UGA and SECIS element is required for selenocysteine to insert into nascent selenoprotein peptides ..... 7

**Figure 6**, Four cultured epithelial breast cancer cell lines used in the present study under a phase-contrast microscope (10x). ..... 15

**Figure 7,** Possible mechanisms in chemoprotective effects of Se ..... 28

**Figure 8**, Crosslinks between MAPK/ERK2 pathway and Akt/PKB pathway controls the apoptotic signal of a cell. ..... 31

**Figure 9,** Selenite reduction pathway. ..... 37

**Figure 10,** Lord-qPCR in quantifying DNA damage. ..... 66

**Figure 11**, Percentage of cells per plate (%) from MDA-MB-436, MDA-MB-231, and MCF-7 cell lines. ..... 82

**Figure 12**, Mycoplasma test of cell lines MDA-MB-436 and MCF-7. ..... 83

**Figure 13,** Mycoplasma PCR test of cell line MDA-MB-231 and Sum149pt. ..... 84

**Figure 14**, PCR amplification of DNA from MDA-MB-231 for *BRCA1* mutations. ..... 85

**Figure 15,** PCR amplification of DNA from MDA-MB-231 for *p53, KRAS,*

and *BRAF* mutations. ..... 86

**Figure 16,** Genomic DNA sequence comparison of four human breast cancer cell lines at position 160,933 in the *BRCA1* gene..... 87

**Figure 17,** Genomic DNA sequence comparison of four cell lines for the expected mutation in Sum149pt at cDNA 2288 position with T deletion on *BRCA1* gene..... 88

**Figure 18,** Presence of expected mutations on the MDA-MB-231 cell line. ..... 89

**Figure 19,** Representative images of comets captured under the 10X Fluorescent Axiostar plus transmitted light microscope. ..... 91

**Figure 20,** Comet assay of all four breast cancer cell lines to examine the level of DNA damage after 24 hours incubation with 2 µM selenite or MSA. ..... 92

**Figure 21**, Gel electrophoresis of PCR product from MDA-MB-436 DNA with Lord-qPCR primers. ..... 94

**Figure 22,** Bioinformatics analysis of Lord-qPCR primers which expect to target *p53* gene..... 96

**Figure 23**, Bioinformatics analysis of Lord-qPCR primers targeting mitochondrial DNA. ..... 97

**Figure 24**, Melt curve from Lord-qPCR reaction of MDA-MB-436 with Ko8 mitochondrial primer..... 98

**Figure 25**, Lord-qPCR with mitochondrial primers to assess the level of mitochondrial DNA damage in three breast cancer cell lines upon Se treatment. ..... 99

**Figure 26**, Lord-qPCR result with *p53* primers on three breast cancer cell lines..... 100

**Figure 27,** Gel electrophoresis of RNA from MDA-MB-436 cell line on 1% non-denaturing agarose gel to show the RNA integrity. ..... 102

**Figure 28,** PCR amplification of p53 cDNA in MDA-MB-436 cells. ..... 103

**Figure 29,** Electropherogram of gel purified *p53* PCR product (bottom band; 155 bp) from lane three of **Figure 28**. ..... 104

**Figure 30**, Evidence of amplified fragments from **Figure 28** were extracted from the *p53* gene.. ..... 105

**Figure 31,** End-point PCR of Ko12 primer set on MDA-MB-436 DNA. .. 107

**Figure 32,** Comparison of the level of DNA damage estimated with *B2M* and *p53* primers in Lord-qPCR on MDA-MB-436 cell line. ... 108

**Figure 33**, Formazan test to determine the optimal concentration to use in MTT experiments..... 109

**Figure 34**, MSA and selenite cytotoxicity to four breast cancer cell lines. ..... 111

**Figure 35,** Cytotoxicity of 2 µM MSA or selenite with/without 8.33 µM cisplatin on the MDA-MB-436 cell line. ..... 113

**Figure 36**, Cytotoxicity of 2 µM MSA or selenite with/without cisplatin on MDA-MB-231 cell line..... 114

**Figure 37**, Melt curve from Lord-qPCR reaction of MDA-MB-436 with Ko6 p53 primer. ..... 151

**Figure 38**, Melt curve from Lord-qPCR reaction of MDA-MB-436 with Ko12 B2M primer..... 152

# List of Equations

**Equation 1**, Equation to calculate the concentration of cells with a haemocytometer. ..... 44

**Equation 2**, Calculation for cell viability with trypan blue stain. ..... 44

**Equation 3**, Calculation for growth assay to calculate the percentage of cells present..... 46

**Equation 4**, Calculation of tail moment for comet assay..... 58

**Equation 5,** Formula for the standard error of mean. ..... 59

**Equation 6**, Calculation for MTT assay to calculate the percentage of inhibition of cell under a specific condition. ..... 64

**Equation 7,** Equation for adjusting *Cp* value with amplification efficiency. ..... 71

**Equation 8,** Delta *Cp* for normalising lesion in treated sample..... 71

**Equation 9**, Equation to calculate lesion rate based on the delta *Cp* value ..... 72

# List of Abbreviations

| | |
|---|---|
| ATM | Ataxia-Telangiectasia |
| ATR | Ataxia telangiectasia and Rad3-related protein |
| BIC | Cancer Information Core |
| *BRCA1* | Breast cancer susceptibility gene 1 |
| BRCT | BRCA1 C-Terminal domain |
| CDK | Cyclin dependent kinase |
| CHEK2 | Checkpoint Kinase 2 |
| Cp | Crossing point (qPCR) |
| Cys | Cysteine |
| DC | Cisplatin drug control |
| DEPC | Diethylpyrocarbonate |
| *E. coli* | *Escherichia coli* |
| ER | Estrogen Receptor |
| ERK | Extracellular signal regulated protein kinase |
| Gadd45a | Growth Arrest and DNA Damage |
| GPx | Glutathione peroxidase |
| GSH | Glutathione |
| HER2 | Epidermal Growth Factor Receptor 2 |
| $IC_{50}$ | Inhibitory concentration |
| LOD | Logarithms of the likelihood ratios for linkage |
| MAP | Mitogen-activated protein |
| MMP | Matrix metalloproteinase |
| MSA | Methylseleninic acid |

| | |
|---|---|
| MSC | Methylselenocysteine |
| MSeCN | Methylselenocyanate |
| NBS1 | Nibrin |
| NER | Nucleotide excision DNA repair pathway |
| NPC | Nutritional Prevention of Cancer trial |
| OD | Optical density |
| P | Passage |
| p53 | Tumour Protein 53 |
| PARP | Poly (ADP-ribose) polymerase |
| PBMC | Peripheral blood monoclonal cells |
| PR | Progesterone Receptor |
| PSC | PBS solvent control |
| PSSC | PBS and saline solvent control |
| PTEN | Phosphatase and Tensin Homolog |
| RDA | Recommended daily allowance |
| Ref 1 | Redox factor 1 |
| RING | Really Interesting New Gene domain |
| RNS | Reactive nitrogen species |
| ROS | Reactive oxygen species |
| Se | Selenium |
| Sec | Selenocysteine |
| SECIS | Selenoprotein insertion sequence |
| SELECT | Selenium and Vitamin E Cancer Prevention Trial |
| SeMet | Selenomethionine |
| SEP15 | 15kDa selenoprotein |
| SSC | Saline solvent control |

| | |
|---|---|
| SSe | Sodium selenite |
| Trx | Thioredoxin |
| TrxR | Thioredoxin reductase |
| TSG | Tumour suppressor gene |
| uPA | Urokinase-type plasminogen activator |
| VEGF | Vascular endothelial growth factor |
| WBC | White blood cells |
| XPC | Xeroderma pigmentosum complementation group C |

# Chapter 1:

# Introduction and Literature Review

## 1.1 Introduction

Selenium (Se) is a non-metal trace element with the atomic number 34 and on the periodic table, it is located in between sulphur and tellurium. Se was first discovered in 1817 by Swedish chemists Jöns Jakob Berzelius and Johan Gottlieb Gahn (Berzelius, 1818) and it exists as a black crystal or red powder after purification (**Figure 1**). This element was originally known for its toxic effect in humans such as impairment of immunity, gastrointestinal disturbance, and disruption of endocrine functions (Vinceti et al., 2001). However, in 1954 the beneficial effects were shown in the bacterium *Escherichia coli* (*E. coli*), where Se is important for the active form of formic dehydrogenase that is required for growth (Pinsent, 1954). Subsequent studies also found that Se is an essential element, especially in mammals (Oldfield, 2006). Se is essential for human health and functions through specific “selenoproteins” encoded by RNA codon UGA and incorporating selenocysteine; to date, twenty-five selenoproteins have been described in mammals (Rayman, 2009). Se deficiency can cause numerous health problems, including an increased risk of mortality, decreased immune and cognitive function, and increased cancer incidence (Rayman, 2012).

**Figure 1**, Appearance of Se (Oelen, 2011).

However, the effects of Se are controversial, and it appears to have a U-shaped association with human health; high levels of Se can cause an increased risk of type 2 diabetes and peripheral neuropathy and may induce DNA damage. (Rayman, 2012). Apart from the dose, other factors such as different chemical forms of Se and polymorphisms in the selenoproteins can affect the balance of efficacy and toxicity of Se supplementation.

In the present study, we selected two chemical forms of Se for testing *in vitro* against four breast cancer cell lines that differ in their mutation status. The two different Se compounds, organic methylseleninic acid (MSA) and inorganic sodium selenite (**Figure 2**), are metabolised via different routes. Previous studies show that inorganic selenite appears to be more cytotoxic than the organic Se compound (Jiang et al., 2002). In this literature review, we will focus on the genetics of breast cancer and the effects of Se on cancer development.

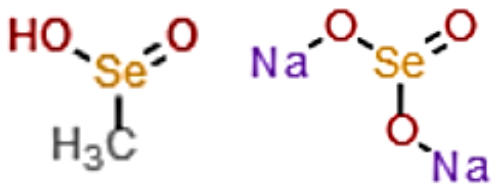


**Figure 2**, Chemical structure of MSA (left) and sodium selenite (right). Pictures modified from Sanmartín et al. (2012).

## 1.2 Dietary source and geographical distribution of Se

For humans, the main source of Se is from our diet. Food items such as tuna, milk, bread, and cereal are high in Se. Brazil nuts have the highest content, which can reach up to 512 mg/kg (Rayman, 2008). However, the daily intake of Se in human varies widely from one geological location to another, which depends on the amount of Se in the crop soil. For example, Canada, USA, and Japan have higher Se intake compared to east Europe, parts of China, and New Zealand (Rayman, 2012).

The recommended daily allowance (RDA) from the National Institutes of Health, USA is 55 µg/day (**Table 1**). Intake of 1540-1600 µg/day show slight adverse effects, and intake up to 3200-5000 µg/day may cause selenosis. Symptoms of this condition include brittle hair and nails, garlic breath, and skin lesions. The average Se intake in Europe is 40 µg/day compared to 93 µg/day in women and 134 µg/day in man in the USA (Rayman, 2008). However, in New Zealand the average intake in 1987 was 28 µg/day, which is much lower than the RDA (Robinson & Thomson, 1987). It is known that New Zealand has Se-deficient soil. The daily Se intake in New Zealand has increased over the past decades especially in the North Island due to the importation of wheat products from Australia. In contrast, the South Island

uses locally grown wheat for baking goods. For example, Se concentration in white bread ranges from 25 µg/kg in Dunedin, 80-104 µg/kg in Napier, and 78-114 µg/kg in Auckland (Thomson, 2004). In addition to food sources, Se supplementation can be used to increase its intake.

| Age (years) | Male | Female | Pregnancy | Lactation |
|---|---|---|---|---|
| Birth to 0.5 | 15 µg | 15 µg | | |
| 0.6-1 | 20 µg | 20 µg | | |
| 1-3 | 20 µg | 20 µg | | |
| 4-8 | 30 µg | 30 µg | | |
| 9-13 | 40 µg | 40 µg | 60 µg | 70 µg |
| 14-18 | 55 µg | 55 µg | 60 µg | 70 µg |
| 19-50 | 55 µg | 55 µg | | |
| 51+ | 55 µg | 55 µg | | |

**Table 1**, Recommended Se dietary allowances from the USA Department of Health and Human Services ("Selenium Dietary Supplement Fact Sheet," 2013).

### 1.3 Se metabolism

Se enters the human body mostly in its organic form as selenomethionine, selenocysteine, and Se-methylselenocysteine. Animal protein is rich in these forms of Se. In comparison, inorganic Se such as sodium selenite (SSe) can be obtained from Se supplements. Se can participate in different mechanisms with or without binding to selenoproteins. The overall metabolism in Se is summarised in **Figure 3**.

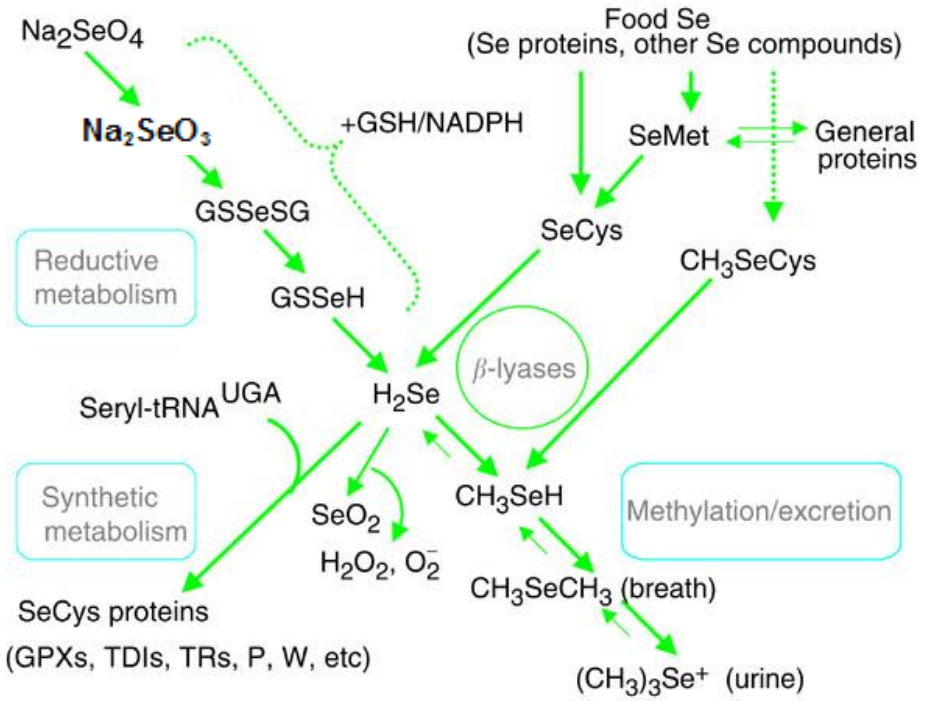


**Figure 3**, Se metabolic pathway (Combs, 2004). Abbreviation for Se compounds: $Na_2SeO_4$, selenate; $Na_2SeO_3$, selenite; $CH_3SeH$, methylselenocystine; SeMet, selenomethionine; SeCys, selenocysteine; GSSeH, selenoglutathione; GSSeSG, selenodiglutathione; $H_2Se$, hydrogen selenide; $SeO_2$, Se dioxide; $CH_3SeH$, methylselenol; $CH_3SeCH_3$, dimethylselenide; $(CH_3)_3Se^+$, trimethylselenonium; GPXs, glutathione peroxidases; TDIs, iodothyronine 5'-deiodinases; TRs, thioredoxin reductases, P, selenoprotein P; W, selenoprotein W

Selenite can be reduced to hydrogen selenide ($H_2Se$) by glutathione (GSH); selenocysteine can also be metabolised into this key molecule. $H_2Se$ is the central molecule in Se metabolism, where it can function as a precursor to the synthesis of selenoproteins or it can be methylated into mono-, di-, or tri-methylated Se, which will be excreted through the kidney. Trimethylated Se is dominant after a high dose of Se and can be detected in breath (Letavayová et al., 2006).

Different forms of Se can have different efficacy in tumour development, and it appears that methylselenol ($CH_3SeH$) is the critical metabolite for the tumour-specific actions of Se (Ip et al., 1991). Se compounds that are able to produce a steady stream of monomethylated Se, such as Se-methylselenocysteine ($CH_3SeCys$), selenocysteine (SeCys), and a novel Se compound methylselenic acid (MSA), are likely to possess potential as anti-tumour agents (Ip et al., 1991).

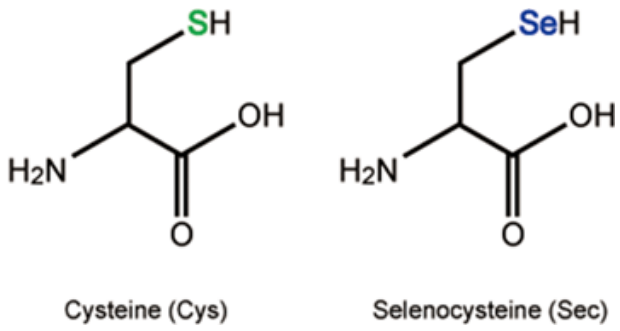


**Figure 4**, Structural differences between cysteine (Cys) and selenocysteine (Sec) (Chiba et al., 2010).

### 1.3.1 Selenoprotein synthesis

Following the intake of Se from the consumption of animal proteins and/or vitamin supplements, it is metabolised in the liver into hydrogen selenide ($H_2Se$) (see **Figure 3**) and converted to selenocysteine via a specialised tRNA molecule. Selenocysteine is a cysteine analogue with seleno-group replacing the thiol group on cysteine (**Figure 4**). The selenocysteine-specific tRNA is different from standard tRNA in a structural manner. Selenocysteine is encoded by UGA codon on mRNA, but because UGA is also a stop codon it can cause translation to terminate prematurely and cause the release of

nascent peptides into the cytoplasm. The selenoprotein insertion sequence (SECIS), which is downstream of the UGA codon, is defined with specific sequences and secondary structure on mRNA. The differential structure on $tRNA^{sec}$, along with the assistance of other protein factors, allows it to recognise the UGA codon and the downstream SECIS element (**Figure 5**). This selenocysteine-specific characteristic post-translationally regulates the expression of selenoproteins depending on the availability of Se; when Se is available, the vicinity of UGA codon is folded into secondary structures, which will be recognised by $tRNA^{sec}$ and read-through on mRNA sequences. Alternatively, when Se is depleted, mRNA remains as linear structure and UGA encodes for a termination signal resulting in premature termination and produces non-functional selenoprotein peptides (Commans & Böck, 1999).

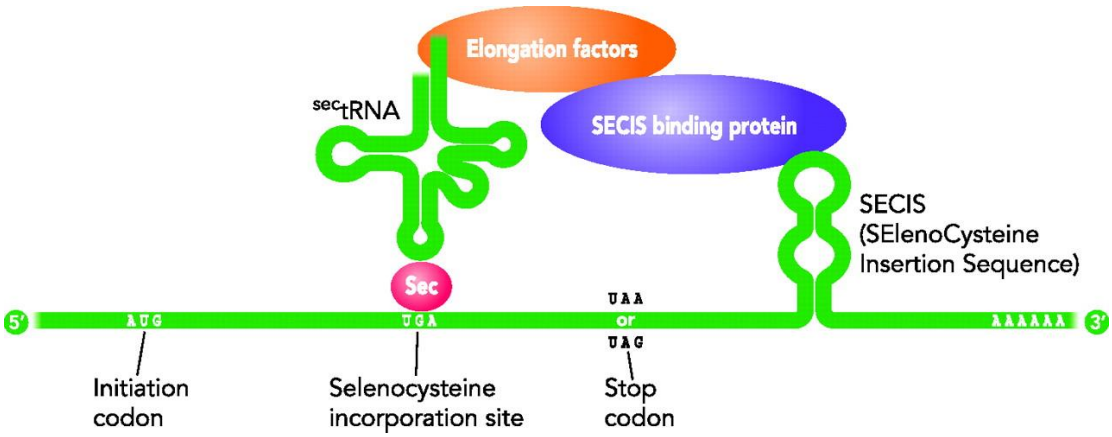


**Figure 5**, Schematic diagram to show incorporation of codon UGA and SECIS element is required for selenocysteine to insert into nascent selenoprotein peptides (Moghadaszadeh & Beggs, 2006).

## 1.4 Se function in healthy cells

One function of Se in normal cells is to stimulate the expression of

selenoproteins, and some of them are antioxidants which can counteract free radicals and prevent oxidative damage. For example, glutathione peroxidase (GPx) is a well-known reactive oxygen species (ROS) scavenger that reduces hydrogen peroxides ($H_2O_2$) and lipid peroxides; as a result, it can reduce oxidative stress in cells. Not surprisingly, the effect of Se supplementation is more significant in individuals with low GPx, whereas individuals with saturated GPx activity are less affected. Other selenoproteins such as 15 kDa selenoprotein (SEP15) and selenoprotein P are also antioxidants, which can reduce oxidative damage when induced by Se (Rayman, 2005).

### 1.5 Effect of Se supplementation and cancer

The first study that demonstrated an association between cancer and dietary Se intake was published in 1977 (Schrauzer et al., 1977). The authors correlated cancer mortality and Se intake from 27 different countries (excluding New Zealand) resulting in an inverse correlation: the lower the Se intake the higher the cancer mortality. Subsequent case-control studies have shown that Se supplementation may be helpful in decreasing some types of cancers, such as prostate (Etminan et al., 2005), bladder (Amaral et al., 2010), colon (Jacobs et al., 2004), and lung (Zhuo et al., 2004). The largest clinical trial with the strongest evidence of the anti-cancer role of Se was the Nutritional Prevention of Cancer trial (NPC) that started in 1996. This trial involved 1312 subjects with a history of non-melanoma skin cancer who were randomised to take either placebo or 200 µg Se supplement daily. The primary endpoint of further skin cancers showed no effect from Se, but analysis of secondary endpoints, seven years after the trial had started,

showed 50% and 37% reduction in total cancer mortality and total cancer incidence, respectively (Clark et al., 1996). Therefore, Se may function as a chemoprotective agent.

This possible chemoprotective function of Se led to the development of the Se and Vitamin E Cancer Prevention Trial (SELECT) to determine the effects of Se on the incidence of prostate cancer. This phase III placebo-controlled trial randomised a total of 35,533 healthy volunteers that were recruited across USA and Canada, to placebo or Se 200 µg/day as organic L-selenomethionine. However, the authors of this trial reported that regular Se supplementation did not reduce prostate cancer incidence (Ledesma et al., 2011). One possible explanation for the negative result is that the pre-treatment serum Se concentration in subjects was relatively high (and within the recommended optimal range (Rayman, 2012)) compared to the other studies that had showed a beneficial effect of Se in preventing cancer (Clark et al., 1996).

The effect of Se is also observed *in vitro* and in animal models. In a mouse model, Se was shown to reduce breast cancer incidence after exposure to carcinogens (this will be discussed in depth in section 1.6). In *in vitro* studies, incubation of non-tumorous fibroblast cell lines with Se not only had preventive effects toward cell damage but also had DNA-repairing effects, where the lesions established by carcinogens could be fixed at a higher rate (Ip, 1998). Although the mechanisms in reducing cancer incidence by Se are still unclear, it is likely to involve cell/DNA protection, oxidative stress reduction, and promotion of DNA repair (Bera et al., 2013). More recent

studies suggest Se is not only acting as a chemoprotective agent but also has a synergistic effect with chemotherapy drugs to enhance cancer cell-killing ability while at the same time protecting healthy cells from anticancer drug-induced toxicity (Cao et al., 2004). The mechanism for this effect involves increased tumour apoptosis and cell cycle arrest with high Se supplementation. The mechanism of Se in cancer development will be discussed in depth in later sections. For the purpose of this Masters thesis, we will focus only on breast cancer cell lines and investigate the effects of Se compounds.

## 1.6 Breast cancer

Breast cancer is the second most common cancer worldwide, but it is the most common cancer in women. There were 1.68 million cases and 522,000 deaths reported worldwide in 2012 (Siegel et al., 2012). In New Zealand, 3,000 breast cancer cases are diagnosed with 600 deaths reported each year ("Cancer: New registrations and deaths 2012," 2015). The aetiology of breast cancer is complicated and can involve carcinogens such as smoking, stressed lifestyle, radiation, and genetic factors.

### 1.6.1 Major mutations in breast cancer

Cancer is the result from the accumulation of both germline and somatic mutations. The most common breast cancer mutations are found in the breast cancer susceptibility genes 1 (*BRCA1*) and 2 (*BRCA2*). They are inherited in an autosomal dominant manner, which means a mutation in one allele is enough to result in a phenotype. Mutations in these two genes account for 90% of the genetic risk and are found in 60-80% of affected

individuals (Ford et al., 1994; Hartmann et al., 2001). The *BRCA1* locus was first identified in 1990 where researchers conducted a genetic mapping analysis on 23 extended families including 146 breast cancer patients across America and Canada (Hall et al., 1990). The resulting LOD score (logarithm of the likelihood ratios for linkage) was 5.98 which suggests evidence of linkage between the *BRCA1* gene and breast cancer on chromosome 17q. The *BRCA1* gene was cloned in 1994 and contains 5592 bp of a coding nucleotide sequence spanning 22 exons on chromosome 17q21.1 and encodes an 1863 amino acid protein (Durocher et al., 1996; Miki et al., 1994).

There are 1700 mutations reported on *BRCA1*, and 858 mutations have been confirmed with clinical significance (Clark et al., 2012). The result of these mutations can reduce or lose the function of BRCA1 protein by altering the protein structure. There are three domains on BRCA1 that are mutated with high frequency. These include the RING domains, regions encoded by exons 11-13, and BRCT domain. RING (Really Interesting New Gene) domain is a highly conserved alpha helix structure which encompasses 1-109 amino acid sequence on BRCA1. This domain is responsible for the E3-ubiquitin ligase function of BRCA1 protein. E3-ubiquitin ligase is important for ubiquitination to substrate and targeting to proteasome destruction. E3 act as an adaptor of E2 ubiquitin-conjugating enzymes and assists the transfer of ubiquitin to substrates. Mutations that disrupt the ubiquitin ligase function on BRCA1 increase predisposition to breast cancer. Secondly, regions encoded by exon 11-13 cover binding sites for proteins such as Rad50, Rad51, and c-myc (see later paragraph), which

are responsible for DNA repair. This area of the gene also includes two nuclear localisation sequences which are important for translocating BRCA1 from cytosol to nucleus. Lastly, BRCT domain (BRCA1 C-terminal) is a highly conserved domain in many other proteins and is mostly involved in DNA repair. This area of BRCA1 mediates the phosphorylation of ATM (Ataxia-Telangiectasia) and ATR (Ataxia-Telangiectasia and Rad3-related protein) which are two kinases activated by double-stranded DNA break; phosphorylation of BRCA1 can be recruited to the site with DNA damage. This domain is therefore responsible for sensing DNA lesions. Mutations here are therefore expected to be detrimental (Clark et al., 2012).

BRCA1 protein can localise inside the cell nucleus and exists as a multi-protein complex with BRCA2, RAD51, BARD1 and other DNA repair proteins. This complex senses DNA damage, such as double-strand breaks and mismatching codons. It coordinates the damage-sensing proteins as well as the repair ones. In addition, it serves as part of the transcriptional machinery (Elstrodt et al., 2006). *BRCA1* is therefore a tumour suppressor gene (TSG) that plays an important role sensing DNA damage, coordinates repairing proteins, and is also incorporated as part of the transcription factor to upregulate the machinery for cell cycle arrest and DNA repair. TSGs are a group of genes that function as a gatekeeper for cancer development by fixing genetic lesions that can result in cancer, and/or directing cells through apoptotic pathways when the repair cannot be done. Therefore, mutations in *BRCA1* are associated with increased breast/ovarian cancer risk due to defective repair process and therefore are prone to tumour transformation.

Other genetic mutations associated with breast cancer include Tumour Protein 53 (*TP53*), Phosphatase and Tensin Homolog (*PTEN*), Checkpoint Kinase 2 (*CHEK2*), Ataxia-Telangiectasia (*ATM*), Nibrin (*NBS1*), and DNA Repair Protein (*RAD50*) genes; they account for a smaller portion of genetic risk in breast cancer (Hu & Diamond, 2003). Among all the mutations above, *TP53* is the most common mutation throughout all cancer types; it is a tumour-suppressor gene, which is responsible for activating proteins for cell cycle arrest, triggering apoptosis, and inducing DNA repair, and therefore preventing the formation of cancer.

### 1.6.2 Breast cancer cell line classification

There are at least 41 commercially available breast cancer cell lines for scientific research (Elstrodt et al., 2006). Breast cancer cell lines are normally classified based on their expression level of oestrogen receptor (ER), progesterone receptor (PR), and epidermal growth factor receptor 2 (HER2). ER- and PR- positive breast cancer cells have the potential to respond to oestrogen and progesterone hormones, respectively. HER-2 positive is defined as a cell with overexpression of the receptor.

The four breast cancer cell lines used in this study were MCF-7, Sum149pt, MDA-MB-436, and MDA-MB-231 (**Figure 6**). The first, Michigan Cancer Foundation 7 (MCF-7), was extracted from a metastatic breast tumour from a 69-year-old Caucasian female. This ER and PR positive, non-*BRCA1* mutated breast cancer cell line overexpresses the oncogene *WNT7B,* which activates the downstream cellular pathway and promotes cancer metastasis (McGrath, 2014). The second, MDA-MB-436, is a metastatic breast cancer

cell line isolated from a 43-year-old Caucasian female. The mutation is found at nucleotide position 5396 (G> A) in exon 20 of the *BRCA1* gene and causes upregulation of tubulin and actin, which are components of the microskeleton (Elstrodt et al., 2006). This cell line is “triple negative” (negative for ER, PR and HER-2) but *BRCA1* mutated. The third, Sum149pt, is a breast cancer primary cell line with deletion at the 2288 nucleotide location and it is also a triple negative, *BRCA1* mutated cell line. Finally, the MDA-MB-231 breast cancer cell line was isolated from a 51-year-old Caucasian female and is aneuploid, where the cells are trisomic; it is HER-2 positive, non-*BRCA1* mutated (Lehmann et al., 2011). The four cell lines used are summarised in **Table 2**. The advantage of using a cancer cell line is the unlimited growth and flask-adhering characteristic, which allow easier experimental handling.

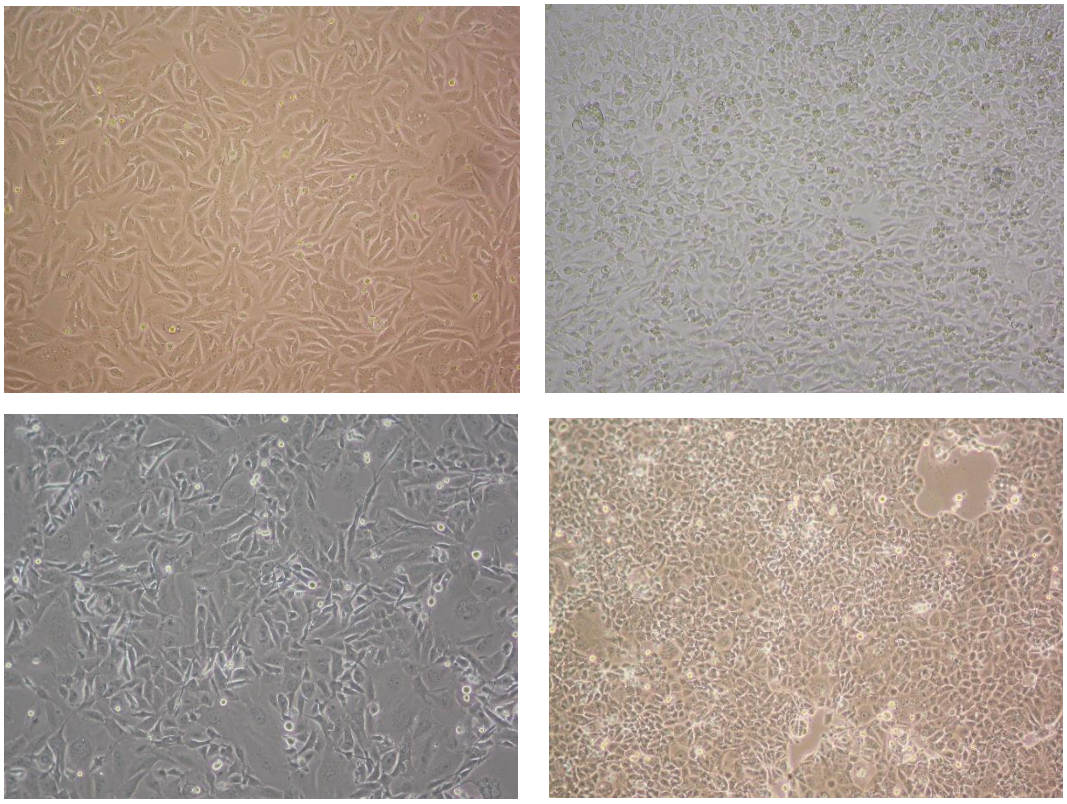

**Figure 6**, Four cultured epithelial breast cancer cell lines used in the present study under a phase-contrast microscope (10x). Top left: Sum149pt; top right: MDA-MB-436; bottom left: MDA-MB-231; bottom right: MCF-7. Photos were taken by Annie Ko at 90% confluency.

| Cell line | Origin of cells | Triple negative* | Mutation | Gene sequence |
|---|---|---|---|---|
| SUM149pt | Primary | **Yes** | ***BRCA1*** | c.2288delT |
| MDA-MB-436 | Metastasis (pleural effusion) | **Yes** | ***BRCA1***<br>*RB1* | c.5277+1G>A<br>c.607_608ins227 |
| MDA-MB-231 | Metastasis (pleural effusion) | **Yes** | *CDKN2A*<br>*KRAS*<br>*NF2*<br>*TP53* | c.1391G>T<br>c.1_471del471<br>c.38G>A<br>c.691G>T<br>c.839G>A |
| MCF-7 | Metastasis (pleural effusion) | **No**<br>*$ER^{+}$, $PR^{+/-}$, $HER2^{-}$* | *CDKN2A*<br>*CDKN2a(p14)*<br>*PIK3CA* | c.1_471del471<br>c.317_522del206<br>c.1633G>A |

**Table 2**, Summary of the four breast cancer cell lines (modified from Lehmann et al. (2011)).

*Triple negative stands for ER, PR, and HER-2 negative cell line.

### 1.6.3 Common chemotherapy drugs in breast cancer

While breast cancer may be treated with hormones, it is also commonly treated with cytotoxic chemotherapy drugs, both after surgery (as adjuvant therapy including radiation therapy, chemotherapy, and hormonal therapy) and for the recurrent or metastatic disease. Here, I will briefly review the chemotherapy drugs doxorubicin, docetaxel, and cisplatin and hormonal therapy, tamoxifen. These drugs have been examined in combination with Se in *in vitro* and/or *in vivo* models. The effect of combined therapy will be discussed in later sections.

Cisplatin as a chemotherapy drug was discovered in 1965 where the researchers found its effect in inhibiting binary fission of *E. coli* bacteria. Later studies proved the mechanism of action to be through crosslinking with DNA bases, and guanine is the preferred nucleotide (Rosenberg et al., 1965). Cisplatin can cross-link DNA strands in many different ways, which can interrupt cell division and DNA repair pathways, leading to apoptosis when repair is impossible (Wang & Lippard, 2005). Aside from nausea and vomiting, other common side effects of cisplatin include kidney toxicity (nephrotoxicity), bone marrow suppression, and anaemia. Previous studies show that breast cancer cells with *BRCA1* mutations are more susceptible to cisplatin treatment; *BRCA1*$^{-/-}$ appears to be five times more sensitive compared to the wild type (Bhattacharyya et al., 2000; Silver et al., 2010). This phenomenon can be explained by the loss of DNA repair ability with a defect in *BRCA1* expression and thus cells are more likely to undergo apoptosis.

Doxorubicin is an anthracycline antitumour antibiotic. Although both doxorubicin and cisplatin have a site of action on DNA, their mechanisms of action are different. Doxorubicin intercalates the DNA strands and inhibits the enzyme topoisomerase II, which is used to unwind DNA double strands, thus preventing DNA replication and transcription.

Docetaxel also targets fast-proliferating cells, but instead of preventing DNA replication, it inhibits cell division by binding to microtubules and preventing their depolymerisation. Inhibition of microtubule disassembly results in failure of mitotic division between metaphase and anaphase, and the accumulation of microtubules inside cells can indirectly trigger apoptosis and result in cell death (Lyseng-Williamson & Fenton, 2005).

In addition to chemotherapy, hormonal therapy is a common breast cancer treatment. One of the most common hormonal drugs used is tamoxifen. This drug is taken orally as a prodrug, which requires enzymatic conversion in the liver to active metabolites. The active form of the drug have higher affinity to ER and compete with native oestrogen for binding on breast cells. The binding of tamoxifen metabolites in the ER alters the downstream signalling pathway and gene expression. This alteration needs to include suppression of HER-2 expression, as overexpression of HER-2 is associated with tamoxifen resistance (Wang et al., 2004).

## 1.7 Se and breast cancer

### 1.7.1 Chemoprotective effect of Se on breast cancer

Similar effect to breast cancer as to other tumour types mentioned above,

Se can protect cells from oxidative damage and promote repair once the damage is formed. An *in vitro* study found that Se can improve the association of BRCA1 protein with p53, another key DNA-repairing factor (Fischer et al., 2006). In contrast, mutations in *BRCA1* can decrease the efficiency of its protein binding with other proteins. Therefore, individuals carrying mutations in *BRCA1* could have significant improvement in DNA repair when administered Se supplements. More detailed mechanisms will be discussed in later sections.

#### 1.7.1.1 Epidemiology studies on chemoprotective effect of Se

Kotsopoulos et al. (2010) sampled toenails from *BRCA1* mutation carriers and non-carriers, to correlate the Se content with the amount of cellular DNA damage. The results from 25 non-*BRCA1* carriers against 25 *BRCA1* carriers from Canada showed toenail Se cannot be used as a predictor of DNA damage in all populations. However, there was an inverse association observed in the *BRCA1* carrier group, suggesting possible benefit from Se supplementation in this group and further imply a protective role against breast cancer (Kotsopoulos et al., 2010).

The effect of selenoprotein genotypes is also seen in breast cancer. One study compared interactions between serum Se concentration and the genotype of the Se-dependent GPx1 enzyme (SNP: rs1050450) among healthy controls and breast cancer patients (Jaworska - Bieniek et al., 2012). The result suggested the optimal Se concentration in breast cancer, which refers to the concentration associated with the least number of breast cancer patients and the highest number of healthy controls, was 100-120

µg/L. However, for individuals carrying homozygous TT genotypes of GPx1, the optimal concentration was lowered to around 75 µg/L (**Table 3**).

| Quartiles | Concentration Se (µg/L) | No. Cases | No. Controls |
|---|---|---|---|
| I | 49.73 – 72.51 | 29 | 26 |
| II | 72.63 – 82.73 | 20 | 36 |
| III | 83.00 – 95.76 | 27 | 26 |
| IV | 96.74 – 160.97 | 26 | 30 |

**Table 3,** Association between serum Se concentration with the breast cancer risks in GPx1 TT variant carriers (Jaworska - Bieniek et al., 2012).

The mechanisms that bring about in the chemoprotective effects of Se against breast cancer cells can protect normal cells from cytotoxic damage from chemotherapy drugs. One study examined the protective role of Se against kidney and bone marrow toxicities in patients undergoing cisplatin treatment (Hu et al., 1997). A 4000 µg dose of Se (as seleno-kappacarrageenan) was given to patients from four days before to four days after cisplatin administration. The Se compound used is an organic Se as a raw material produced by red algae. The study showed a significantly higher number of white blood cells (WBC) and fewer blood transfusions in patients who received the combined Se and cisplatin treatment compared to the cisplatin-only group. Also, Se-treated patients appeared to have lower nephrotoxicity, which was assessed by measuring urinary enzymes that are highly expressed in damaged renal tubules. To conclude, this study suggested that Se, when administered with cisplatin, can protect the body from nephrotoxicity and bone marrow suppression. The reduction of toxicity

from Se may result in a potential increase in the amount of cisplatin patients can tolerate without exposure to a higher risk of side effects.

#### 1.7.1.2 *In vitro* studies on chemoprotective effect of Se

One key piece of evidence supporting the role of Se in DNA repair was reported by Kowalska et al., 2005. Briefly, WBC isolated from *BRCA1* carriers were incubated and exposed to a DNA-damaging cytotoxic drug, bleomycin. The DNA damage was measured by counting chromatid aberrations with Giemsa stain and compared to the cells from non-carriers. The results showed that cells from *BRCA1* carriers contained significantly higher induced damage (0.58 chromosome breaks/cell) than the non-carrier samples (0.39/cell). Subsequently, carriers were supplemented orally with 138 µg/day of selenite for 1-3 months, after which the level of damage returned back to similar levels (0.40/cell) to the non-carriers (Kowalska et al., 2005).

### 1.7.2 Therapeutic effect of Se on breast cancer

In addition to the chemoprotective effect of Se, it can also inhibit tumour growth and metastasis by arresting the cell cycle and directing cells to enter apoptosis. Many lines of evidence also show its synergistic effect when combined with chemotherapy drugs, in which Se can protect healthy cells from cytotoxic drug damage while improving tumour cell apoptosis in a dose-dependent manner (Cao et al., 2004; Lobb, 2011). Details regarding the mechanism for this effect will be discussed in later sections.

### 1.7.2.1 *In vitro* studies on therapeutic effect of Se

Evidence of Se's effect on apoptosis was proposed by Dong et al., 2002. Global gene expression was measured using a microarray with cDNA from cultured MCF-7 cells after 6 hrs treatment with MSA. Thirty genes were up-regulated after Se treatment and they could be categorised into three groups: 1. signalling molecules such as extracellular signal-regulated protein kinase (ERK), and mitogen-activated protein (MAP); 2. apoptosis-regulating genes; 3. cell cycle-regulating genes such as cyclin, and cyclin dependent kinase (CDK). Upregulation of these key proteins can induce the apoptotic pathway and inhibit cancer cell growth. This study provided strong evidence of the effect of Se in cancer cell apoptosis and cell cycle arrest (Dong et al., 2002). Furthermore, He et al., 2013 applied Se-containing tea polysaccharide to MCF-7 cells and reported a significant reduction in tumour cell growth with an $IC_{50}$ of 140.1 µg/mL. This result was supported by an increase in pro-apoptotic proteins and activation of caspases, which are essential factors for apoptosis, thus suggesting cell cycle arrest and apoptosis (He et al., 2013). This study is in line with previous studies on prostate cancer, where they suggest the action from organic Se is on caspase-dependent apoptosis and G1-cell cycle arrest (Wang et al., 2002).

As the tumour-killing ability of Se was proven *in vitro*, many studies started to combine chemotherapy with Se in various cancer cell types. In 2011, one study investigated the combined treatment between chemotherapy and MSA on acute monocytic leukaemia cells (THP-1) and peripheral blood mononuclear cells (PBMC) (Lobb, 2011). In this study, they observed an enhanced cytotoxic effect on cancer cells when treated with MSA and

chemotherapy. The same effect was not seen on non-malignant PBMC. They also observed an increased level of glutathione (GSH) in PBMC cells while it was reduced in THP-1 cells after combined treatment with MSA and chemotherapy. The level of intracellular GSH in cells correlates with their ability to detoxify xenobiotics. Therefore, the differential changes in GSH in PBMC and THP-1 cells suggest MSA increased the ability of healthy cells to detoxify cytotoxic drugs while reducing the capacity of the leukaemia cells to do so. Overall this study showed evidence of increased therapeutic efficacy when combined with a Se compound towards malignant cells while healthy cells were protected from drug damage via induction of GSH (Lobb, 2011).

To be specific to breast cancer, Li et al., 2007 combined doxorubicin with MSA in treating doxorubicin-resistant MCF-7 cells for 24 hours. This study showed a significant increase in doxorubicin sensitivity and enhanced apoptosis in MCF-7 cells with MSA in comparison to doxorubicin treatment alone. Their biochemical analysis also revealed a change of phosphorylation pattern in key proteins that increase tumour apoptosis (Li et al., 2007).

Another study found that MSA can suppress the expression of ERα and prevent uncontrollable proliferation from ER activation (Lee et al., 2005). Based on this observation, $ERα^{+}$ breast cancer cell line should be more sensitive to Se as the stimulant for proliferation is inhibited. Indeed, in the same study, they compared the $ERα^{+}$/ $ERβ^{-}$ and $ERα^{-}$/ $ERβ^{+}$ breast cancer cell lines MCF-7 and MDA-MB-231, respectively, and found that the ER

downstream proliferation pathway was inhibited in MCF-7 while MDA-MB-231 remain unchanged (Lee et al., 2005). Another study investigated the combined effect of Se and docetaxel, and significantly increased cell apoptosis, growth inhibition, and cell cycle arrest were observed in MDA-MB-231 but not in MCF-7 cells (Park et al., 2015). Although the result of the two studies appeared contradicted as Se should synergistically inhibit with ER-dependent proliferation on MCF-7 cell line, however, the net result of chemoprotective and anti-tumour effect from Se can be complicated. Also, one drawback of the latter study is that there is no specification of the type of Se compound they used throughout the paper, which makes the further investigation difficult. All these studies mentioned above present evidence of a synergistic effect of Se compounds and chemotherapy drugs towards breast cancer cells, although the efficacy depends on the dosage, cell line, and type of Se compound used.

Aside from doxorubicin and docetaxel, previous *in vitro* studies also combine cisplatin and Se. Zhang et al. (2014) used HepG2 human hepatocellular carcinoma, MCF-7, and HK-2 non-malignant kidney cell line to examine the combined effects of cisplatin and organic MSA. They pretreated the cells with 10 μM of MSA for 6 hours followed by 24 hours of co-incubation with 40 μM of cisplatin. Both the cancer cell lines, HepG2 and MCF-7, showed the synergistic efficacy of MSA and cisplatin in both cell viability and level of DNA damage, but the same effect was not seen in the normal kidney cell line. The result indicates the combined therapy have some cancer specificity. Furthermore, western blot studies of the HepG2 cells showed down-regulation of anti-apoptotic protein families and up-

regulation of pro-apoptotic proteins as a consequence of co-treatment. Higher levels of p53 phosphorylation and down-regulation of phospho-MDM2 were also seen in HepG2 but not the HK-2 cell line; phospho-MDM2 is responsible for binding and degrading p53. This observation suggests that the activation of the p53-mediated apoptotic pathway may play a vital role in MSA and cisplatin preferential synergism.

Studies using *BRCA1*-mutated breast cancer cells have shown that inorganic selenite is more cytotoxic to breast cancer cells at much lower concentrations than MSA *in vitro*. Using the Sum149pt cell line, Mayall et al., 2014 found the inhibitory concentration ($IC_{50}$) of MSA and selenite to the Sum149pt cell line was 45 µM and 900 µM, respectively (Mayall et al., 2014b). A comet assay showed increased DNA damage when the cell line was treated with elevated levels of selenite. This finding is in line with the previous studies where the inorganic forms of Se appear to be more genotoxic to cells than organic Se (Valdiglesias et al., 2010).

#### 1.7.2.2 *In vivo* studies on therapeutic effect of Se

Chen et al., 2013 investigated the effect of dietary Se supplementation on tumour development using *in vivo* mouse models. Eight mice were fed with inorganic selenite, six with organic selenomethionine, and seven with organic MSA for three months prior to breast cancer cell inoculation (Chen et al., 2013). The primary tumour growth and the level of metastasis were measured and compared between Se-deficient and Se-adequate groups, and also between different forms of Se. They observed mice fed with inorganic selenite had a short-term delay of cancer growth whereas the

organic Se MSA and selenomethionine (SeMet) groups showed extensive tumour growth inhibition. Also, selenite-treated mice showed extensive metastasis, especially in the bone and kidney, whereas mice in the organic Se groups, especially SeMet, show decreased the level of metastasis. There was no significant difference in tumour growth inhibition and level of metastasis between the Se-deficient and Se-adequate groups.

This study presented *in vivo* evidence that, while Se supplementation can inhibit tumour growth and reduce metastasis, the effect is dependent on the form of Se. Organic Se such as SeMet and MSA are more effective in controlling breast cancer growth and metastasis than selenite. In fact, this study concluded that selenite is an unsuitable compound to reduce breast cancer development due to the increased incidence of bone and kidney metastasis (Chen et al., 2013). Indeed, a randomised study from 2012 supplied supranutritional dose of selenite (250 mg/day) to 1135 women with a BRCA1 mutation, 60 cases of cancer incidence were reported from the Se-supplemented group, as oppose to 45 cases from the placebo group. An insignificantly increased breast cancer incidence was seen with selenite supplementation. The result does not support the usage of Se on BRCA1 carriers for chemoprotection, and again emphasise the differential effects from a different chemical form of Se (Lubinski et al., 2011).

Another study, by Li et al., 2009, examined the combined effect of tamoxifen with or without methylselenocysteine (MSC) on *in vivo* MCF-7 xenograft mouse models Li et al. (2009). The size of the tumour was measured twice a week, and significant tumour growth inhibition was observed when treated

with both MSC and tamoxifen in comparison to tamoxifen-only. Immunohistochemistry measured the protein expression levels of ERα, and the ERα-targeting genes, PR and cyclin D1 showed significant reduction of protein expression. Tamoxifen, as explained previously, is a common hormonal therapy drug used to treat $ER^+$ breast cancer cells by acting as an antagonist of oestrogen and bind to the ER. As mentioned in the previous section, a study provided *in vitro* evidence of Se inhibiting ERα expression. Based on this finding, the administration of Se with tamoxifen is expected to significantly suppress ERα expression and reduce binding of oestrogen, respectively.

### 1.8 Mechanisms of anticancer effects of Se

The anti-carcinogenic and cancer-killing effect of Se can be summarised in four different categories: 1. neutralise reactive oxygen species (ROS) and prevent DNA damage; 2. repair DNA damage and avoid formation of mutations; 3. cell cycle arrest and programme cancer cells towards the apoptotic pathways; 4. prevent local growth and metastasis of tumours. The response from the cells, in part, depends on the dosage applied and chemical form of Se administered. Several studies show that Se along with other chemotherapy drugs can not only protect healthy cells from drug-induced cytotoxic damage but also increase the tumour-killing effect from chemotherapy drugs (Cao et al., 2004; Lobb, 2011). In this literature review, we will predominantly focus on the mechanism of chemoprotective and cancer-killing effect of Se, and will only briefly introduce the mechanism in slowing down cancer progression (invasion and metastasis).

### 1.8.1 Anti-oxidant and DNA repair

DNA damage occurs at a rate of 60,000 times per human cell per day (Bernstein et al., 2013). DNA damage can be naturally-occurring, induced by carcinogenesis or by exogenous agents such as UV light, ionising radiation, and industrial chemicals. In many metabolic processes such as respiration, a large amount of ROS, lipid peroxidation products, and reactive nitrogen species (RNS) are released in the cells. These chemicals attack the backbone of DNA creating single-stranded and double-stranded breaks, depurination, and/or depyrimidinations. DNA damage triggers the expression of downstream effectors to arrest the cell cycle and repair the damage, or programme the cell towards apoptotic pathways. Alternatively, if the damage signal is ignored and continuously replicated, mutations are established, resulting in oncogenesis.

At the nutritional level (55- 200 µg/day/person), Se appears to protect cells against ROS, promote DNA repair, and promote cell cycle progression under physiological states. In section 1.3.1 we reviewed the effect of selenoproteins such as GPx and selenoprotein P where they acting as a free radical scavenger. The reaction of GPx with hydrogen peroxide is: $2GSH + H_2O_2 \rightarrow GS–SG + 2H_2O$. The reduction of $H_2O_2$ prevents the formation of free radicals and reduces DNA damage (Bhabak & Mugesh, 2010).

Se compounds can not only protect DNA from damage through specific selenoproteins but also improve repair of damaged DNA. The possible mechanisms of DNA repair and DNA protection are summarised in a

schematic diagram in **Figure 7**. Se, in particular SeMet, prevents cancer formation in a p53-dependent manner. SeMet selectively induces the DNA repair cycle of p53, leaving the other two pathways unchanged (Fischer et al., 2006). SeMet can reduce the key cysteine residues 277/275 on p53 via redox factor 1 (Ref-1). Evidence of this process is seen *in vitro* on both human and mouse fibroblast cells (Seo et al., 2002a; Seo et al., 2002b). Mouse fibroblasts with either null p53 or null Ref-1 will block the DNA repair response from SeMet (Seo et al., 2002b). Fifteen hours pretreatment is required prior DNA-damage application to see the effect of repair. Redox state of Ref-1 is regulated by thioredoxin (Trx), which is modulated by another selenoprotein, thioredoxin reductase (TrxR); Trx therefore indirectly controls the redox state of p53.

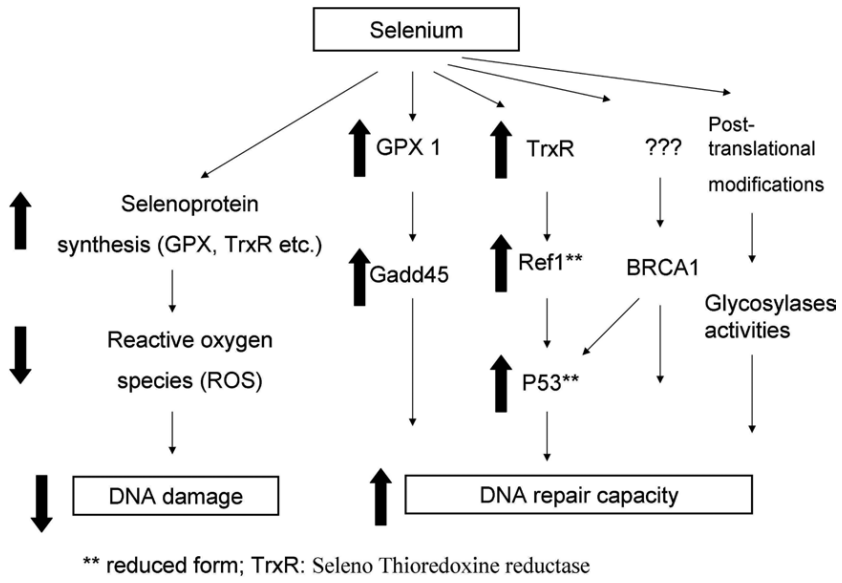


**Figure 7,** Possible mechanisms in chemoprotective effects of Se (Bera et al., 2013)

BRCA1 protein is a well-known DNA-repairing protein which can not only activate downstream DNA-repairing effectors but also join into a repair complex and fix damage directly. The interaction between BRCA1 and

Rad51 protein can repair DNA double-stranded breaks (Boulton, 2006). BRCA1 protein is also able to directly associate with p53 and activates the nucleotide excision repair (NER) DNA repair pathway, which promotes sequence-specific binding and activates downstream DNA-repairing genes, such as *XPC, p48XPE,* and *GADD45a* (Growth Arrest and DNA Damage). These expressed proteins are directly associated with DNA repair (Adimoolam & Ford, 2002). One study found that Ref-1 and Brca1 can interact with p53 concurrently. This suggests that Ref-1 can be a potential regulator of the NER pathway (Fischer et al., 2006). Despite the activation of the NER pathway by p53, other studies suggest induction of GPx by Se can also up-regulate the expression of the enzyme Gadd45, a stress sensor which functions in DNA replication and damage repair (Zeng et al., 2003). Breast cancer cell lines with GPx knocked out cannot induce Gadd45 expression (Nasr et al., 2004).

Another action of Se is to prevent carcinogenesis by inhibiting phase I enzymes and inducing phase II enzymes. The phase I enzymes can convert a carcinogen into a reactive species that attacks DNA, whereas phase II enzymes can detoxify the carcinogens (Ip & Lisk, 1997).

### 1.8.2 Apoptosis

In supranutritional doses (>400 µg/day) Se compounds can arrest the cell cycle and programme the cell towards apoptosis (Seo et al., 2002a). Organic and inorganic Se compounds appear to induce different routes of apoptosis and cell cycle arrest. Inorganic Se compounds, such as selenite, preferentially induce the caspase-independent apoptotic pathway. It causes

DNA single-stranded breaks which activate p53 and upregulates the expression of pro-apoptotic proteins, such as Bax (Jiang et al., 2002). Increased production of pro-apoptotic proteins will release cytochrome c from mitochondria and induce nuclease which results in nucleosome fragmentation that causes sub-apoptotic death or necrosis.

On the other hand, organic Se compounds, such as MSA will trigger the caspase-dependent apoptotic pathway. Organic Se compounds exert this action through Akt/PKB and MAPK/ERK pathway. These two pathways are important in controlling cell proliferation, growth, and apoptotic signal. Increased phosphorylation of Akt and ERK-2 protein will prevent the activation of key components in apoptosis (Chandler L. Walker, 2013). The relationship between the two pathways can be seen in **Figure 8**.

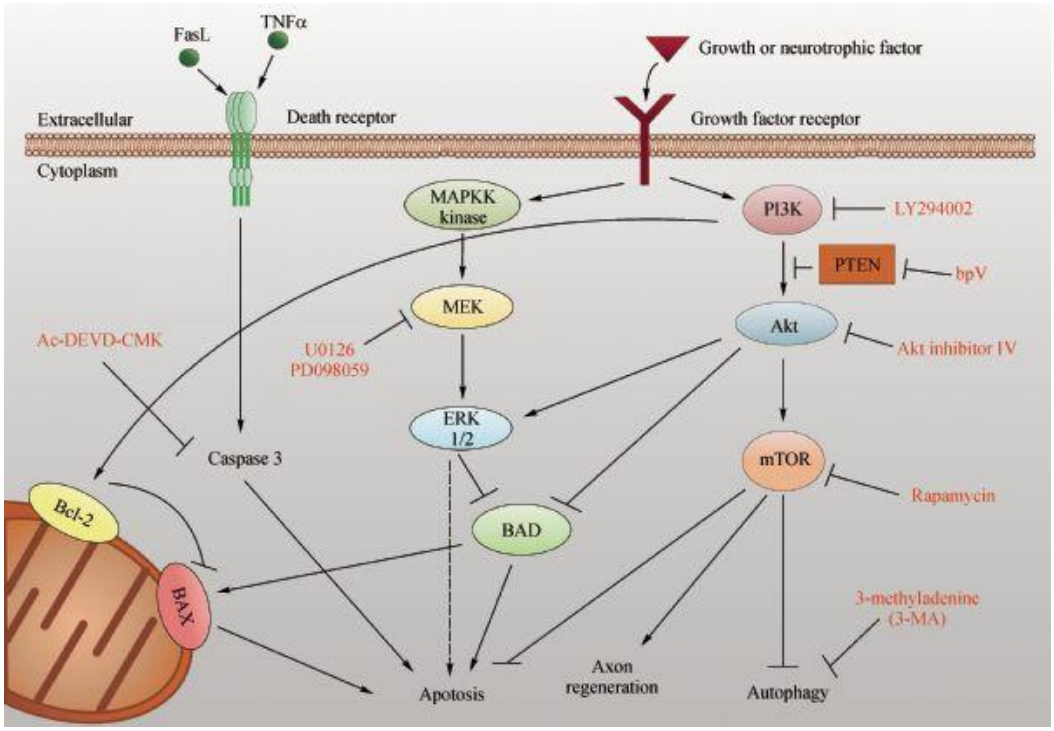


**Figure 8**, Crosslinks between MAPK/ERK2 pathway and Akt/PKB pathway controls the apoptotic signal of a cell (Chandler L. Walker, 2013). In this diagram, Akt phosphorylation inhibits the activation of ERK1/2 which further prevents the activation of pro-apoptotic protein, BAD, and results in cell survival.

Prostate cancer cells treated with MSA show decreased phosphorylation of both Akt and ERK-2 kinase, while other components of this pathway such as MAPK, and JNK1/2 remain unchanged (Zhao et al., 2006). Decreased phosphorylation of Akt and ERK-2 promote activation of pro-apoptotic proteins such as Bad and Bax. They then translocate to the surface of mitochondria and cause the release of cytochrome c into the cytoplasm. Cytochrome C acts as a death signal and binds to the apoptotic protease activating factor-1 (Apaf-1), which then binds to procaspase-9 forming an apoptosome. Formation of apoptosomes can trigger downstream activation of caspase-3 and caspase-7, which break the protein scaffold inside cells

and result in cell shrinkage and death (Dejean et al., 2006). Organic Se also arrests the cell cycle in G1-S phase by up-regulating the cyclin-dependent kinase (cdk) inhibitors p16, p21, and p27, which decreases the activation of cdk4, cdk6, and cdk2, respectively. Decreased activation of cdk by Se causes decreased phosphorylation in cyclin D and results in G1 cell cycle arrest in endothelial cells (Wang et al., 2008).

In addition to the differential effects of organic and inorganic Se compounds in cancer cells, it is also clear that one Se compound can act differently within non-malignant and malignant cells. In a study from 2002, enzymatically-generated methylselenol was incubated with a cultured human prostate cancer (cell line DU145) and human umbilical vein endothelial cells (HUVEC). The results of this study showed increased apoptotic morphological changes, such as DNA nucleosomal fragmentation and poly (ADP-ribose) polymerase (PARP) cleavage in the cancer cell line. PARP belongs to a family of proteins involved in cellular damage repair, and it is cleaved and inactivated by caspase during apoptosis. The biochemical analysis also showed the same pattern of phosphorylation on Akt and ERK-2 as when treated with MSA. In contrast, HUVECs did not show any sign of apoptosis with the same Se exposure, but rather had a G1–S cell cycle arrest effect. This pattern in HUVECs from methylselenol mimics the effect observed from MSA (Wang et al., 2002).

For breast cancer, one study from 2007 investigated the effect of MSA with doxorubicin *in vitro* on MCF-7 cells. In this study, they found cancer cells that are resistant to doxorubicin treatment have an increased level of

phosphorylation of Akt kinase, which then triggers downstream cell survival signalling and represses pro-apoptotic proteins. Treatment with MSA appears to reverse this effect by reducing the level of phosphorylation of Akt. This result is supported by measuring the level of phosphorylation of GSK3β and FOXO3A, which are downstream effectors of activated Akt and are acting as anti-apoptotic proteins when phosphorylated. Therefore, the combined treatment of doxorubicin and MSA can increase drug sensitivity by modulating Akt signalling (Li et al., 2007).

In comparison, a 2005 study suggested a separate mechanism of MSA effects on the MCF-7 breast cancer cell line. As mentioned above, MCF-7 is an ERα positive breast cancer cells; the fast proliferation of MCF-7 cells is facilitated by overexpression of ERα. In this study, they showed the effect of MSA in reducing RNA and protein expression of ER-α by MCF-7 cells, and they also examined the expression of a downstream effector of ERα, c-myc, by measuring the luciferase activity link to the *c-myc* gene (Lee et al., 2005). This research represents a novel mechanism of Se in oestrogen-responsive breast cancer cells by repressing the ER and thereby reducing cancer cell proliferation.

### 1.8.3 Inhibition of cancer invasion and metastasis

One key step in cancer metastasis is the attachment of cancer cells to extracellular matrix for seeding. Any factors that inhibit the adhesion have the potential to decrease cancer invasion/metastasis. One study from 2001 using an *in vitro* human fibrosarcoma cell line showed that cell adhesion to collagen matrix was inhibited by selenite treatment via decreased

expression of urokinase-type plasminogen activator (uPA), and matrix metalloproteinase (MMP)-2 and -9; all are factors involved in matrix degradation (Yoon et al., 2001). This effect appears to be mediated via suppression of two transcription factors, NF-κB and AP-1. In addition to cell-matrix adhesion, another factor that affects tumour metastasis is vascular endothelial growth factor (VEGF). High expression of this protein activates the receptors on vascular endothelial cells and triggers the proliferation of vascular cells and results in angiogenesis.

Other research examined the effects of selenite, MSA, and methylselenocyanate (MSeCN) on *in vitro* HUVECs, human prostate cancer cells, and breast cancer (MCF-7 and MDA-MB-468) cells. HUVECs showed decreased the gelatinolytic activity of MMP-2 within 0.5 hours upon Se application. Alternatively, for prostate cancer and breast cancer cells, exposure to MSA but not selenite caused a reduction of cellular and secreted VEGF. This study showed that Se, especially in a mono-methylated form, inhibits cancer invasion and metastasis via reducing the activity of MMP-2 and VEGF proteins (Jiang et al., 2000).

### 1.9 Differential efficacy of different Se compounds

Different Se compounds appear to have different efficacy in activating both DNA repair in healthy cells and inducing apoptosis in cancer cells. For example, mice were supplemented with four different types of Se a week prior to tumour induction, and the efficacy of each compound was measured based on the number of tumours that developed (Ip et al., 1991). The relative efficacy of Se compounds found was in the order of Se-

methylselenocysteine, selenite, selenocystine, and dimethyl selenoxide, from highest to lowest efficacy. These results suggest that methylselenol is the key metabolite in Se metabolism, and any Se compound that can generate a steady stream of monomethylated Se has higher efficacy (Ip et al., 1991). Although selenocystine is close to the $H_2Se$ pool, its non-specific incorporation into selenoproteins causes random loss of Se and reduces its efficacy.

The second part of this study compared the efficacy of mono-, di-, and tri-methylated Se in restoring GPx in Se-depleted mice. The results showed that monomethylated Se is more efficient than di- and tri- methylated Se compounds. This suggests that complete demethylation is an essential process in Se metabolism (Ip et al., 1991). The example of DNA repair pathway via p53 was shown to react differently according to the Se compound used.

A follow-up study published in 2000 showed strong evidence that a mono-methylated Se compound is the key metabolite of Se (Ip et al., 2000). This study investigated MSA, a pre-formed mono-methylated metabolite, which is a simplified version of Se-methylselenocysteine without the complex amino acid covers. Se-methylselenocysteine requires β-lyase to convert it into monomethylated Se. MSA in comparison to Se-methylselenocysteine was much more potent in inducing apoptosis and inhibiting the growth of mouse mammary tumour cells *in vitro*. However, when examining the chemoprotective effect of these two compounds on an *in vivo* mouse model, no significant differences were shown between them. A possible

explanation for this phenomenon is that β-lyase is present in many tissues and therefore it is not anymore a limiting factor in forming monomethylated compounds from Se-methylselenocysteine, thus removing differences between it and MSA.

Se effects on a DNA repair pathway via p53 also differed with the Se compound used. A study from 2004 compared the post-translational modification of p53 from selenite, MSA and SeMet in human lung cancer cells *in vitro*. They showed that all three Se compounds can promote a redox response from p53 via cysteine residues. However, the cells incubated with selenite did not show any improvement in DNA repair and cell survival. Alternatively, MSA and SeMet both showed upregulation of DNA repair proteins, although MSA exhibited a more efficient dose response (1-5 μM) than SeMet (10-20 μM). The reason, as mentioned above, is likely due to enzyme conversion required for SeMet to methylselenol which reduces its efficacy. In addition to redox response from p53, they also found MSA and selenite are able to phosphorylate some threonine and serine residues on p53, respectively, but SeMet did not induce any phosphorylation. Selenite promoted phosphorylation on serine 20, 37, and 46 residues while MSA-induced threonine phosphorylation. The three phosphorylated serine residues by selenite are known to associate with an apoptotic pathway by p53. Differential phosphorylation sites on p53 by selenite and MSA could be the reason behind differences in the genotoxicity of different Se compounds (Smith et al., 2004).

## 1.10 Pro-oxidant effect of Se

Although accumulating published data demonstrates the beneficial effect of Se against cancer, several studies have reported adverse effects and DNA damage with Se supplements. High concentrations of Se, especially in inorganic form, can induce DNA breaks. Selenite can oxidise glutathione (GSH) and form superoxide anion ($O_2^-$) radicals and elemental Se ($Se^0$) through the intermediate GSSeSG (**Figure 9**). The free radical itself has low toxicity but it can yield $H_2O_2$ and undergo Fenton's reaction, reducing metal ions to form the hydroxyl (OH) radical which is highly damaging to DNA (Letavayová et al., 2006).

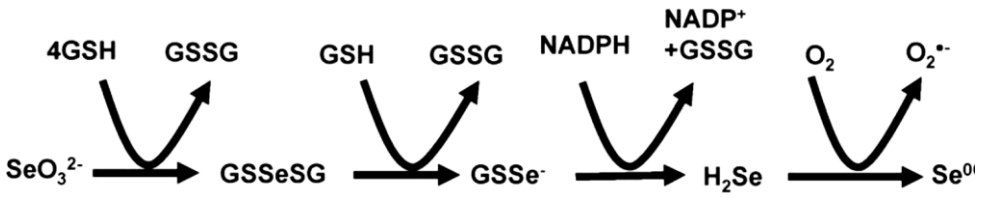


**Figure 9,** Selenite reduction pathway (Seko et al., 1989).

Conversely, methylselenol ($CH_3SeH$), which is produced from SeMet and hydrogen selenide, can convert to selenide anion (RSe-), which can then generate $O_2^-$ and create oxidative stress. Although the oxidative stress may result in apoptosis and prevent cancer growth, too many Se anions can create oxidative damage in DNA (Chaudiere et al., 1992). Although both organic and inorganic Se can cause DNA damage, the dosage limits are different. For example, *in vitro*, 5-10 μM selenite can induce single-stranded break and acute cell lysis whereas, for methylselenocysteine, 10-50 μM is required to induce cell death, mainly via apoptosis rather than necrosis. This result indicates different forms of Se can induce different metabolic pathways to cause DNA damage (Wilson et al., 1992).

## 1.11 Focus of present research

Previous studies have shown that organic and inorganic Se appear to work on different pathways in a cell and therefore have different effects on cell viability. Furthermore, patients with *BRCA1* mutations seem to be more sensitive than non-*BRCA1* mutated ones. Therefore, firstly we aim to investigate the *in vitro* effect of two Se compounds, organic MSA and inorganic selenite, on *BRCA1*-mutated (MDA-MB-436 and Sum149pt) and non-mutated (MCF-7 and MDA-MB-231) breast cancer cell lines. We will examine the cytotoxic and genotoxic effect of Se by analysing cell viability and level of DNA damage with colorimetric MTT assay, and comet assay, respectively. We hypothesised that the breast cancer cells with a *BRCA1* mutation are more sensitive to DNA damage and death from Se treatment, especially to the inorganic form. Previous research on Se in breast cancer cells with *BRCA1* mutations are mostly epidemiological studies or *in vitro* studies with a focus on DNA repair effects of Se (Fischer et al., 2006; Jaworska et al., 2012; Kotsopoulos et al., 2010; Kowalska et al., 2005). To the best of our knowledge, no evidence demonstrating the direct relationship between the *BRCA1* mutations and the cytotoxic effect of Se has been reported. We aim to explore this in this research study. The second aim of the study is based on the result of the first objective, we will examine the combined effect of the chemotherapeutic drug, cisplatin, with selenite or MSA on both *BRCA1*-mutated and non-mutated breast cancer cell lines. The combined cytotoxicity will be measured with MTT assay again. Lastly, we will also validate a new technique called Long run real-time PCR (Lord-qPCR) for quantifying DNA lesions created by selenite and MSA. This

technique detects the DNA damage based on the amplification efficiency on DNA template with qPCR. The quality of result from this method can be compared with the previous result from the conventional comet assay.

# Chapter 2:

# Material and Methods

The following sterile plastic-ware was sourced: 0.2 mL Axygen™ PCR tube, 0.6 mL Eppendorf Tube®, 2 mL Eppendorf Tube®, 15 mL and 50 mL Fisher Scientific Falcon™ tube, Jet Biofil® T25 flask and T75 flask, Jet Biofil® cultured-treated flat bottom 24- and 96- well plate, 10 mL Terumo® sterile syringe, Sartorius Stedim Minisart® syringe filter and Biologix® 3 mL Pasteur pipette. In addition, the following glassware was used: Scott bottles, serological pipette tips, 26 x 76 $mm^2$ Fronine microscope slides, 20 $mm^2$ and 22 x 40 $mm^2$ coverslips. Double distilled water (mQ water) with a resistivity of 18 MΩ.cm. Solutions were sterilised by autoclaving or filtering (sterile syringe and 0.2 µM filter). Recipes for every solution used in the present research are listed in Appendix 1.

All the commercial breast cancer cell lines used in this study were sourced from the University of Waikato inventory. Under the guidelines of the University of Waikato Human Ethics Committee, ethics approval was not required. Cells were cultured using aseptic techniques and all the work was conducted in a Heraeus® Herasafe® KS 18 safety cabinet class II.

## 2.1 Breast cancer cells

Two *BRCA1*-mutated and two non-*BRCA1*-mutated human breast cancer cell lines were used in this project and are summarised in **Table 4** below.

## 2.2 Reviving of *in vitro* cancer cells

A cryovial containing the breast cancer cells was removed from a -80°C freezer and transferred to an ice box. The cells were quickly thawed by immersing the cryovial into a 37°C water bath for two minutes until only a small piece of ice was visible. The cells were then transferred to a tissue culture hood where 2 mL of pre-warmed 37°C of the appropriate complete media was carefully dropped and then mixed gently with a pipette. The entire solution was then transferred to a labelled T25 flask and allowed to grow in a 5% $CO_2$, 37°C Thermo Scientific™ Heracell™ 240i incubator. The next day, the cells were visualised under a microscope to confirm the revival and adherence to the flask.

| **Cell line** | **Mutated Gene(s)** | **NCBI Accession Number** |
|---|---|---|
| SUM149pt | ***BRCA1*** | NG_005905.2 |
| MDA-MB-436 | ***BRCA1*** | |
| | *RB1* | NG_009009.1 |
| MDA-MB-231 | *CDKN2A* | NG_007485.1 |
| | *KRAS* | NG_007524.1 |
| | *NF2* | NG_009057.1 |
| | *TP53* | NG_017013.2 |
| | *BRAF* | NG_007873.3 |
| MCF-7 | *CDKN2A* | NG_007485.1 |
| | *CDKN2a(p14)* | |
| | *PIK3CA* | NG_012113.2 |

**Table 4**, Summary of the breast cancer cell lines used in this study with Genbank Accession number from NCBI.

## 2.3 Cell culturing

All cell culture experiments were carried out in a physical containment

facility level two (PC2) laboratory. The complete culture media for growing the breast cancer cell lines were decided based on the recipes recommended from ATCC® and/or published journal articles (Kao et al., 2009; Price et al., 1990; Proia et al., 2011; Sheridan et al., 2006). MCF-7, MDA-MB-436, and MDA-MB-231 breast cancer cell lines were grown in minimum essential media (MEM) from Gibco® supplemented with 10% Fetal Bovine Serum (FBS), 1% Insulin, 1% 100x Penicillin/Streptomycin. Sum149pt cell line was grown in Ham's F-12 media from Sigma-Aldrich® with 5% FBS, 1% 100x Penicillin/Streptomycin, 0.5% Hydrocortisone, 0.1% Insulin, and 1% Hepes. The passage number of MCF-7, MDA-MB-436, MDA-MB-231, and Sum149pt were P63, P15, P20, and P20, respectively. The cells we used for experiments were no more than ten passages on top of the original passage number. Cells were grown in a T25 flask with 25 $cm^2$ surface area for the cell to adhere. The conditions for incubation were set at 37°C with 5% $CO_2$. Media was replaced on alternate days. Pictures of the cultured four cell lines can be seen in **Figure 6**.

### 2.4 Sub-culturing cells

Cells were split when they reached 85%-90% confluency to keep cells growing under exponential phase. Old media was removed with a Pasteur pipette, followed by addition of 2 mL 1 X PBS (pH 7.4) to wash the cells and then discarded. Washing the cells with PBS removes media left in the flask, that would prevent interference with the trypsin cleavage. To lift the adhered cells from the bottom of the flask, 2 mL of pre-warmed 0.25% trypsin-EDTA from Gibco® was added to the flask and incubated at 37°C for 3 to 5 minutes. After the incubation, 4 mL of pre-incubated media was added to the cell

solution to terminate the reaction between cell and trypsin. The cell mixture was then centrifuged in the Heraeus® Megafuge® 1.0 at 200 x *g* for 5 minutes at room temperature (RT). After separating the cells and solution, the supernatant was then removed and the cell pellet was resuspended in 6 mL of pre-warmed media by gently pipetting the solution and cells up and down. The cell solution was then split into two T25 flasks with 3 mL each and continued growing in a 37°C incubator.

### 2.5 Measuring cell concentration using a Haemocytometer

Cell solution used for cell counting was taken from the solution after adding media to trypsin and before centrifugation to spin down cell pellet (section 2.4). Before taking out cells to count, the solution was mixed by pipetting; for MDA-MB-436, SUM149pt, and MDA-MB-231 cell line, the solution was pipetted up and down 10 times; for MCF-7 cell lines, due to a characteristic clumping issue, the cell solution was pipetted 50 times to fully resuspend the cells. To measure cell concentration, 50 µL of cell solution was transferred to a 0.6 mL Eppendorf tube followed by addition of 50 µL trypan blue dye to stain the cells. The mixture was gently pipetted up and down ten times to mix thoroughly. The Haemocytometer was cleaned with 70% alcohol, air dried, and covered with a 22 mm width coverslip. Ten microlitres of dye mixture were transferred to each Neubauer chamber on the haemocytometer. Each chamber has a counting grid drawn. In the present study, cells were counted in each of four corners at top and bottom and averaged the number by eight to estimate cell counted in each square. According to the manuscript given by the manufacturer, the distance between coverslip and haemocytometer is 0.1 mm and the big square is

0.1 mm x 0.1 mm, therefore, the volume of solution counted is 0.1 µL. To calculate the concentration of cells in 1 mL, we used the formula (**Equation 1**) below:

$$\text{Concentration (Cell/mL)} = Average\ cell\ number\ in\ each\ square \times 2\ (dilution\ factor) \times 10000$$

**Equation 1**, Equation to calculate the concentration of cells with a haemocytometer.

To calculate the total number of cells in the solution, the final number was multiplied by the total volume in the cell solution mixture.

### *2.6* Cell viability counts with Trypan blue

Trypan blue dye was used to estimate the cell viability. Dead cells lose their membrane integrity which allows the trypan blue diffuse into cells and appear as blue colonies under a microscope. In contrast, healthy cells with intact membrane appear as white colonies. In each square counted, both blue and white cells were recorded and percentage viability of cells was calculated with **Equation 2** below:

$$\%\ \text{cell viability} = \left(\frac{\text{Unstained cells}}{\text{total cells}}\right) \times 100$$

**Equation 2**, Calculation for cell viability with trypan blue stain.

### 2.7 Freezing cultured cells

Once all the assays on cultured cells were completed, the remaining cells were frozen down in cryovials with freezing media and stored at -80°C.

Freezing media was made up with the corresponding complete cell media supplemented with fresh 5% Dimethyl sulfoxide (DMSO). Cells were harvested as stated in section 2.4 and the population was counted as outlined in sections 2.5 and 2.6. Cells were resuspended with freezing media to a concentration of 1.5 x $10^6$ cells/mL, and 1 mL aliquoted into each labelled CryoTube™. The CryoTubes™ were then kept in a freezing container from Thermo Fisher Nalgene® and left in a -80°C freezer. The cryo-container was filled with isopropanol which allows the temperature to decline with steady speed (-1°C per minute). Once the cell media were completely frozen, the vials were transferred to a labelled box in a -80°C freezer for long-term storage.

### 2.8 Growth assay of cultured breast cancer cells

To assess the growth rate of a cell line, cells were grown to 90% confluency in a T25 flask followed by cell harvest procedure described in section 2.4. Cells were diluted down to a concentration 2.5 x $10^5$ cells/mL and plated on a cell culture treated 24-well plate. The layout of different timing to harvest was specified in **Table 5**, and the remaining wells were filled with 1xPBS to prevent evaporation of media.

| | | | | | |
|---|---|---|---|---|---|
| 24 hours | 24 hours | 48 hours | 48 hours | 72 hours | 72 hours |
| 24 hours | | 48 hours | | 72 hours | |
| | | | | | |

**Table 5**, 24-well plate arrangement for growth control

After 24 hours, the first three wells were harvested individually by the addition of 500 µL trypsin followed by neutralisation with 1 mL of warm media after 5 minutes of trypsinisation at 37°C. The cell mixture was then transferred to a 2 mL tube for cell counting (procedure outlined in section 2.5). The same steps were repeated for wells with 48 and 72 hours incubation from the first day. Once the amount of viable cells was acquired over the three-day period, the percentage of cells present at different timing was calculated by dividing the number by the original number of cells plated (2.5 x $10^5$ cells). The formula (**Equation 3**) is specified below:

**Equation 3**, Calculation for growth assay to calculate the percentage of cells present.

$$\%\ \text{of cell present} = \frac{\text{calculated cell number at different timing}}{\text{Original cell number input}} \times 100\%$$

The experiment was repeated twice for statistical significance and analysed with Microsoft Excel; p-value <0.05 was considered statistically significant.

## 2.9 DNA extraction from cultured breast cancer cells

Cancer cells were grown in conditions stated in section 2.3. Adhering cells were lifted with the method specified in section 2.4. Cell pellets were resuspended in 10 µL of freshly thawed 10 mg/mL proteinase K, and 190 µL of digestion buffer containing 10 mM Tris-Cl (pH 8.0), 10 mM, EDTA (pH 8.0), 100 mM NaCl, and 0.5% SDS. The samples were digested overnight at 65°C on a 600 rpm shaking Eppendorf ThermoMixer™. After overnight incubation, samples were cooled to room temperature (RT) followed by twenty seconds of vortex to mix the solution. An equal volume of organic solvent, chloroform, was used to separate the DNA from protein in the lysed

cell solutions. The sample was incubated for five minutes on a Stuart™ SB2 rotator and the two phases separated by five minutes of centrifugation at 10000 x *g* in the Eppendorf centrifuge (5415R). Cellular protein was partitioned into the lower organic phase leaving the nucleic acid in the upper aqueous layer. The upper layer of the sample mixture was carefully transferred to a new 2 mL Eppendorf tube. To precipitate the DNA out of the aqueous solution, two volumes of ice-cold absolute ethanol and one-tenth volume of 3 M sodium acetate (pH 5.5) was added and the samples were then left in -20°C freezer for one hour to allow DNA precipitation. After the freezing step, samples were centrifuged at 14000 x *g* for 20 minutes at 4°C to settle the DNA pellet. The supernatant was carefully removed and the pellet washed with 1 mL of 70% ethanol. The sample was gently inverted several times to mix. The sample was then centrifuged at the same speed as previously for 15 minutes followed by drying with opened lids for 10 minutes to allow evaporation of the ethanol. The DNA pellet was resuspended in 50 µL of TE buffer (pH 8.0) and the concentration and quality of DNA were determined using the Thermo Scientific Nanodrop™ 2000c at wavelengths 230, 260, and 280 nm. The readings provide a ratio of 260/280 and 260/230, which indicate the purity of nucleic acid and the amount of residual organic solvent carry-over from the extraction process, respectively. A ratio of 260/280 at 1.8-2.0 is considered pure with nucleic acid; expected 260/230 ratio is commonly within the range 2.0-2.2. The DNA samples were stored at 4°C for further experimental analysis.

### 2.10 Testing for mycoplasma contamination using PCR

Mycoplasma is a group of micro-organisms that are defined as lacking a

rigid cell wall (Barile & Kruse Jr, 1973) and are a major issue causing cell contamination. Heavily contaminated culture media appears cloudy or turbid and sometimes with clumps floating. However, due to the common addition of antibiotics to media, sometimes contamination can be hindered and not reach the eye-detectable level. The presence of mycoplasma in cultures can create stress for cells and alter cellular metabolism, as well as inhibiting cell growth and causing DNA damage. It is therefore important to test for the presence of mycoplasma prior starting any experiment. The method used here is the PCR-based mycoplasma detection. This method amplifies the conserved 16S rRNA region in mycoplasma (Hopert et al., 1993; Uphoff & Drexler, 2002). Briefly, a 2x PCR master mix iTaq™ from iNtRON Biotechnology was used with published primers. The master mix contains iTaq™ DNA polymerase (5 U/mL), dNTPs, reaction buffer, stabiliser and enhancer, and gel loading dye. The six published primers for detecting Mycoplasma are listed in Table 6 (Uphoff & Drexler, 2011).

| **Forward primer (5')** | **Reverse primer (3')** |
|---|---|
| cgc ctg agt agt acg t**w**c gc | gcg gtg tgt aca a**r**a ccc ga |
| tgc ctg **r**gt agt aca ttc gc | gcg gtg tgt aca aac ccc ga |
| cgc ctg agt atg ctc gc | |
| cgc ctg ggt agt aca ttc gc | |

**Table 6,** Primer sets for mycoplasma detection. The combination of different 5' and 3' primers covers detection of a different strain of mycoplasma (Uphoff & Drexler, 2011). **R**= mixture of a and g nucleotides, and **w**= mixture of a and t.

Three PCR controls were set up on the ice. Firstly, an internal control obtained from Leibniz Institute DSMZ (Deutsche Sammlung von

Mikroorganismen und Zellkulturen GmbH) in Germany was used in this experiment to confirm the complete reaction of PCR with efficient primers and PCR components. This lyophilised internal control DNA sample was suspended in 100 µL of mQ water and diluted ten times according to the DSMZ guidelines (Mayall et al., 2014a). The internal control is a 516 bp mycoplasma sequence from a strain *Acholeplasma laidlawii*, cloned to a 3995 bp plasmid. The cloned mycoplasma sequence was disrupted by insertion of extra 476 bp fragment which results in a 1 kb band as opposed to the expected 516 bp band appearing on the positive control. Secondly, DNA added for the positive control reaction was kindly provided by Crown Research Institute AgResearch, Hamilton, New Zealand, as DNA extracted from a contaminated mouse embryo fibroblast cell line. Positive control DNA was prepared from a former study in 2014 with Quick-gDNA™ MiniPrep DNA extraction kit (Zymo Research) and stored in -20°C (Mayall et al., 2014a). Finally, a negative control was set up by replacing sample DNA with mQ water; an absence of the band was expected on agarose gel unless PCR contamination occurred. The PCR reaction was set up in a PCR hood (except the final DNA addition) with content listed in **Table 7** using sample DNA extracted from cultured cells in this study.

| | 2x PCR iTaq™ master mix (µL) | 5µM primer mix (µL) | Positive control DNA (µL) | 50 ng/µL of Sample DNA (µL) | Internal control (µL) | mQ Water (µL) |
|---|---|---|---|---|---|---|
| Negative control | 12.5 | 1 | | | | 11.5 |
| Negative control + internal control | 12.5 | 1 | | | 1 | 10.5 |
| Positive control | 12.5 | 1 | 1 | | | 10.5 |
| Positive control + internal control | 12.5 | 1 | 1 | | 1 | 9.5 |
| Sample DNA | 12.5 | 1 | | 1 | | 10.5 |
| Sample DNA + internal control | 12.5 | 1 | | 1 | 1 | 9.5 |

**Table 7**, Composition of PCR reaction mixture for mycoplasma detection.

PCR was run in the MJ RESEARCH PTC-200 DNA Engine with the cycling conditions listed in **Table 8**. Five microliters of all PCR products were loaded on a 1 % agarose gel. The agarose gel was made up of 0.4 g of HyAgarose™ LE Agarose dissolved in 40 mL of 1 x Tris-acetate-EDTA (TAE) buffer; the mixture was microwaved for 1 minute with high power (700W), cooled to 60°C, followed by the addition of 2 µL of 10 mg/mL Ethidium Bromide DNA stain. The gel was then run at 90 volts for 30 minutes in an Owl™ EasyCast™ B1A Mini Gel Electrophoresis System. The agarose gel was visualised with the Omega Lum™ G imaging system. PCR with the addition of internal control DNA was expected to show a band size of 986

bp, and sample DNA with mycoplasma contamination was expected to show a band at the size of 510 bp on the agarose gel.

| **Cycle step** | **Temperature (°C)** | **Time** | **Cycle number** |
|---|---|---|---|
| Initial denaturation | 94 | 2 min | 1 |
| Denaturation | 94 | 20 sec | 35 |
| Annealing | 63 | 20 sec | |
| Elongation | 72 | 60 sec | |
| Final elongation | 72 | 5 min | 1 |

**Table 8**, Cycling conditions of PCR for mycoplasma detection

## 2.11 Confirmation of DNA mutation in the cultured breast cancer cell lines

PCR and DNA sequencing were used to confirm the identity of each cell line through detecting the presence/absence of specific mutations. Primers used were listed below in **Table 9**:

| Target genes | Primer | Sequence (5'-3') | Size (bp) | Method | Length (bp) | Tm (°C) | GC% |
|---|---|---|---|---|---|---|---|
| Breast cancer 1, early onset (*BRCA1*) | KM2F | ACATGACAGCGATACTTTCCC | 250 | DNA | 21 | 58 | 47 |
| | KM2R | ACCAGGTACCAATGAAATACTGC | | | 23 | 58 | 43 |
| | KM4F | TGGTTGGGATGGAAGAGTGA | 400 | DNA | 20 | 58.26 | 50 |
| | KM4R | GATCTGCCTGCCTCAGTCTC | | | 20 | 59.9 | 60 |
| | KM5R | TTCTTTCAGCATGATTTTGAAGTCA | | | 25 | 57.96 | 32 |
| Tumour protein p53 (*TP53*) | KO9F | GCTTTGAGGTGCGTGTTTGT | 247 | DNA | 20 | 59.9 | 50 |
| | KO9R | CTTCTTTGGCTGGGGAGAGG | | | 20 | 60.03 | 60 |
| Kirsten rat sarcoma viral oncogene homolog (*KRAS*) | KO10F | ACGTCTGCAGTCAACTGGAA | 251 | DNA | 20 | 59.54 | 50 |
| | KO10R | GCTGTATCGTCAAGGCACTCT | | | 21 | 60.13 | 52.38 |
| B-Raf proto-oncogene, serine/threonine kinase (*BRAF*) | KO11F | AGACGGGACTCGAGTGATGA | 300 | DNA | 20 | 60.04 | 55 |
| | KO11R | AGTCCCGACTGCTGTGAACA | | | 20 | 61.4 | 55 |

**Table 9**, PCR primers designed to detect mutations in the breast cancer cell lines. KM stands for Kirsty Mayall who is the former masterate student in our lab. Ko is my last name, which labels the primers designed in the present study.

PCR reactions were set up with the ingredients listed in **Table 10**.

| **Component** | **Working concentration** | **Final concentration** | **Volume/ PCR tube** |
|---|---|---|---|
| HOT FIREPol® DNA Polymerase (Solis BioDyne) | 5 U/µL | 0.05 U/µL | 0.2 µL |
| $MgCl_2$ | 25 mM | 1.9 mM | 1.5 µL |
| Buffer B2 (Solis BioDyne) | 10X | 1X | 2 µL |
| dNTP | 20 mM | 200 µM | 0.2 µL |
| Forward Primer | 10 µM | 0.25 µM | 0.5 µL |
| Reverse Primer | 10 µM | 0.25 µM | 0.5 µL |
| DNA template | 20 ng/µL | 2 ng/µL | 2 µL |
| mQ $H_2O$ | | | 13.1 µL |
| **Total volume** | | | 20 µL |

**Table 10**, Composition of the PCR reaction mix.

All PCR reactions were run with the cycling conditions listed below in Table 11. The reaction products along with 100 bp ladder from Invitrogen™ were either load on 1% agarose gel and run under electrophoresis (90 volts, 30 minutes) with TAE buffer, or stored at 4°C until required for gel electrophoresis analysis.

| **Cycle step** | **Temperature (°C)** | **Time** | **Cycle number** |
|---|---|---|---|
| Initial denaturation | 95 | 15 min | 1 |
| Denaturation | 95 | 20 sec | 34 |
| Annealing | 61 | 20 sec | |
| Elongation | 72 | 60 sec | |
| Final elongation | 72 | 12 min | 1 |

**Table 11**, PCR cycling conditions to amplify positions with desired mutations.

After confirmation of the size of PCR product on the agarose gel, two methodologies were used to purify the DNA for sequencing. The Zymoclean™ Gel DNA recovery kit (Cat No: D4001) was used with the observation of smearing or unspecific PCR products, where the desired band size on the agarose gel was cut out and purified according to the manufacturer's instructions. Alternatively, if the PCR product appeared as a single sharp band on the agarose gel, the DNA clean and concentrator™-5 kit (Cat No: D4013) from Zymo Research was used to purify PCR products. Following purification, samples were then sent to Waikato DNA Sequencing Facility, Hamilton, New Zealand to sequence with 5 µM of appropriate primers (**Table 9**). The result was then matched with a reference sequence from The National Center for Biotechnology Information (NCBI: http://www.ncbi.nlm.nih.gov/) database via Geneious software (version 8.0.5) supplied from University of Waikato to confirm the presence or absence of specific mutations (**Table 4**).

### 2.12 Comet assays for testing DNA damage from Se

The comet assay, also known as single-cell gel electrophoresis (SCGE), is the most common method used to assess the level of DNA strand breaks in eukaryotic cells. This technique was first developed by Ostling and Johanson (1984) who demonstrated the first "comets" with damaged DNA under an electrophoretic field. Three main steps involved in the comet assay include encapsulation, lysis, and electrophoresis. Briefly, sample cells were fixed onto a glass slide followed by lysis of the cellular membrane to expose DNA, which allows it to migrate under an electric current. The smaller DNA fragments migrate further, therefore a longer comet tail is expected in highly

DNA-fragmented cells. The level of DNA damage can be predicted by measuring the length and intensity of comet tails.

Here firstly, we harvested the cells from a flask following the steps in section 2.4 and cell count to measure the total amount of cells as in section 2.5. The cells were resuspended in the volume that makes up the final concentration to $2.5x10^5$ cells/mL for MDA-MB-231, MDA-MB-436, and SUM149pt cell line, and $1x10^6$ cells for MCF-7. As MCF-7 cell line is the most slow-growing cell line, it therefore requires greater cell input to adhere within 24 hours. The diluted cell solution was then aliquot as 1 mL to 9 wells on a cell culture treated 24 well-plate. The plate was organised as below in **Table 12**. Each treatment was organised as a triplicate; two replicates were used in comet assay and one well was further used for Lord-qPCR experiment (see section 2.14). To avoid evaporation, 1xPBS was used to fill the remaining empty wells. Cells were incubated in a 37°C incubator with 5% $CO_2$ for 24 hours to adhere to the plate.

| | | | | | |
|---|---|---|---|---|---|
| Control | Control | Selenite | Selenite | MSA | MSA |
| Control (Lord-q) | | Selenite (Lord-q) | | MSA (Lord-q) | |
| | | | | | |

**Table 12**, Sample layout for comet assay on a 24-well plate. Lord-q is the wells of the cell where the DNA is extracted for later Lord-qPCR assay.

After 24 hours, media was aspirated from the plate and fresh media added

with its corresponding drug with the formula indicated below. The formula for cell lines (MCF-7, MDA-MB-231, and MDA-MB-436) using MEM media is outlined in **Table 13**, and the formula with Ham's F12 media (Sum149pt) is in **Table 14**. The volume of each component was multiplied 3.5 times for preparing sufficient volume for the triplicates and avoid pipetting errors. Corresponding complete media was added to the control wells. The adhered cells with drug-formulated media were incubated for 24 hours in a 37°C incubator with 5% $CO_2$.

| **Media components** | **20 µM Selenite in 1 mL (µL)** | **Triplicates Selenite media (µL)** | **20 µM MSA in 1 mL (µL)** | **Triplicates MSA media (µL)** |
|---|---|---|---|---|
| FBS | 100 | 350 | 100 | 350 |
| Insulin | 10 | 35 | 10 | 35 |
| 100x Pen/Strep | 10 | 35 | 10 | 35 |
| 100 µM Selenite | 20 | 70 | | |
| 100 µM MSA | | | 20 | 70 |
| MEM | 860 | 2580 | 860 | 2580 |
| Total (µL) | 1000 | 3500 | 1000 | 3500 |

**Table 13**, Formula to make up Se media with MEM media for MDA-MB-436, MDA-MB-231, and MCF-7 cell lines.

To prepare for the comet assay, 1% normal melting point agarose (NMPA) with 1xPBS was melted by incubation in a 35°C water bath for one hour. Glass microscope slides (25 mm x 75 mm) were cleaned with 70% ethanol

and lint-free Kimberly-Clark® Kimwipes™, and labelled appropriately with a diamond pencil. The cleaned slides were then immersed into the 1% NMPA to cover 2/3 of the slide. The agarose was then stored at RT to solidify overnight.

| **Media components** | **20 µM Selenite in 1 mL (µL)** | **Triplicates Selenite media (µL)** | **20 µM MSA in 1 mL (µL)** | **Triplicates MSA media (µL)** |
|---|---|---|---|---|
| FBS | 50 | 175 | 50 | 175 |
| Insulin | 5 | 17.5 | 5 | 17.5 |
| 100x Pen/Strep | 10 | 35 | 10 | 35 |
| Hepes | 10 | 35 | 10 | 35 |
| Hydrocortisol | 1 | 3.5 | 1 | 3.5 |
| 100 µM Selenite | 20 | 70 | | |
| 100 µM MSA | | | 20 | 70 |
| MEM | 904 | 3164 | 904 | 3164 |
| Total (µL) | 1000 | 3500 | 1000 | 3500 |

**Table 14**, Formula to make up Se media with Ham's F12 media for Sum149pt cell line.

After 24 hours Se incubation, cells were harvested and counted with the method from sections 2.4 and 2.5. Cells from each well were diluted with 1xPBS to $5x10^4$ cells/10 µL. The slides with NMPA prepared a day before were then coated with a mixture of 10 µL of the fresh cells and 80 µL of 0.5% low melting point agarose (LMPA) in 1xPBS. A 20 mm x 40 mm coverslip was gently placed on top. The slides were kept in 4°C cold room for 20 minutes to solidify. The coverslips were then removed and the slides were

immersed into lysis solution containing 0.5% Triton X100, 3.5 mM SDS, 2.5 M NaCl, 100 mM EDTA, and 10 mM Tris (pH 10.0), 300 mM NaOH for 90 minutes at RT. Once the cells were lysed, the resultant “nucleoid” was unwound with alkaline buffer for 30 minutes followed by electrophoresis with Owl™ separation system gel tank powered by BioRad PowerPac™ 300 for 20 minutes, 300 mA, 17 volts at 4°C in the dark, as light may introduce additional DNA damage.

After electrophoresis, the slides were neutralised and rinsed with neutralisation buffer and sterile water and dried at RT. The slides were stored in dark for no more than two weeks to maintain the sensitivity of fluorescence. To capture the comet cells, the slides were stained with 100 µL of 1/1000 SYBR® Gold (Thermo Fisher) at 4°C for 10 minutes followed by two 5 minute washing steps with pre-chilled water. The stained comet was then examined under Axiostar plus transmitted light microscope. Fifty comets were captured from each slide and duplicate slides were prepared, which gave 100 comets for each sample. The fluorescent comets were then input into software TriTek CometScore for calculating the percentage of DNA in tail and tail moment (**Equation 4**) with 90% cut-off to eliminate background noise.

$$\text{Tail moment} = \text{length of comet tail} \times \text{percentage of DNA in comet tail}$$

**Equation 4**, Calculation of tail moment for comet assay.

The average of percentage DNA in tail and tail moment was calculated with Microsoft Office Excel 2013 for each of the duplicated control, selenite, and

MSA-treated samples. An average of two technical replicates was obtained from the individual experiment. For statistical significance, three biological replicates were completed separately. Error bars were calculated as the standard error of mean (SEM) with the formula outlined in **Equation 5**. To compare the percentage of DNA in tail and tail moment between controls, selenite- and MSA-treated samples, and a one-tailed *t*-test was carried out. A p-value smaller than 0.05 is considered statistically significant.

$$SEM = \frac{S}{\sqrt{n}}$$

**Equation 5,** Formula for the standard error of mean. *S* is the sample standard deviation; *n* is the size of the sample.

### 2.13 MTT assay for testing Se cytotoxicity

MTT assay is a colorimetric assay used to assess the metabolic activity of cells. Tetrazolium dye MTT (3-(4,5-dimethylthiazol-2-yl)-2,5-diphenyltetrazolium bromide) can react with mitochondrial NAD(P)H-dependent cellular oxidoreductase enzymes to form insoluble purple formazan crystals. The colour intensity reflects the amount of cells with metabolic activity, therefore this method is commonly used to measure the viability of cell population.

#### 2.13.1 Determining cell concentration

The concentration of cells used for the MTT assay is crucial since a high or low amount can reduce the sensitivity of this assay. Therefore, before beginning the MTT experiment, the optimal concentration of cells was

determined individually for each cell line through cell titration. A cell volume (200 µL) with a concentration ranging from $1x10^4$, $5x10^4$, $1x10^5$, $5x10^5$, to $1x10^6$ cells/mL was added to a culture-treated flat bottom 96-well plate for 24 hours to allow cell adherence. Media was then replaced with 200 µL of warm fresh media and 10 µL of 5 mg/mL of MTT reagent and incubated for 4 hours at 37°C. Once the reaction was completed, culture media in each well was replaced with 100 µL of solubilising solution and shaken on IKA® MS1 Minishaker plate shaker for 15 minutes followed by one-hour incubation at 37°C to dissolve the formazan crystal. The plates were then measured by Bio-Rad Microplate reader model 680 at 570 nm with background reference at 655 nm. Reading at 655 nm was subtracted from 570 nm. The OD reading of each concentration was then analysed graphically with Microsoft Office Excel 2013. The optimal concentration of cells used for MTT assay was chosen from the linear range on the graph.

### 2.13.2 MTT assay with Se

To begin, cancer cells were harvested and the population density was measured as described previously in sections 2.4 and 2.5, respectively. The cell pellet was resuspended in a sufficient amount of media to achieve a concentration of $1.5x10^5$ cells/mL, and 200 µL of the cell solution was transferred to a cell culture treated flat bottom 96-well plate to the wells indicated in **Table 15**, except the blank wells. Different breast cancer cell lines have different growth rates; MCF-7 and Sum149pt were incubated at 37°C with 5% $CO_2$ for 72 hours for the cells to adhere, and MDA-MB-436 and MDA-MB-231 were incubated for 24 hours.

### 2.13.2.1 Se incubation

After the incubation, media with different concentrations of Se were made up and the formula is listed in **Table 16** and **Table 17**. The old media was replaced with new Se and media mixture with corresponding concentrations as arranged in **Table 16,** Formula to make up Se media with their corresponding Se concentrations for MDA-MB-231, MDA-MB-436, and MCF-7 cell lines. Each Se concentration was made up with volume for triplicates (µL). SC stands for solvent control in which cells in a well were exposed to 190 µL of media plus 10 µL of 1xPBS and further incubated with Se for another 24 hours.

| | | | | | | | | | | |
|---|---|---|---|---|---|---|---|---|---|---|
| PBS | → | | | | | | | | | |
| BL | SC | A | B | C | D | E | F | G | H | SC | BL |
| BL | SC | A | B | C | D | E | F | G | H | SC | BL |
| GC | GC | A | B | C | D | E | F | G | H | GC | GC |
| | | | | | | | | | | |
| | | | | | | | | | | |
| | | | | | | | | | | |
| PBS | → | | | | | | | | | |

**Table 15**, MTT assay arrangement on a 96-well plate. A= 1 µM; B= 5 µM; C= 10 µM; D= 50 µM; E= 100 µM; F= 250 µM; G= 500 µM; H= 1000 µM; BL= Blank (media+PBS); SC= Solvent control (cell + media + PBS); GC= Growth control (Cells + media).

| | SC | 1 µM A | 5 µM B | 10 µM C | 50 µM D | 100 µM E | 250 µM F | 500 µM G | 1000 µM H |
|---|---|---|---|---|---|---|---|---|---|
| FBS | 70 | 70 | 70 | 70 | 70 | 70 | 70 | 70 | 70 |
| Insulin | 7 | 7 | 7 | 7 | 7 | 7 | 7 | 7 | 7 |
| Pen/Strep | 7 | 7 | 7 | 7 | 7 | 7 | 7 | 7 | 7 |
| 100 µM Se | | 7 | 35 | | | | | | |
| 1 mM Se | | | | 7 | 35 | 70 | | | |
| 10 mM Se | | | | | | | 17.5 | 35 | 70 |
| MEM | 616 | 609 | 581 | 609 | 581 | 546 | 598.5 | 581 | 546 |
| Total (µL) | 700 | 700 | 700 | 700 | 700 | 700 | 700 | 700 | 700 |

**Table 16**, Formula to make up Se media with their corresponding Se concentrations for MDA-MB-231, MDA-MB-436, and MCF-7 cell lines. Each Se concentration was made up with volume for triplicates (µL). SC stands for solvent control in which cells in a well were exposed to 190 µL of media plus 10 µL of 1xPBS

| | SC | 1 µM A | 5 µM B | 10 µM C | 50 µM D | 100 µM E | 250 µM F | 500 µM G | 1000 µM H |
|---|---|---|---|---|---|---|---|---|---|
| FBS | 35 | 35 | 35 | 35 | 35 | 35 | 35 | 35 | 35 |
| Insulin | 3.5 | 3.5 | 3.5 | 3.5 | 3.5 | 3.5 | 3.5 | 3.5 | 3.5 |
| Pen/Strep | 7 | 7 | 7 | 7 | 7 | 7 | 7 | 7 | 7 |
| Hepes | 7 | 7 | 7 | 7 | 7 | 7 | 7 | 7 | 7 |
| HC | 0.7 | 0.7 | 0.7 | 0.7 | 0.7 | 0.7 | 0.7 | 0.7 | 0.7 |
| 0.1 mM Se | | 7 | 35 | | | | | | |
| 1 mM Se | | | | 7 | 35 | 70 | | | |
| 10 mM Se | | | | | | | 17.5 | 35 | 70 |
| Ham's F12 | 646 | 639. | 611.8 | 639.8 | 611.8 | 576.8 | 629.3 | 611.8 | 576.8 |
| Total (µL) | 700 | 700 | 700 | 700 | 700 | 700 | 700 | 700 | 700 |

**Table 17**, Formula of Se media with their corresponding Se concentrations for Sum149pt cell line. Each Se concentration was made up with volume required for triplicates (µL).

### 2.13.2.2 MTT assay

After the Se incubation, 96-well plates were spun with Heraeus™ Multifuge™ X3R centrifuge at 600 rpm for five minutes at RT to settle the cells. The Se media was then replaced with cell line-specific fresh media and 10 µL of 5 mg/mL of MTT reagent and incubated for 4 hours at 37°C for MTT to reduce into purple formazan crystals. After the MTT reaction, the plates were spun again for 5 minutes, and replaced the MTT media with 100 µL of solubilising solution which was made up of 20% SDS, 50% *N,N*-dimethylformamide, 20mM HCl, and glacial acetic acid to adjust pH to 4.7. Formazan crystals were dissolved with the solubilising solution with shaking

on IKA® MS1 Minishaker plate shaker for 5 minutes and further incubated for one hour. Once all the purple crystals were partitioned into solution, the plates were then measured by Bio-Rad Microplate reader model 680 at 570 nm with background reference at 655 nm. Reading at 655 nm was subtracted from 570 nm.

To analyse the results, the average optical density (OD) of each set of wells per Se concentration was obtained in triplicate. Reading from blank measurement was subtracted from the treated samples to avoid colour interference from the solution. The percentage cell inhibition from the Se treatment was calculated with **Equation 6** below:

$$\%\ \text{inhibition} = 100 - \left[\left(\frac{\text{Corrected sample OD}}{\text{Corrected solvent control OD}}\right) \times 100\right]$$

**Equation 6**, Calculation for MTT assay to calculate the percentage of inhibition of cell under a specific condition. Corrected OD refers to the original OD reading subtracted by reading from blank wells.

SEM from three replicates was calculated as the error bar of data. The inhibitory concentration of Se that kills 50% of a cell population ($IC_{50}$) was obtained graphically with Microsoft Office Excel 2013. To compare the $IC_{50}$ of Se between cell lines, the difference was considered statistically significant only when the two-tailed p-value was <0.05.

### 2.14 Lord-qPCR for DNA damage analysis

Long-run real-time PCR (Lord-qPCR) is a new cost-effective and sensitive method published in 2013 for detecting the level of DNA damage (Lehle et

al., 2013). This method is based on the theory that DNA damage can decrease the amplification efficiency of DNA polymerase to read through templates. To quantify the number of lesions, longer amplicons are required. Assuming damage is evenly distributed throughout a genome, the longer the reading length the more the lesions. Greater lesions require more amplification cycles over the threshold cycle number and enter the exponential phase when compared to the short amplicons the impaired amplification is more significant (**Figure 10**). In the Lord-qPCR, the long amplicon (3-4kb) serves to quantify lesions, and the shorter (40-70 kb) one serves as an internal reference to compare the amplification efficiency. The difference in amplification efficiency between short and long amplicons can be used to calculate the rate of DNA damage. Lord-qPCR appears to be more sensitive than comet assay as it can detect a variety of lesions without being limiting to strand breaks.

Treatment with various concentrations of a DNA-damaging agent, bleomycin, showed that Lord-Q can detect damages created by greater than 10 nM bleomycin whereas comet assay can only detect damage at bleomycin concentrations higher than 500 nM (Lehle et al., 2013). Lord-qPCR can detect up to 0.3 lesions /10 kb. Since this technique is relatively new, only a few researchers have validated its usefulness. A recent study used this method to detect the level of UV and oxidation-induced DNA damage in forensic blood stains (Eurek, 2014). In this study, the author acknowledged the efficient and sensitive nature of Lord-qPCR but also pointed out the downside of this technique which can only assay lesions that can impair the reading of polymerases such as DNA-strand breaks, abasic

sites, and thymer-dimers (Lehle et al., 2013).

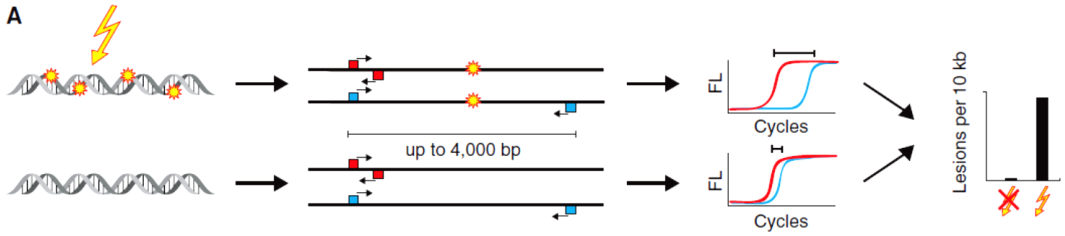


**Figure 10,** Lord-qPCR in quantifying DNA damage. Damage by UV light is indicated by a yellow star on the DNA helix (Left). The DNA fragments with or without damage are amplified using internal reference primers (red) and compared to the amplification rate in longer amplicons (blue primers)**.** The amplification efficiency of long amplicons (blue) is compared to the reference fragments (red) by measuring the cycles required over the detection threshold. The difference in amplification efficiency is used to predict the level of DNA damage (right) (Lehle et al., 2013).

The following method was kindly provided by Evans and Jacobson (2015) with slight modifications for our *in vitro* mammalian cell lines. Lord-qPCR experiments were carried out in MDA-MB-436, MDA-MB-231 and Sum149pt cell lines. Due to time constraints, an experiment on MCF-7 was not performed. DNA was extracted from cancer cells incubated with MSA, selenite, or without Se treatment, with steps specified in section 2.9. The DNA was extracted from the same plate as for the comet assay in **Table 12**. To avoid small volume and pipetting errors, a master mix was prepared with the formula outlined in **Table 18** and stored in -20°C. When setting up the Lord-qPCR, the master mix was thawed on ice and mixed with components listed in **Table 19**. To prove no interference from DNA contamination was present, a negative control was prepared by adding PCR-grade water to

replace the volume of DNA.

| **Component** | **Working concentration** | **Final concentration** | **Volume/ 1 mL** |
|---|---|---|---|
| $MgCl_2$ | 25 mM | 2.5 mM | 100 µL |
| Buffer B1 (Solis BioDyne) | 10X | 1X | 100 µL |
| dNTP | 20 mM | 200 µM | 10 µL |
| Syto® 82 (ThermoFisher) | 5 mM | 2 µM | 0.4 µL |
| mQ $H_2O$ | | | 604.6 µL |

**Table 18**, Formula of Lord-qPCR master mix. Syto® 82 is an orange fluorescent nucleic acid stain that binds to double-stranded DNA to monitor the DNA amplification in real time. B1 buffer is a detergent-free buffer which is commonly used in easily amplified template for comparison to another common PCR buffer, B2.

| **Component** | **Working concentration** | **Final concentration** | **Volume/ PCR tube** |
|---|---|---|---|
| Master Mix | | | 16.3 µL |
| HOT FIRE Pol® DNA Polymerase (Solis BioDyne) | 5 U/µL | 0.05 U/µL | 0.2 µL |
| Forward Primer | 20 µM | 0.5 µM | 0.5 µL |
| Reverse Primer | 20 µM | 0.5 µM | 0.5 µL |
| DNA template | 10 ng/µL | 1.25 ng/µL | 2.5 µL |

**Table 19**, Formula of Lord-qPCR set up. Master mix is the mixture made up in **Table 18**.

The primers used in this experiment target three genes that are listed in **Table 20**. *p53* and *B2M* genes were selected for nuclear DNA damage detection, and mitochondrial DNA damage was tested with a separate set of primers. P53 and mitochondrial-targeting primers were designed previously in the published Lord-qPCR paper (Lehle et al., 2013), whereas the *B2M* targeting primer set is newly designed for this study to further validate results from *p53*-targeting primers. For each gene targeted, there was one set of primers for long fragments (~3 kb) and one set for short fragments (~50 bp). As mentioned above, the short fragment was used as an internal reference, with an assumption that short fragments have little or no damage. In this case, the result for each DNA sample (MSA, selenite, and control) will have two sets of values, one for long fragments and one for short fragments, for analysis.

| Target genes | Primer | Sequence (5'-3') | Size (bp) | Method | Length | Tm (°C) | GC% |
|---|---|---|---|---|---|---|---|
| Cellular tumour antigen *p53* | KO5F | CATAACCGCAAATGGGAAAC | 45 | gDNA | 20 | 55.61 | 45 |
| | KO5R | CGTCCTTTTGATGGCCTTT | | | 19 | 56.1 | 47.37 |
| | KO6F | CATAACCGCAAATGGGAAAC | 3075 | gDNA | 20 | 55.61 | 45 |
| | KO6R | CGGGACGTGAAAGGTTAGAA | | | 20 | 57.56 | 50 |
| Mitochondrial DNA (mtDNA) | KO7F | GGCCACAGCACTTAAACACA | 67 | mtDNA | 20 | 58.97 | 50 |
| | KO7R | TGGTTAGGCTGGTGTTAGGG | | | 20 | 59.01 | 55 |
| | KO8F | ATCGTAGCCTTCTCCACTTC | 3723 | mtDNA | 20 | 56.74 | 50 |
| | KO8R | TGGTTAGGCTGGTGTTAGGG | | | 20 | 59.01 | 55 |
| beta-2-microglobulin (*B2M*) | KO12F | GGGCAAATACCTTGGGTGGA | 3446 | gDNA | 20 | 59.96 | 55 |
| | KO12R | GACGCTTATCGACGCCCTAA | | | 20 | 59.97 | 55 |
| | KO13F | TGGGTCTGCCTGTCATGTTT | 60 | gDNA | 20 | 59.52 | 50 |
| | KO13R | AGTTTGGACTGCATCTGCCT | | | 20 | 59.6 | 50 |

**Table 20**, Lord-qPCR primers used to amplify *H. sapiens* mitochondrial or genomic DNA.

Once all the solutions were added to a qPCR-grade Axygen™ PCR tube on ice, the mixture was briefly mixed by vortex and centrifuged in an Eppendorf centrifuge (5415R) to draw all the liquid together. The real-time PCR was run with Rotor gene® 6000 real-time rotary analyser (Corbett Life Science). A touchdown cycle was set up prior the actual signal-acquiring cycle (**Table 21**) to improve the specificity of primer binding to the desired locus. The final melting step denatures double stranded DNA fragments by raising up the temperature, single peak represents a single product formed in the PCR reaction as all the products melt at a specific temperature. Product specificity of primers can be monitored with the melt curve analysis.

| | **Cycle step** | **Temperature (°C)** | **Time** | **Cycle number** |
|---|---|---|---|---|
| **Cycle 1 (Touchdown)** | Initial denaturation | 95 | 15 min | 1 |
| | Denaturation | 95 | 10 sec | 10 |
| | Annealing | 65 (-0.5°C/cycle) | 10 sec | |
| | Elongation | 72 | 4 min | |
| **Cycle 2 (Signal acquiring )** | Denaturation | 95 | 15 sec | 45 |
| | Annealing | 60 | 15 sec | |
| | Elongation | 72 | 4 min | |
| | Final melt | 65-95 | | 1 |

**Table 21**, Cycling conditions for Lord-qPCR

To analyse the results of Lord-qPCR, values of the threshold cycle crossing point (*Cp*) and amplification efficiency (E) were extracted from each sample

for calculation with Microsoft Office Excel 2013. For each replica, there were three DNA treatments with selenite, MSA, or no Se addition (control). Each treatment had two set of values, for long fragments and short fragments as a reference. The efficiency of each sample was used to adjust the *Cp* with the formula in **Equation 7**.

$$\text{Adjusted Cp} = \frac{Efficiency}{2} \times \text{Cp}$$

**Equation 7,** Equation for adjusting *Cp* value with amplification efficiency. E = 2 is the perfect reaction in qPCR which indicates 100% efficiency. The sample E number divided by 2 converts the value to percentage efficiency, which was used to adjust the *Cp* value (Evans & Jacobson, 2015).

Further, to normalise the lesions from treated samples with control samples, delta difference between control and treated was calculated by subtracting control *Cp* (adjusted) from corresponding treated *Cp* (adjusted). The formula is outlined in **Equation 8**.

$$\Delta\text{Cp} = \text{Treated Cp} - \text{Control Cp}$$

**Equation 8,** Delta *Cp* for normalising lesion in treated sample. The *Cp* value in the calculation was the adjusted number from previous formula.

After delta *Cp* value for long and short amplicons was acquired for each Se treatment, the lesion rate can be calculated with the formula in **Equation 9**. This formula was adapted from Rothfuss et al. (2010) where they calculate the lesion rate by subtracting the delta *Cp* in short amplicons from long amplicons. This formula, as discussed above, uses short fragments as a

reference to quantify DNA damage in treated samples. Lesion rate per 10kb DNA of selenite- or MSA-treated samples can then be predicted.

$$\text{Lesion rate (lesion per 10kb DNA)} = (1 - 2^{(\Delta Cp_{long} - \Delta Cp_{short})} \times \frac{10000\ (bp)}{Size\ of\ long\ fragment\ (bp)})$$

**Equation 9**, Equation to calculate lesion rate based on the delta *Cp* value (Rothfuss et al., 2010).

Two technical replicates and three biological replicates were performed for selenite and MSA treatment in each cell line. The calculated lesions for each treatment sample were summarised in a column chart with Microsoft Office Excel 2013. Error bars were calculated as SEM from three biological replicates. The difference between cell lines was analysed with a one-tailed *t*-test and was considered significant with p-value < 0.05.

## 2.15 Primer validation

Primers targeting *p53* and mitochondria were extracted from published research Lehle et al. (2013). To validate the location that the primers target are *p53* and mitochondria, the two set of primers were used in end point PCR on MDA-MB-436 DNA followed by amplified fragment sequencing. The PCR reactions were set up with as described in **Table 22**. Conditions for PCR reaction are outlined in **Table 23** and the reaction was carried out with MJ RESEARCH PTC-200 DNA Engine. The PCR product was loaded onto a 1% agarose gel with 1 x TAE buffer followed by electrophoresis with 90 volts for 30 minutes. The gel was then visualised under UV light to confirm success in PCR reaction based on the band size. The size of the band was

expected to be 3075 bp and 3723 bp for *p53* and mitochondrial DNA, respectively. Once the presence of the desired amplicons was confirmed, the rest of the PCR product was purified with the DNA clean and concentrator$^{TM}$kit (Cat No: D4013) as specified by Zymo Research. The purified PCR product was then sent to Waikato DNA Sequencing Facility, Hamilton, New Zealand. The sequenced result acquired was compared against information on Human Genome Browser (https://genome.ucsc.edu/) to confirm the amplified loci.

| **Component** | **Working concentration** | **Final concentration** | **Volume/ PCR tube** |
|---|---|---|---|
| 2x PCR master mix iTaq$^{TM}$ (iNtRON Biotechnology) | 2x | 1x | 10 µL |
| Forward Primer | 10 µM | 0.5 µM | 1 µL |
| Reverse Primer | 10 µM | 0.5 µM | 1 µL |
| DNA template | 10 ng/µL | 1.25 ng/µL | 2.5 µL |
| mQ $H_2O$ | | | 5.5 µL |
| **Total volume** | | | 20 µL |

**Table 22,** PCR composition for validating primers used in Lord-qPCR.

| | Cycle step | Temperature (°C) | Time | Cycle number |
|---|---|---|---|---|
| Cycle 1 (Touchdown) | Initial denaturation | 94 | 5 min | 1 |
| | Denaturation | 94 | 15 Sec | 10 |
| | Annealing | 65 (-0.5°C/cycle) | 15 Sec | |
| | Elongation | 72 | 4 min | |
| Cycle 2 | Denaturation | 94 | 15 Sec | 35 |
| | Annealing | 60 | 15 Sec | |
| | Elongation | 72 | 4 min | |
| | Final elongation | 72 | 10 min | 1 |

**Table 23,** Cycling condition of PCR for Lord-qPCR primer validation.

## 2.16 Confirmation of mRNA expression using LORD-qPCR primers

To demonstrate that a specific p53 mRNA transcript was indeed expressed, RNA from the *in vitro* cancer cell lines was extracted, reverse-transcribed into cDNA, amplified with the LORD-qPCR primers and then sequenced.

### 2.16.1 RNA extraction from cultured cells

*In vitro* breast cancer cells from a 90% confluent T25 flask (~5x$10^6$ cells) were used for RNA extraction. To lyse the cells, 1 mL of TRIzol® reagent from Life Technologies was added to the flask and pipetted up and down several times. Instructions were followed as stated by the manufacturer. Briefly, the homogenised sample was incubated at RT for 5 minutes to allow complete dissociation of nucleoprotein complex. Two hundred microliters of chloroform was added to the lysate to separate RNA from DNA and protein. The sample was mixed for 15 seconds by inversion and further incubated for 3 minutes at RT. The sample was then centrifuged at 12000 x *g* for 15

minutes at 4°C to separate the phases. The top aqueous layer with RNA was transferred to a new tube. Ten microliters of RNase-free glycogen and 0.5 mL of 100% of isopropanol were added sequentially to the sample and further incubated for 10 minutes to precipitate RNA out of the aqueous solution. The sample was then centrifuged at 12000 x *g* for 10 minutes at 4°C to pellet the RNA precipitant. The supernatant was removed followed by addition of 1 mL of 70% ethanol and a 5-second vortex to wash the RNA pellet. The sample was centrifuged at 7500 x *g* for 5 minutes at 4°C followed by removal of the supernatant. The RNA pellet was dried for 5 minutes at RT and resuspended in 20 µL of RNase-free water. The concentration was measured using Thermo Scientific Nanodrop™ 2000c spectrophotometer. Pure RNA was expected to have 260/280 ratio of 2.0 in comparison to 1.8 for DNA. The RNA sample was stored at -80°C until required for further experiments.

### 2.16.2 cDNA construction

Prior beginning of cDNA construction, the extracted RNA was treated with DNA-Free RNA Kit™ from Zymo Research to eliminate any potential DNA contamination that was carried over from RNA extraction. The procedure was followed as specified by the manufacturer. After eliminating potential DNA contamination, the presence of reverse transcriptase inhibitor could further interfere with a PCR reaction. RNA Clean & Concentrator™-5 from Zymo research was used here as a column purification method to purify RNA and eliminate reverse transcriptase inhibitor. Once the ultra-pure RNA was obtained, Tetro cDNA synthesis kit from Bioline was used to reverse transcribe the RNA as specified by the manufacturer. The formula of the

reaction mix is specified in **Table 24**.

All the solutions were mixed by vortex and centrifuged briefly before use, then gently pipetted several times to mix after being combined in an RNase-free PCR tube. A negative control was also prepared with the same formulation as below (**Table 24**) except reverse transcriptase was replaced with DEPC-treated water. The negative control allows for detection of any genomic DNA contamination. To begin the reverse transcription, samples were incubated at 25°C for 10 minutes followed by 45°C for 30 minutes, and the reaction terminated by 85°C incubation for 5 minutes. All steps were carried out with BioRad PTC-100® Thermal Cycler. The final cDNA sample and the negative control was stored at -20°C for further use.

| **Component** | **Volume (µL)** |
|---|---|
| Total RNA (up to 5 µg) | *n** |
| Random hexamer primer | 1 |
| 10 mM dNTP mix | 1 |
| 5x RT buffer | 4 |
| 10 U/µL Ribosafe RNase Inhibitor | 1 |
| 200 U/µL Tetro Reverse Transcriptase | 1 |
| DEPC-treated water | Add up final volume to 20 µL |

**Table 24**, Formula of reverse transcription reaction. **n* volume depends on the concentration of RNA from nanodrop that provides 3-5 µg of RNA. Random hexamer is a mixture of single-stranded hexanucleotides that has the potential to anneal and amplify many random points of DNA.

### 2.16.3 Amplification of the *p53* gene

To prove the presence of p53 transcript, primer set KO9F and KO9R (**Table 9**) were used to amplify breast cancer cDNA. The PCR was set up the same as in **Table 10** with the cycling condition listed in **Table 25**. The PCR product was then loaded onto a 2% agarose gel along with a 100 bp ladder. The gel was then run with 1 x TAE buffer for 30 minutes at 90 V. The size of the band on the gel was expected to be 155 bp for cDNA and 247 bp for genomic DNA contamination. Thus, observation of a 155 bp band can confirm transcription of *p53* in the cultured breast cell lines.

| **Cycle step** | **Temperature (°C)** | **Time** | **Cycle number** |
|---|---|---|---|
| Initial denaturation | 95 | 15 min | 1 |
| Denaturation | 95 | 20 sec | 34 |
| Annealing | 58 | 20 sec | |
| Elongation | 72 | 40 sec | |
| Final elongation | 72 | 12 min | 1 |

**Table 25**, PCR cycling condition for confirming expression of p53 mRNA transcript in cancer cell lines

### 2.17 Combined treatment of cisplatin and Se

Cisplatin, as mentioned previously, is a common chemotherapy drug for treating a variety of cancers. Since Se was reported to have synergistic effects in killing cancer cells when combined with cancer treatment, here we combined Se with cisplatin to determine the interaction *in vitro.* Cisplatin Ebewe® was acquired from Waikato Hospital with a stock concentration of 1 mg/mL. We decided to use 8.33 μM of cisplatin in this experiment which

is the pharmacological plasma concentration achieved in patients (Clavel et al., 1994; Johnsson et al., 1997; Johnsson et al., 1996; Lobb, 2011). The MTT assay was again used here for testing the toxicity towards cells. Due to time limitations, MDA-MB-436 was the only cell line used in this experiment.

Similar to the Se MTT assay above, cancer cells from a confluent T25 flask were trypsinised and counted as specified in sections 2.4, 2.5, and 2.6. Cells were diluted down to $1.5x10^5$ cells/mL with warm complete media and 200 µL of the cell solution was aliquoted into each well except the blank controls in a 96 well plate with layout organised as in **Table 26**. Cells were allowed to adhere in a 37°C and 5% $CO_2$ incubator for 24 hours. After the time, the master mix was made up as in **Table 27**.

| | | | | | | | | | | | |
|---|---|---|---|---|---|---|---|---|---|---|---|
| PBS | → | | | | | | | | | → | |
| BL | PSC | GC | DC | 2 µM- | 2 µM+ | 10 µM- | 10 µM+ | DC | GC | PSC | BL |
| BL | PSC | GC | DC | 2 µM- | 2 µM+ | 10 µM- | 10 µM+ | DC | GC | PSC | BL |
| SSC | SSC | PSSC | PSSC | 2 µM- | 2 µM+ | 10 µM- | 10 µM+ | PSSC | PSSC | SSC | SSC |
| | | | | | | | | | | | |
| | | | | | | | | | | | |
| | | | | | | | | | | | |
| PBS | → | | | | | | | | | → | |

**Table 26**, Layout of 96 well plate for combined treatment between Se and cisplatin.

2 $\mu M^-$= 2 µM of Se without cisplatin; 2 $\mu M^+$= 2 µM Se with cisplatin; 10 $\mu M^-$=10 µM of Se without cisplatin; 10 $\mu M^+$= 10 µM Se with cisplatin; BL= Blank (media+PBS); PSC= PBS Solvent control (cell + media + PBS); SSC= saline solvent control; PSSC= PBS and Saline combination solvent control; GC= Growth control (Cells + media); DC= cisplatin drug control

The old media in the plate was replaced by 200 µL of 2- and 10- mixture above to its corresponding wells and 195 µL to DC, 2+ and 10+ wells as specified in **Table 26**. The cancer cells were then incubated with Se alone for six hours followed by addition of 5 µL of 100 µg/mL of cisplatin to individual wells of DC, 2 µM+, and 10 µM+ and further incubation for 24 hours. After completing the drug/Se incubation, the MTT assay was carried out as in section 2.13.2.2. Similar to **Equation 6**, the corrected OD was then divided by its corresponding solvent control; Se and cisplatin combined, Se only, and cisplatin only wells were divided by the OD reading of PSSC, PSC, and SSC solvent control wells respectively to calculate the percentage inhibition. The final values were analysed with a bar graph in Microsoft Office Excel 2013. Error bar on the graph was calculated as SEM; the difference between values was considered significant if the p-value was $<0.05$.

| | DC | 2- | 2+ | 10- | 10+ |
|---|---|---|---|---|---|
| FBS | 90 | 70 | 70 | 70 | 70 |
| Insulin | 9 | 7 | 7 | 7 | 7 |
| Pen/Strep | 9 | 7 | 7 | 7 | 7 |
| 100 μM Se | | 14 | 14 | 70 | 70 |
| Stock | 769.5 | 602 | 584.5 | 546 | 528.5 |
| Total (μL) | 877.5 | 700 | 682.5 | 700 | 682.5 |

**Table 27**, Composition of combined drug mixture for MTT assay in triplicates (DC has four wells therefore all the ingredient were four times). DC (drug control): 8.33 μM cisplatin only; 2-: 2 μM of Se only; 2+: 2 μM of Se and 8.33 μM of cisplatin; 10-: 10 μM of Se only; 10+: 10 μM of Se and 8.33 μM of cisplatin. BL and PSC were filled with 190 μL of media and 10 μL of PBS; SSC was 190 μL of media and 10 μL of saline; PSSC was 190 μL of media and 5 μL of saline and 5 μL of PBS; GC was 200 μL of complete media.

# Chapter 3:

# Experimental Results

## 3.1 Mammalian Cell Culture

Four breast cancer cells lines were revived from -80°C and their morphology were inspected to confirm epithelial cell structure (**Figure 6**).

## 3.2 Growth assay

A growth assay measures the amount of cells that adhere to a 24 well plate after 24, 48, and 72 hours of incubation; the initial input is 1.5 x $10^6$ cells. The present study is a continuation of research from 2014 (Mayall et al., 2014b), growth assay of cell line Sum149pt was completed last year with similar growth rate as MDA-MB-436. **Figure 11** shows that MDA-MB-231 is the fastest growing cell line followed by MDA-MB-436 and Sum149pt, and eventually MCF-7. To ensure enough cells for the assays, MDA-MB-436, MDA-MB-231 and Sum149pt were allowed 24 hours to adhere; MCF-7 was incubated for 72 hours prior to beginning of the assay.

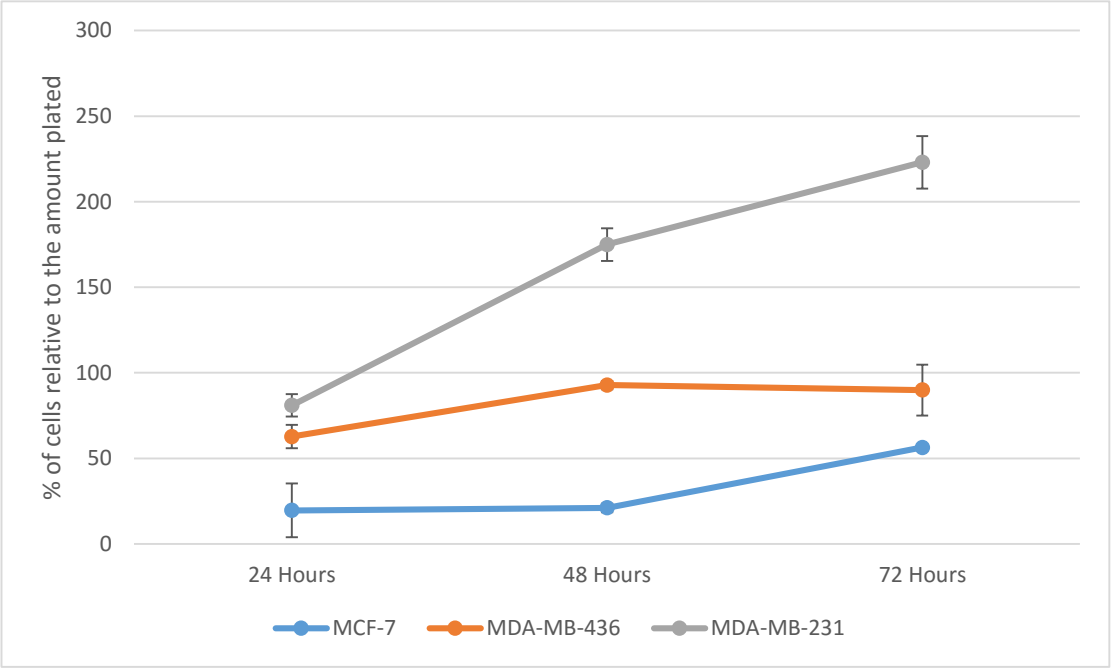


**Figure 11**, Percentage of cells per plate (%) from MDA-MB-436, MDA-MB-231, and MCF-7 cell lines. Error bars were calculated with SEM. *n*=3

### 3.3 Mycoplasma contamination PCR test

The presence of mycoplasma contamination from the cultured cell was tested by PCR, and the size of the amplified products was visualised with agarose gel after electrophoresis. The presence of mycoplasma DNA was expected to show a 510 bp band, and the internal control was expected to present a 986 bp band, respectively. **Figure 12** shows the gel electrophoresis result for PCR analysis of the MDA-MB-436 and MCF-7 cells. **Figure 13** contains results for MDA-MB-231 and Sum149pt. In both figures, a clear band at 980 bp in the samples with the inclusion of the internal control is observed. The positive control shows a positive band at 510 bp and no band in the negative control. Small faint bands with size around 1,500 bp were also noticed; this may be the result of over-amplification and can be improved by reducing the cycle numbers in PCR. The faint band can also be due to non-specific annealing from primers;

increasing annealing temperature can minimise the band. The results present an evidence of the cell lines used being mycoplasma contamination-free.

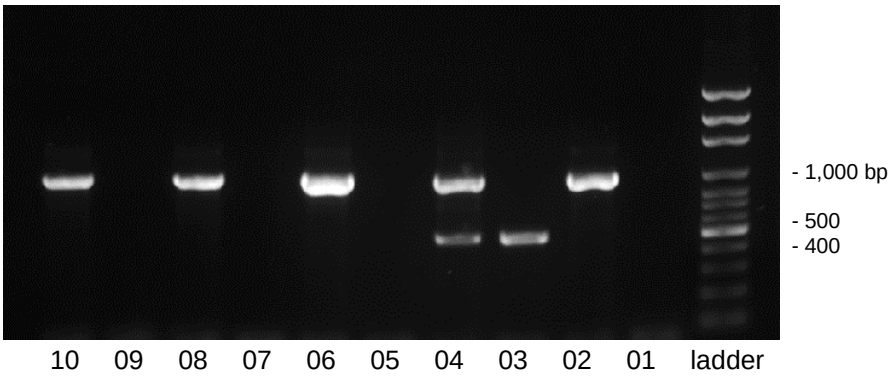


**Figure 12**, Mycoplasma test of cell lines MDA-MB-436 and MCF-7. Ten PCR samples were loaded onto a 1% agarose gel containing Ethidium Bromide and electrophoresed at 90 V for 30 min. Ladder: 100 bp DNA ladder from Solis BioDyne. 01, negative control; 02, negative control plus internal control; 03, positive control; 04, positive control plus internal control; 05, test MCF-7 DNA; 06, test MCF-7 plus internal control; 07, test MDA-MB-436 DNA; 08, test MDA-MB-436 plus internal control; 09, control MCF-7 DNA; 10, control MCF-7 DNA plus internal control.

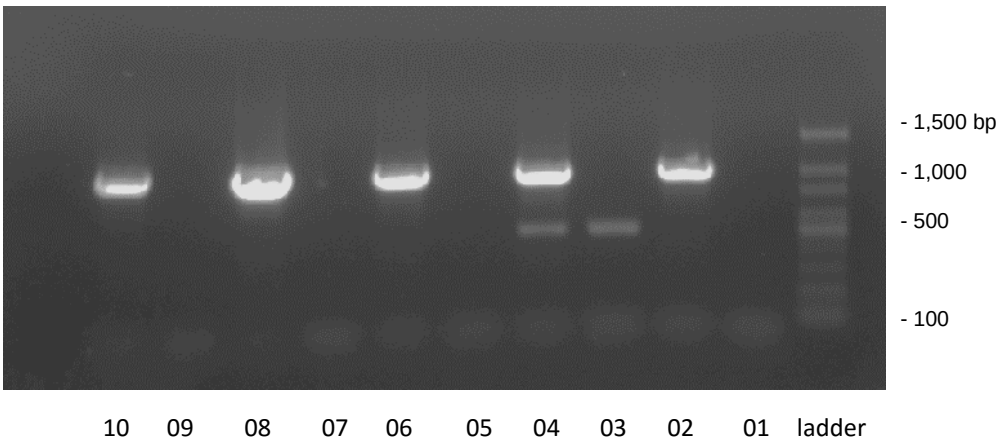


**Figure 13,** Mycoplasma PCR test of cell line MDA-MB-231 and Sum149pt. 01. PCR products were electrophoresed for 30 minutes at 90 V on a 1% 1 X TAE, agarose gel stained with Ethidium Bromide and compared to the 100 bp molecular ladder from GenScript. 01, negative control; 02, negative control plus internal control; 03, positive control; 04, positive control plus internal control; 05, test MDA-MB-231 DNA; 06, test MDA-MB-231 DNA plus internal control; 07, test Sum149pt DNA; 08, test Sum149pt plus internal control; 09, control MCF-7 DNA; 10, control MCF-7 DNA plus internal control. The faint bands at the bottom of each lane are the result of primer dimerisation where primers bind to each other and present as double-stranded nucleotides.

## 3.4 Validation of the reported mutations in the cell lines

To confirm the cell lines were the ones we expected, DNA was extracted from cells and amplified using primers that were designed to target the reported cell line mutations. **Figure 14** and **Figure 15** are the PCR product of MDA-MB-231 DNA, with primers targeting *BRCA1* mutations shown in **Figure 14** and primers targeting mutations on *p53, KRAS,* and *BRAF* gene in **Figure 15**. MDA-MB-231 DNA was amplified into the expected PCR product based on the size confirmed on the agarose gel. In **Figure 14**, lane two and lane three show a faint band below the expected amplicons, this suggests the non-specific targeting of KM4 primers; the outcome can be

improved by increasing the annealing temperature in PCR cycles. This product requires gel purification to proceed to sequencing because of the off-target product from PCR. In other results with a single sharp band, the PCR products were purified with column purification method (see Chapter 2) to remove excessive PCR reactants such as primers, buffer, and Taq enzyme to avoid interference with DNA sequencing. The ultra-pure DNA can then be sequenced.

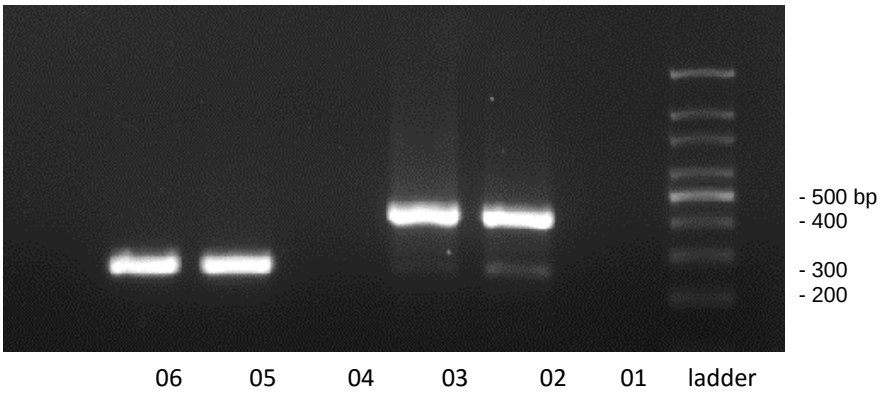


**Figure 14**, PCR amplification of DNA from MDA-MB-231 for *BRCA1* mutations. DNA extracted from MDA-MB-231 was amplified with corresponding primers. The size of amplicons was confirmed by electrophoresis on 1% TAE agarose gel with Ethidium Bromide staining. Products were electrophoresed at 90 V for 30 minutes and the size of bands was compared against 100 bp ladder from GenScript; the scale of the ladder is listed on the right-hand side of the photo. **01-03)** Amplified products from KM4 primer set targets expected *BRCA1* mutation on MDA-MB-436; the expected product size is 400 bp. **01)** Negative control with KM4 primers. **02)** Positive control of KM4 primers with previously validated MDA-MB-436 DNA. **03)** KM4 primers with MDA-MB-231 DNA. **04-06)** Products from KM2 primers which target expected *BRCA1* mutation on Sum149pt; the expected product size is 250 bp. **04)** Negative control of KM2 primers. **05)** Positive control of KM2 with previously validated MDA-MB-436 DNA. **06)** MDA-MB-231 DNA with KM2 primers.

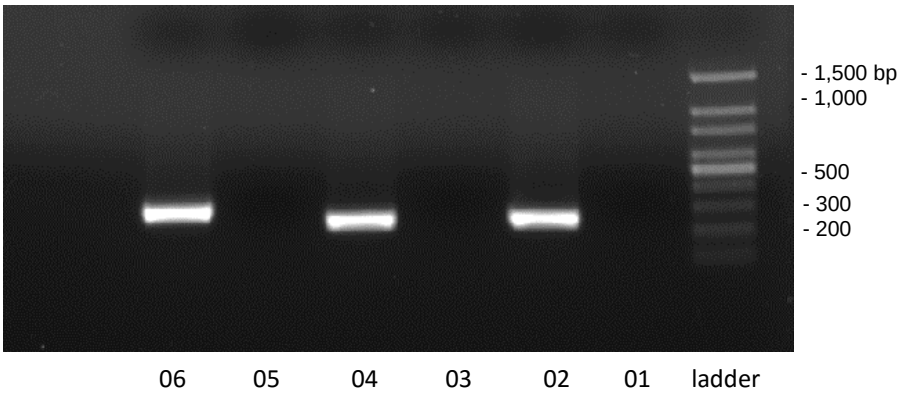


**Figure 15,** PCR amplification of DNA from MDA-MB-231 for *p53, KRAS,* and *BRAF* mutations. DNA extracted from MDA-MB-231 was amplified with corresponding primers. Amplicons were electrophoresed on 1% TAE agarose gel with Ethidium Bromide staining at 90 V for 30 minutes, and the size of bands was compared against 100 bp ladder from GenScript; the size of the ladder is listed on the right-hand side of the photo. **01), 03)**, and **05)** Negative control with Ko9, Ko10, and Ko11 primers, respectively. **02)** Ko9 primers with MDA-MB-231 DNA. Ko9 primers target *p53* mutation on MDA-MB-231; the expected band size is 247 bp. **04)** Ko10 primers with MDA-MB-231 DNA. Ko10 primers target *KRAS* mutation on MDA-MB-231; the expected band size is 251 bp. **06)** Ko11 primers with MDA-MB-231 DNA. Ko11 primers target *BRAF* mutation on MDA-MB-231; the expected band size is 300 bp.

*BRCA1* mutations on Sum149pt and MDA-MB-436 were validated (**Figure 16** and **Figure 17**) with a comparison to the other three cell lines that should not have the same mutation in the locations. As the present study is continued from previous year study, MDA-MB-231 is the only new cell line begin this year. The quality of sequenced PCR products was more than 70% of the high-quality sequence, which confirmed the quality of sequencing. To prove the cell line is MDA-MB-231, the expected genes with

mutations were sequenced and compared to the genomic sequence from the NCBI database.

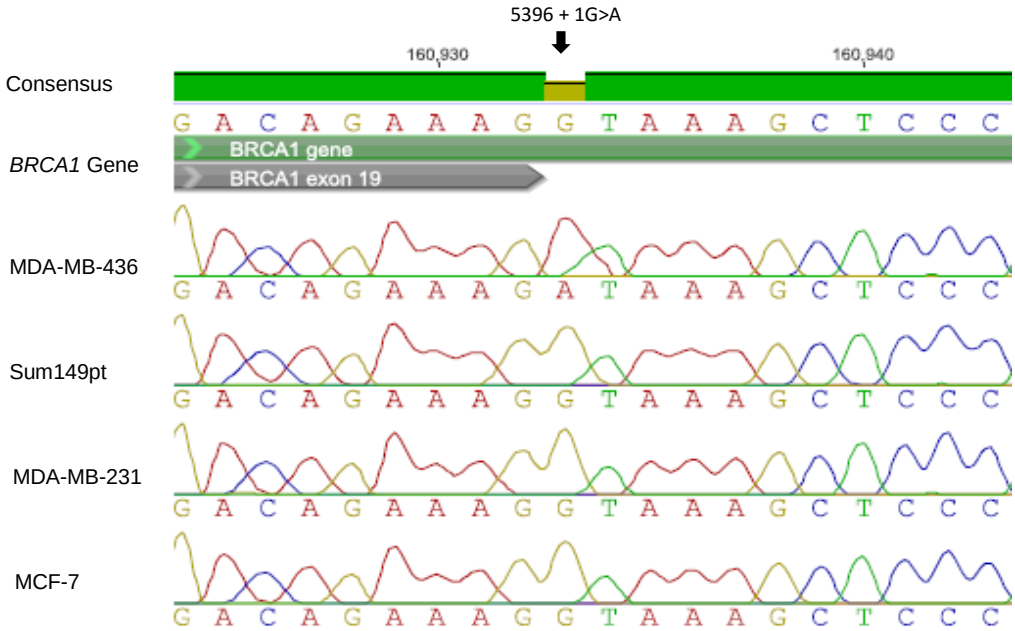


**Figure 16,** Genomic DNA sequence comparison of four human breast cancer cell lines at position 160,933 in the *BRCA1* gene. The electropherogram of each sequenced cell line is shown. The nucleotide was sequenced with KM4F and KM5R. The reference gene is acquired from NCBI database with Genbank accession number: NG_005905.2. The A mutation is depicted in the MDA-MB-436 cell line (5396+1 G>A position on cDNA; 160,933 bp on gDNA).

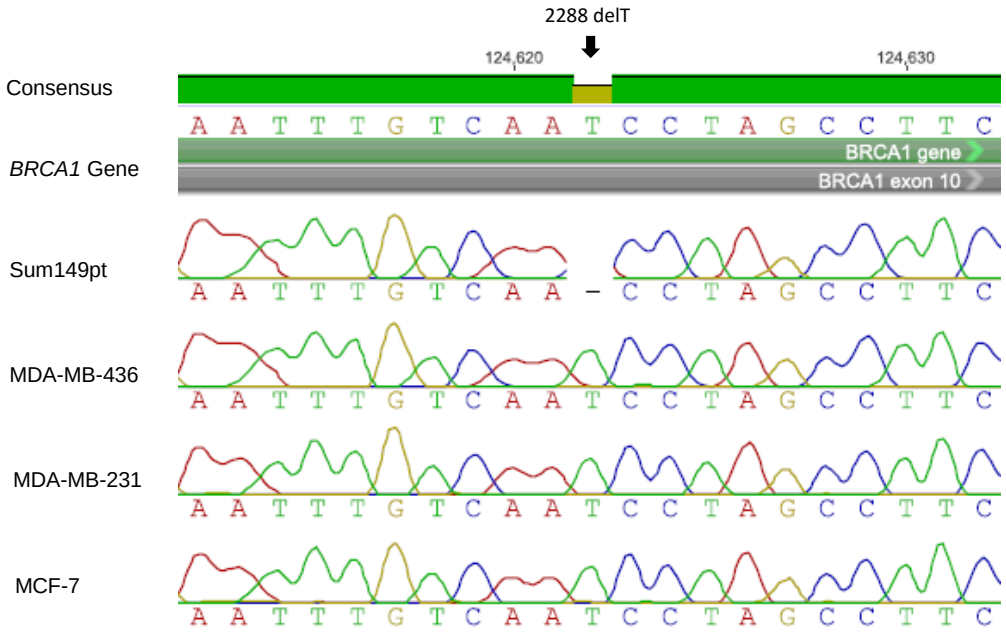


**Figure 17,** Genomic DNA sequence comparison of four cell lines for the expected mutation in Sum149pt at cDNA 2288 position with T deletion on *BRCA1* gene; the position is equivalent to gDNA at 124,622 bp. Nucleotide was sequenced with KM2 primer set. Reference gene is acquired from NCBI database with Genbank accession number: NG_005905.2.

**Figure 18** presents the outcomes of three genes sequenced with expected mutations. *P53* and *KRAS* mutations were validated in the expected position and base substitution. The mutation c1391G>T in *BRAF* gene which is expected at 148,148 bp of genomic sequence was not seen. However from the chromatogram, there are overlapping peaks of G and T at the 148,148 position which suggests the possibility of having heterozygous genes to present an equal reading of G and T nucleotide.

By checking the absence or presence of expected mutations, the identity of each cell line can be confirmed. This allows us to use the confirmed cell

lines to examine the effect of Se via the comet assay and MTT assay.

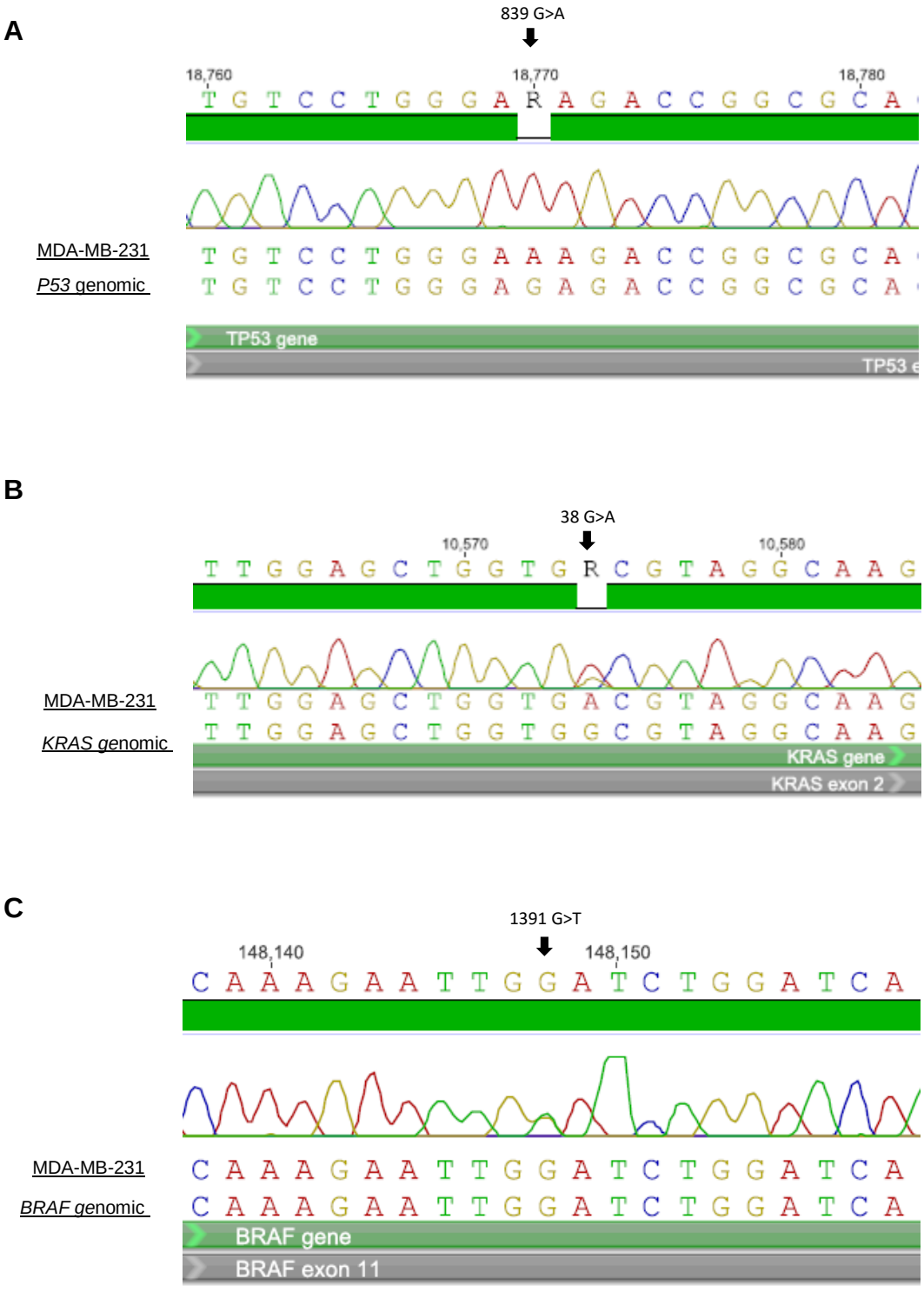


**Figure 18,** Presence of expected mutations on the MDA-MB-231 cell line. **A,** proof of the presence of the expected *p53* mutation at c.839G>A (gDNA at 18,770 position). The nucleotide was sequenced with Ko9 primers. Reference gene was acquired from NCBI

database with Genbank accession number: NG_017013.2. **B,** proof of *KRAS* mutation at c.38G>A (gDNA at 10,574 position). The nucleotide was sequenced with Ko10 primers. Reference gene was acquired from NCBI database with Genbank accession number: NG_007524. **C,** absence *BRAF* mutation at c.1391G>T (gDNA at 148,148 position). The nucleotide was sequenced with Ko11 primers. Reference gene was acquired from NCBI database with Genbank accession number: NG_007873.

### 3.5 Comet assay

The comet assay measures the level of DNA damage based on the intensity and length of the “comet” tail. An example of comets visualised under the fluorescence microscope is shown in **Figure 19** from MDA-MB-436 cells treated with either 2 µM selenite or MSA for 24 hrs. Highly damaged cells present high intensity of comet tails (**Figure 19C**). Based on the pictures below, cells incubated with selenite (**Figure 19C**) show much greater tail intensity compared to the control samples (**Figure 19A**); a slight comet tail was observed in cells treated with MSA (**Figure 19B**).

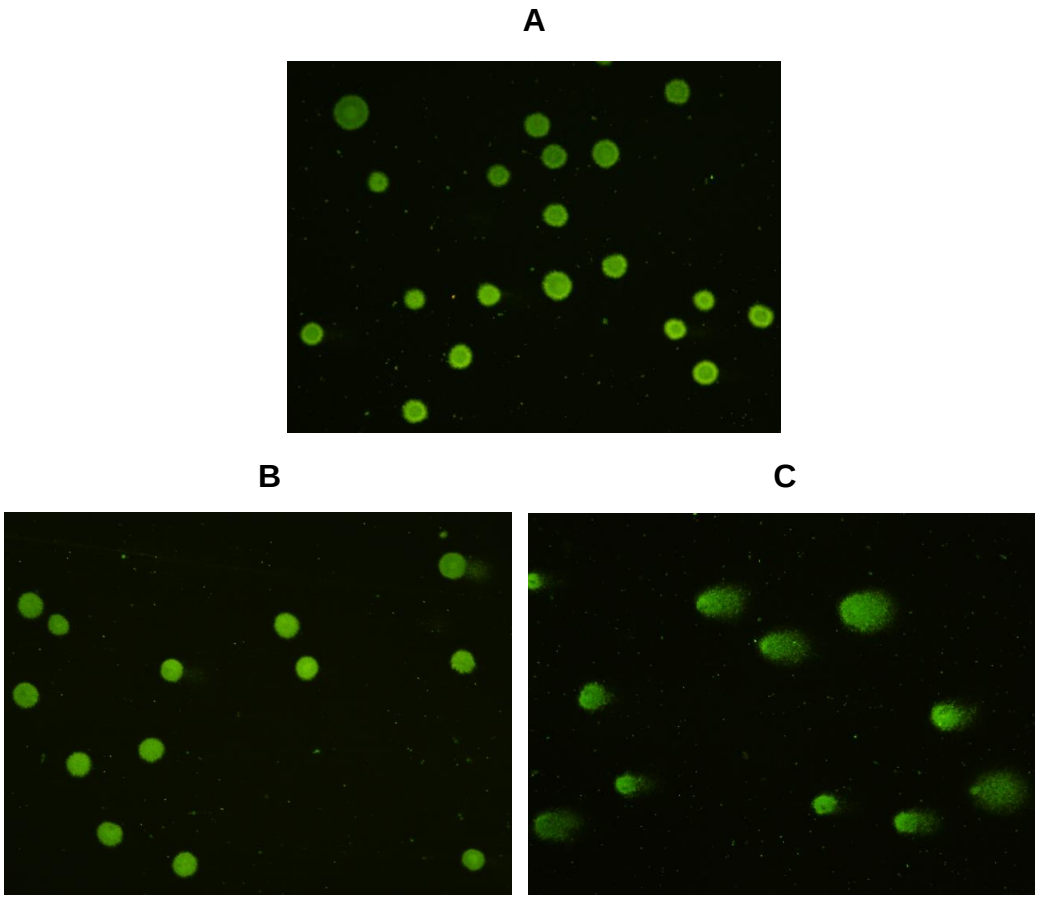


**Figure 19,** Representative images of comets captured under the 10X Fluorescent Axiostar plus transmitted light microscope. Images were produced after SYBR® Gold staining on *BRCA1*-mutated MDA-MB-436 cells that were incubated without Se (A), with 2 µM MSA (B), or 2 µM selenite (C).

The captured comet pictures were analysed with CometScore software which measures the length and the intensity of comet tail and calculates the percentage of DNA in the tail sector. Results of comet assays from four cell lines incubated with selenite and MSA are presented in **Figure 20**. The graphs compare the percentage DNA in tail and tail moment (which accounts for the percentage of DNA in the tail with a length of the comet tail). Fifty comets were captured from each comet slide, two slides were prepared for each sample as technical replicas, therefore 100 comets were analysed for each sample.

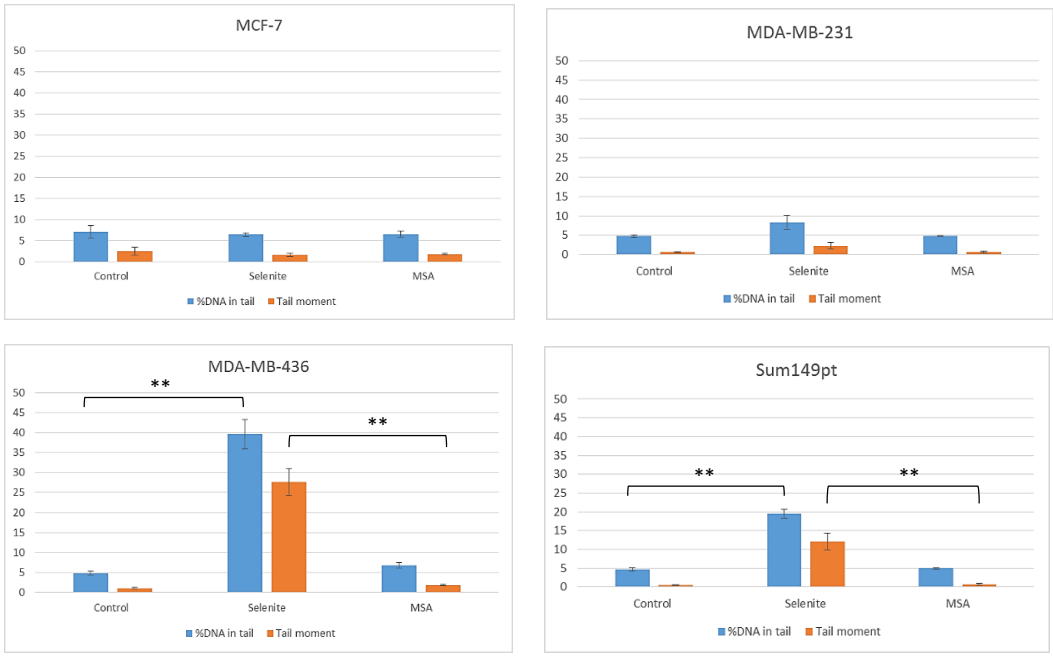


**Figure 20,** Comet assay of all four breast cancer cell lines to examine the level of DNA damage after 24 hours incubation with 2 µM selenite or MSA. The two graphs on top are the results from non-*BRCA1* mutated breast cancer cell lines (MCF-7 and MDA-MB-231). The two bottom graphs are from *BRCA1*-mutated breast cancer cell lines (MDA-MB-436 and Sum149pt). The results were obtained from three technical replicates and three biological replicates. *n*=3, **p < 0.01.

Significantly higher levels of DNA damage (P <0.01) were shown in MDA-MB-436 and Sum149pt cell lines with selenite treatment; these two cell lines are *BRCA1*-mutated. In contrast, MCF-7 and MDA-MB-231 cells, which are non-*BRCA1* mutated cell lines, have a similarly low level of DNA damage when treated with selenite, MSA, and control media.

## 3.6 Lord-qPCR

The purpose of this experiment was to validate the usefulness of Lord-qPCR by comparing the resulting data with the previous conventional comet assay.

### 3.6.1 Preparation of DNA template

DNA tested with Lord-qPCR was extracted from corresponding cell lines after 24 hours incubation with 2 µM of MSA or selenite. The cells were incubated alongside cells for the comet assay to minimise experimental variation. The quality of DNA extracted was confirmed based on the 260/280 and 260/230 ratio from the NanoDrop$^{TM}$ spectrophotometer. DNA can proceed to Lord-qPCR with a 260/280 ratio between 1.8–2.0, and 260/230 value between 2.0–2.2.

### 3.6.2 Primer validation using standard PCR and DNA sequencing

Prior setting up a Lord-qPCR, published primers for the *p53* (3,075 bp) and mitochondrial gene (3,723 bp) (Lehle et al., 2013) were validated by standard PCR followed by sequencing of the amplified fragment, and bioinformatic analysis against the Human Genome Browser (Kent WJ, 2002). **Figure 21** shows that the amplified product of MDA-MB-436 DNA with primers that target *p53* and mitochondrial DNA. Smearing PCR products on the gel suggests an excessive DNA template; this can be improved by decreasing DNA input. A faint band in lane 3 suggests off-targeting of the primer set. This result can be improved by increasing annealing temperature in the PCR cycle. The amplicons then underwent gel purification to remove off-targeting amplicons and excessive PCR reagents. The ultra-pure amplified products were then sequenced.

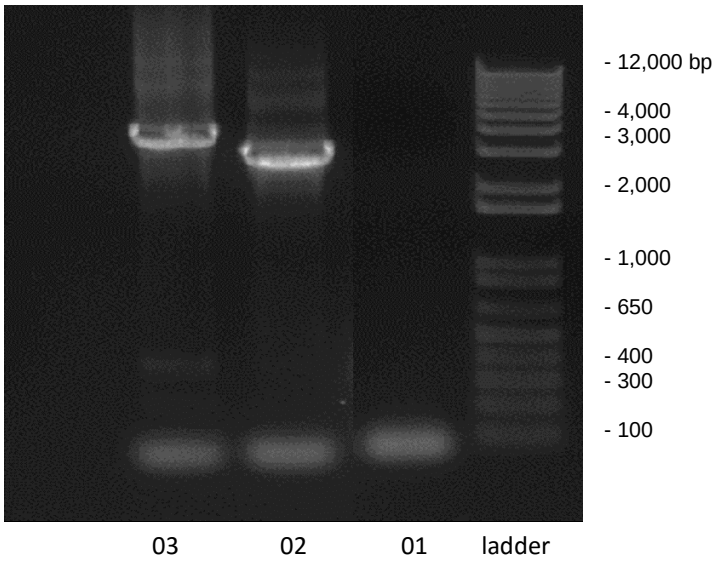


**Figure 21**, Gel electrophoresis of PCR product from MDA-MB-436 DNA with Lord-qPCR primers. DNA extracted from MDA-MB-436 was amplified with corresponding primers. Amplicons were electrophoresed on 1% TAE agarose gel with Ethidium Bromide staining at 90 V for 30 minutes, and the size of bands was compared against 1 kb plus ladder from Invitrogen; the size of the ladder is listed on the right-hand side of the photo. **01)** negative control of Ko6 primers. **02)** MDA-MB-436 DNA amplified with Ko6 primers which targets *p53* gene; the size of the product is 3075 bp. **03)** MDA-MB-436 DNA amplified with Ko8 primers which targets mitochondrial DNA; the size of the product is 3,723 bp.

The sequencing result was then compared against the Human Genome Browser to confirm the genomic loci targeted by the primers. **Figure 22** and **Figure 23** show the locations that the primers target to. In the genomic loci we focused on, there are fifteen isoforms of *p53* and five isoforms of *WRAP53*. The sample amplified fragment (**Figure 22**) overlaps with nine isoforms at the end of the *p53* gene with 99.8% pairwise identity. The sequence range also covered two isoforms (out of five) of another gene, *WRAP53;* this gene is a natural *p53* anti-sense which codes for a transcript that can regulate expression of p53 post-transcriptionally.

Interestingly, an epigenetic tag (H3K27Ac) is denoted in this area. According to the ENCODE result, the information of epigenetic tag was acquired from seven human cell lines; one (K562), is a malignant leukaemia cell line; the other six are normal non-malignant human epithelial cells. None of the breast cancer cell lines used in the present study was covered by the seven cell lines. **Figure 23** presents the evidence of mitochondrial primers targeting mitochondrial DNA. The amplified fragment is matching the coding region on mitochondria. The bioinformatics analysis demonstrates that the two published primer sets target their specified location in the nuclear and mitochondrial genome.

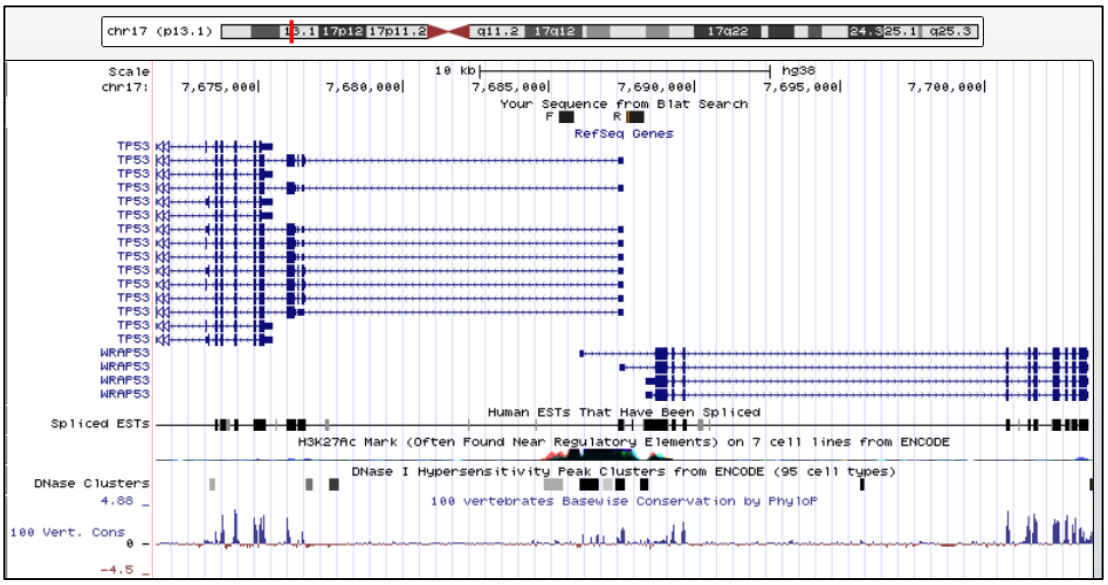


**Figure 22,** Bioinformatics analysis of Lord-qPCR primers which expect to target *p53* gene. Genomic DNA from MDA-MB-436 was amplified with Ko6 primer set. The sequencing result is therefore presented as a section at beginning and end of the amplicons by forward and reverse primer, respectively. The amplified fragment was then sequenced and compared against human genome browser to confirm the genomic loci that the primers target. Top: ideogram of human chromosome 17 and the red vertical bar indicates the position on 17p13.2. Underneath, the scale and genomic position relative to our sequence input. Below the sequence input, fifteen isoforms of *p53* and 4 isoforms of *WRAP53.* Our sequence covers nine isoforms of *p53* and two isoforms of *WRAP53.* The solid blue square on the p53 transcript is exon 1 of the *p53* gene.


**Figure 23**, Bioinformatics analysis of Lord-qPCR primers targeting mitochondrial DNA. Mitochondrial DNA from MDA-MB-436 was amplified with Ko8 primer set. The amplified fragment was then sequenced and compared against human genome browser to confirm the loci that the primers target. Top: ideogram of mitochondrial DNA and complete coverage of red line on the grey bar indicates the full coverage of mitochondria. Underneath: scale and genomic position relative to sample sequence. Top right-hand side: sequenced fragment. Beneath the sample sequence: a column for human mRNA which indicates the coding region. From the graph, our sample sequence matches with the coding region on mitochondria.

### 3.6.3 Lord-qPCR

Lord-qPCR estimates the level of DNA damage based on amplification efficiency of qPCR. The target specificity can be examined through melt curve analysis from the qPCR reaction. This is the last step of qPCR where a gradual increase of temperature denatures double-stranded amplified fragments; massive reduction of fluorescent signal at one temperature indicates a single size product was amplified without significant off-target from primers. After internal analysis within qPCR software, it presents as a single sharp peak. **Figure 24** presents an example of a melt curve from MDA-MB-436 DNA with Ko8 mitochondrial primer. The single sharp peak

from all DNA samples indicates successful amplification of the desired fragment.

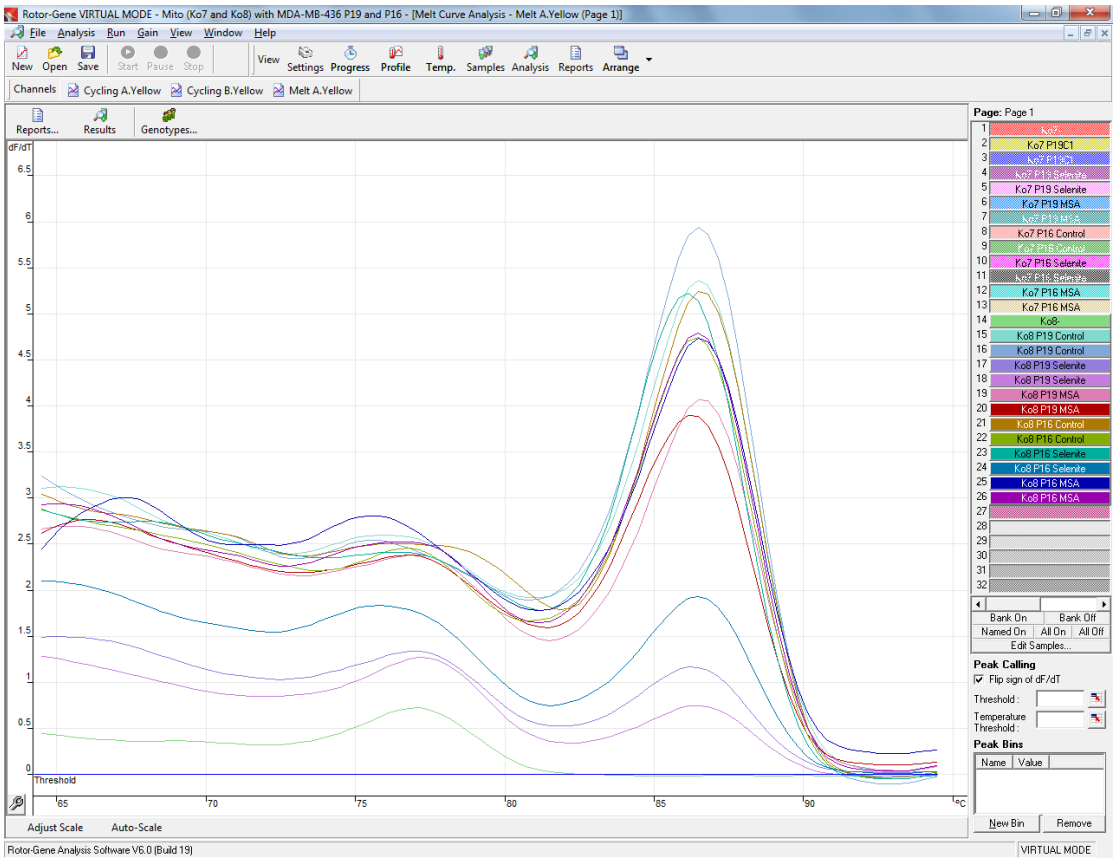


**Figure 24**, Melt curve from Lord-qPCR reaction of MDA-MB-436 with Ko8 mitochondrial primer. A melt curve was acquired at the end of every qPCR run to examine the primer specificity. Single sharp peaks at 86°C indicate only one product was amplified with Ko8 primers. Melting point at high temperature suggests the single amplicon has a larger sequence that requires a higher temperature to denature.

By analysing the amplification efficiency from the qPCR reaction, the value can be converted into quantitative lesions on DNA. **Figure 25** and **Figure 26** compare the number of lesions per 10 kb between MDA-MB-436, MDA-MB-231, and Sum149pt DNA after treatment with 2 µM selenite or MSA. Due to time constraints, MCF-7 was not included in this experiment.

**Figure 25** compares the level of mitochondrial DNA damage. With selenite treatment, the *BRCA1*-mutated MDA-MB-436 and Sum149pt cell lines appeared to have higher damage than MDA-MB-231 but this was not significant (p= 0.26); the same trend was not observed with MSA treatment. Greater DNA damage by inorganic than organic Se in *BRCA1*-mutated cells lines is consistent with our expectations. However, the opposite was seen in the MDA-MB-231 cell line; the phenomenon can be explained by the insensitivity of non-*BRCA1*-mutated cell lines toward Se treatment.

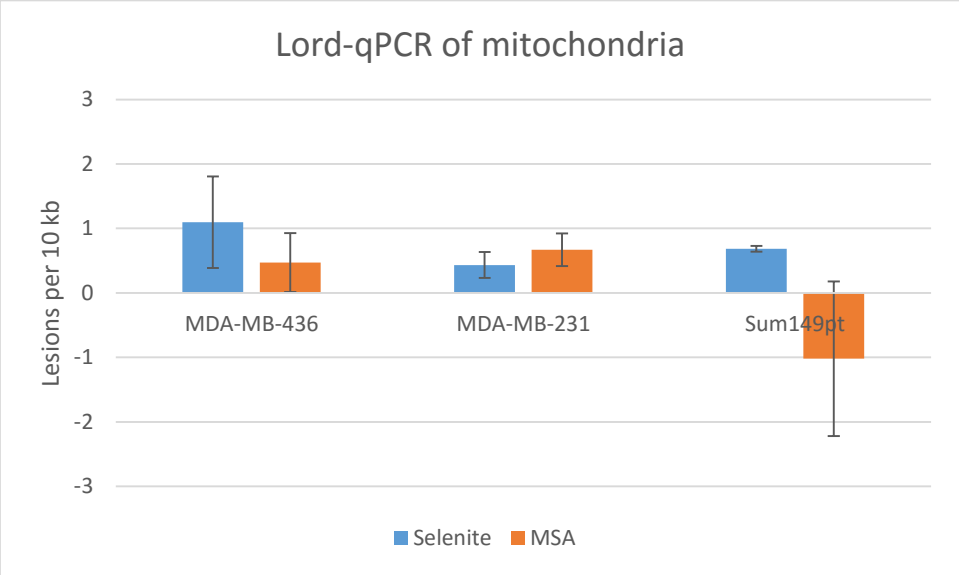


**Figure 25**, Lord-qPCR with mitochondrial primers to assess the level of mitochondrial DNA damage in three breast cancer cell lines upon Se treatment. Comparison of DNA lesions per 10 kb in the three cell lines**.** The quantity of lesion was measured after 24 hours treatment with 2 µM selenite or MSA on a 24-well plate. The data is expressed as mean ± SEM for at least three independent determinations in triplicate for each experimental point (*n*= 3).

**Figure 26** presents a comparison of nuclear DNA damage with primer

targeting the *p53* gene. In the graph, both selenite- and MSA-treated MDA-MB-436 and Sum149pt have higher levels of DNA damage than MDA-MB-231. The differences are not statistically significant ($p > 0.05$) due to highly variable replicates. The overall trends between *BRCA1* and non-*BRCA1* mutated cell lines with Se treatment are in line with the previous comet assay results reported here, where cell lines with *BRCA1* mutations are more sensitive to Se treatment than non-*BRCA1* mutated cell lines.

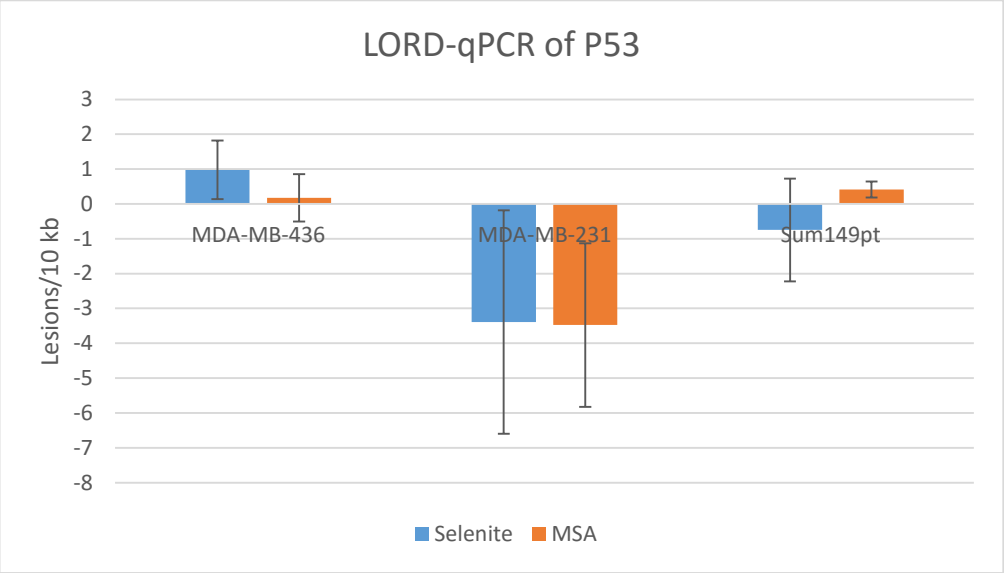


**Figure 26**, Lord-qPCR result with *p53* primers on three breast cancer cell lines. The graph presents the DNA damage after 24 hours incubation with 2 µM of selenite or MSA. The results are expressed as mean ± SEM. The amplification efficiency and threshold cycle number were converted into quantitative lesions with the calculation from (**Equation 9**). Results were obtained from three independent determinations with three replicates in each experiment ($n=3$).

The epigenetic tag raises a question regarding the expression level of *p53.* Low or no expression of a gene can potentially interfere with the effect of a DNA- damaging agent by covering the lesion with histone proteins. This

then leads to the next experiment where we examine the presence of *p53* transcripts in a breast cancer cell line.

### 3.6.4 p53 expression in MDA-MB-436 breast cancer cell line

We next investigated whether the *p53* mRNA transcript was indeed expressed in this breast cancer cell line. Firstly, RNA was extracted from the MDA-MB-436 cell line with a Nanodrop reading of 1130.1 ng/μL, 260/280 ratio 1.84, and 260/230 ratio 1.14. The expected 260/280 ratio for RNA is approximately 2.0 as opposed to 1.8 for DNA; the reading of 1.84 indicates the presence of DNA contamination in the sample. DNase treatment was applied to remove the potential carry-over of DNA contamination from RNA extraction. Moreover, the low 260/230 ratio suggested a large quantity of organic solvent contamination in the DNA solution. The presence of organic solvent can interfere with reverse transcription, therefore the DNase-treated RNA product was then column-purified to remove the organic solvent. The ultra-pure RNA was then reverse-transcribed into cDNA followed by PCR reaction to confirm the presence of the p53 transcript in cells. **Figure 27** shows the integrity of RNA extracted. Intact total RNA run on a denaturing gel will have sharp 28S and 18S rRNA bands (eukaryotic samples). The 28S rRNA band should be approximately twice as intense as the 18S rRNA band. This 2:1 ratio (28S:18S) is a good indication that the RNA is intact. Partially degraded RNA will have a smeared appearance, will lack the sharp rRNA bands, or will not exhibit a 2:1 ratio. Completely degraded RNA will appear as a very low molecular weight smear. By knowing the integrity of RNA, the reverse transcription can then be carried out with the intact RNA as a template.

Secondly, the RNA was reverse transcribed using oligo (DT) primers and then amplified with p53 primers with the expectation of a 155 bp product for cDNA and 247 bp product for gDNA. The primer used here is different from the set for Lord-qPCR; the forward and reverse primer target exon 7 and exon 8 of the *p53* gene, respectively. Therefore, the amplified fragment from genomic DNA is longer than from cDNA due to the inclusion of an intron fragment between exon 7 and 8.

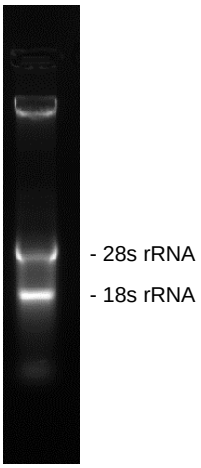


**Figure 27,** Gel electrophoresis of RNA from MDA-MB-436 cell line on 1% non-denaturing agarose gel to show the RNA integrity. The RNA was extracted from the MDA-MB-436 cell line followed by gel electrophoresis at 45 V for 1.5 hours on a 1% TAE agarose gel. Two apparent bright bands represent the 28s and 18s rRNA. This result confirms the integrity of RNA extracted.

**Figure 28** shows the PCR bands of the reverse-transcribed RNA with *p53* primers. In **Figure 28**, no band is seen in cDNA negative control lane which implies no genomic DNA contamination in the RNA sample. Two bands show up in the *p53* sample lane (247 bp and 155 bp) indicate the potential of differential splicing of p53 transcripts in the MDA-MB-436 cell line. The

result presented in **Figure 28** was seen in a repetition of the experiment, i.e. the same bands were seen on the gel, confirming the reproducibility of the result.

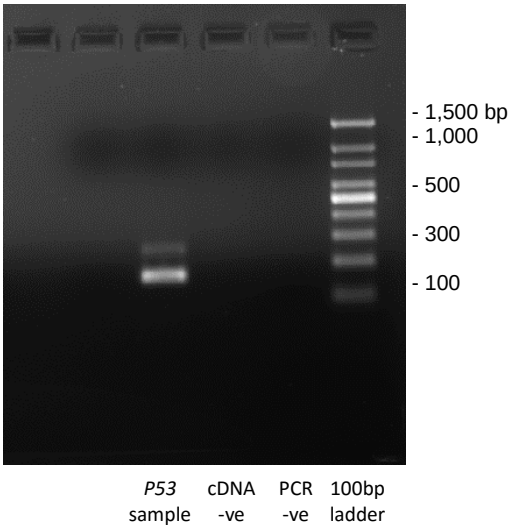


**Figure 28,** PCR amplification of p53 cDNA in MDA-MB-436 cells. cDNA was reverse transcribed from RNA extracted from the MDA-MB-436 cell line followed by PCR amplification with Ko9 primer set. The amplicons were electrophoresed in 1% TAE agarose gel with 90 V for 30 min. The size of bands was compared against 100 bp ladder from GenScript. PCR –ve refers to the negative control of PCR without any cDNA added; cDNA –ve refers to the negative control in reverse transcription without the addition of reverse transcriptase; the *p53* sample is the main sample tested which contains cDNA with *p53* primers. The size of amplified cDNA is expected to be 155bp and 247 bp for genomic DNA contamination or alternative splicing.

Next, the two resulting *p53* PCR bands were gel purified and then sent to the University of Waikato DNA Sequencing Facility to confirm nucleotide identity and alternative splicing of *p53*. **Figure 29** presents the electropherogram of the bottom band from lane three (the sequencing result with Ko9R primer).

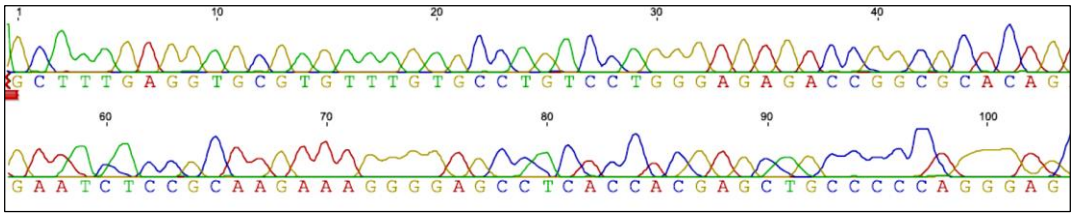


**Figure 29,** Electropherogram of gel purified *p53* PCR product (bottom band; 155 bp) from lane three of **Figure 28**. Sequencing results from Ko9R. The low-quality sequence at the beginning and the end of the fragment were removed. Overall high-quality percentage: 83% (analysed with Geneious Software).

By comparing sample sequences with reference genomic *p53* sequence with Geneious software, **Figure 30** shows the sequence comparison with direct alignment to *p53* genomic sequence. Results show both fragments were amplified from the *p53* gene. For more confidence in the result, the sequences then underwent a BLAST search using NCBI website, and alignment again confirmed that these two sequence match only with the *p53* gene (90% match for top band; 99% for the bottom band).

**A**

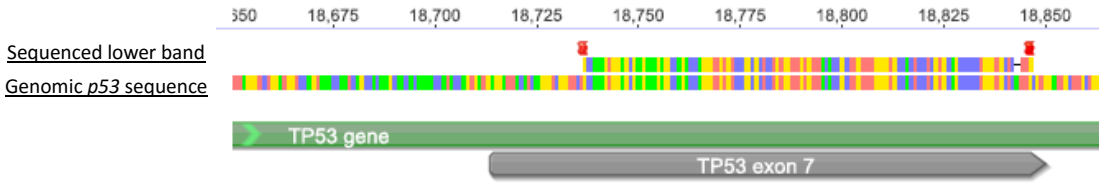


**B**

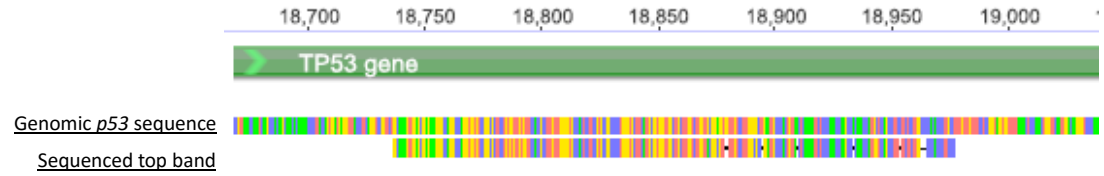


**Figure 30**, Evidence of amplified fragments from **Figure 28** were extracted from the *p53* gene. Sample sequences were compared against genomic *p53* (Genbank accession number: NG_017013.2). Pictures were generated with Geneious software. The scale bar on top indicates nucleotide number on *p53* gene. Coloured vertical bars below *p53* gene (green) represent a combination of different bases; A: red, T: green, C: purple, G: yellow. **A**, alignment of the lower band from lane 3 of **Figure 28** with *p53* gene; the size of quality sequence: 103 bp. Alignment result: 99.1% pairwise identity. **B,** alignment of top band with *p53* gene; the size of quality sequence: 238 bp. Black horizontal bars in between the sample sequence indicate mismatches. Pairwise identity: 90%.

### 3.6.5 Validate result with another primer

To confirm that the results of the Lord-qPCR truly reflect the level of genomic DNA damage rather than being an effect specific to the chosen gene, the same experiment was repeated but with another set of primers that target the housekeeping gene, beta-2-microglobulin (*B2M).* This gene is constantly being transcribed in the nucleus and the chromatin maintained in

an opened conformation which should be prone to DNA damage.

The newly designed *B2M* primers have an expected product size of 3,446 bp; the size was confirmed with end-point PCR. **Figure 31** presents the PCR result with the Ko12 primer set that targets *B2M* gene. From the gel photo, smearing bands suggest over-amplification which can be improved by decreasing the PCR cycle number. Multiple bands seen in some samples suggest the off-targeting of primers, however this phenomenon can be optimised in the qPCR machine by introducing a touchdown step to improve the specificity of primers. Increasing signal-acquiring temperature can restrict the qPCR machine to only receive signals released from larger fragments and leave out signals from small non-specific targeting. However, different sizes of off-target amplicons suggest a possibility of amplification of fragmented DNA. Indeed, BLAST search of the Ko12 primer set does not match with any other gene apart from *B2M*.

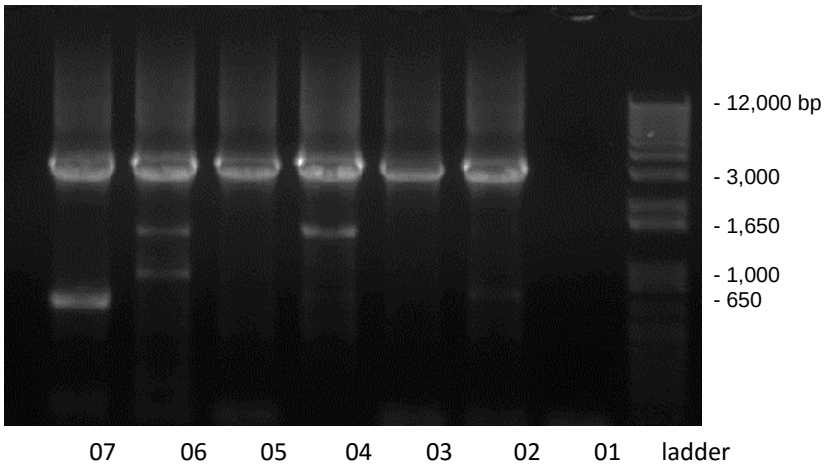


**Figure 31,** End-point PCR of Ko12 primer set on MDA-MB-436 DNA. Ko12 primers target *B2M* housekeeping gene with expected amplicon size of 3446 bp. PCR products were electrophoresed at 90 V for 30 minutes on 1% TAE agarose gel. The size of products was compared against 1 KB plus ladder from Invitrogen. The scale of ladder labelled on the right-hand side of pictures. **01)** negative control of Ko12 primer. **02)** and **03)** replicates of Ko12 primers with non-treated control MDA-MB-436 DNA. **04)** and **05)** replicates of Ko12 primers with selenite-treated MDA-MB-436 DNA. **06)** and **07)** replicates of Ko12 primers with MSA-treated MDA-MB-436 DNA.

The level of genomic DNA damage from *B2M* primer following Lord-qPCR was then compared with the previous result from the *p53* primer set as seen in **Figure 32**. No significant difference was seen between *B2M* and *p53* damage for both selenite (p= 0.27) and MSA treatment (p= 0.46). A slightly higher level of DNA damage was observed in the *B2M* gene than *p53* under selenite treatment, but the variation is statistically insignificant.

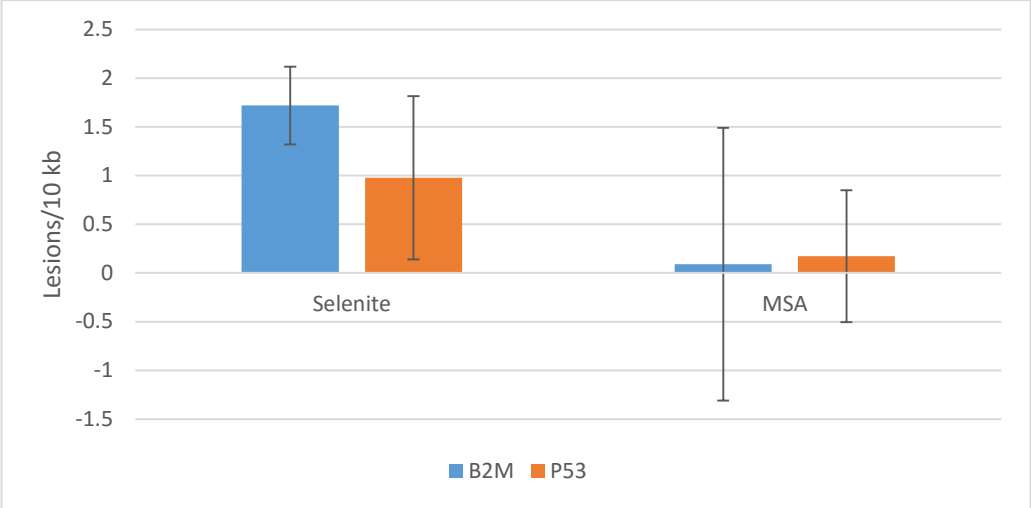


**Figure 32,** Comparison of the level of DNA damage estimated with *B2M* and *p53* primers in Lord-qPCR on MDA-MB-436 cell line. The bar graph is represented as mean ± SEM. *n*=3. P-value between B2M and p53 with selenite treatment is 0.27, for MSA p=0.46.

## 3.7 Se toxicity with MTT assay

### 3.7.1 Formazan test

The concentration of cells used for the MTT assay was determined prior to beginning of the experiment by testing the different concentration of cells with MTT reagent. A formazan test was conducted on the four cancer cell lines used in this study using a cell concentration range of $1x10^4$ to $1x10^6$ cells/mL, respectively (**Figure 33**). Cell viability was determined with Trypan Blue stain. Sum149pt, MDA-MB-231, MDA-MB-436, and MCF-7 cell lines have viability of 85%, 92%, 98%, and 98%, respectively. The reason for this test is to find the optimal concentration of cells to plate out so cells do not become over-confluent, which can interfere with formazan formation. A linear range on the line plot is the optimal concentration that can be detected by MTT assay without hindering from over-confluency. **Figure 33** shows the linear range is below $1.8x10^5$ cells/mL. To acquire a sensitive and reliable

result while obtaining a sufficient volume of cells for the Se cytotoxicity test, a cell concentration of $1.5x10^5$ cells/mL was used for all four breast cancer cell lines for the MTT assay.

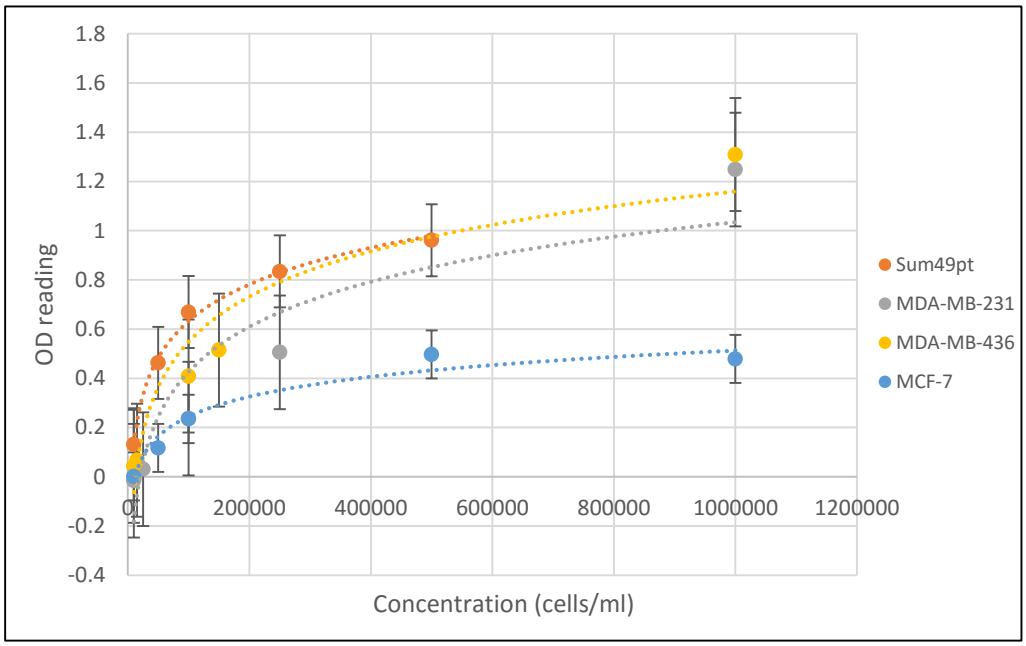


**Figure 33**, Formazan test to determine the optimal concentration to use in MTT experiments. The log graph is OD reading at 570 nm against cell concentration (cells/mL). The OD reading was acquired after 24 hours plating of each cell concentration followed by MTT assay. The data were expressed as mean ± SEM. The results were acquired from triplicate wells (*n*=3).

### 3.7.2 Se cytotoxicity

Breast cancer cells were treated with MSA and selenite independently, with the elemental Se concentration ranging from 0 to 1000 µM. The $IC_{50}$ for each Se compound was deduced graphically (**Figure 34**) as the concentration that killed 50% of the cell population.

Based on the two graphs in **Figure 34**, the $IC_{50}$ values for selenite and MSA are summarised in **Table 28**. The $IC_{50}$ values for MSA are 10–100 times higher than values for selenite in all cell lines, except for the MCF-7 cell line, where the $IC_{50}$ values were the same. This suggests a significantly higher toxicity of selenite than MSA. The two *BRCA1*-mutated cell lines, Sum149pt and MDA-MB-436, are much more sensitive to selenite than MCF-7 and MDA-MB-231. However, the same correlation was not observed with MSA treatment.

| **Breast Cancer Cell Line** | **Selenite (μM)** | **MSA (μM)** |
|---|---|---|
| Sum149pt | 4 | 50 |
| MDA-MB-436 | 5 | 600 |
| MDA-MB-231 | 40 | 800 |
| MCF-7 | 80 | 80 |

**Table 28**, Summary of $IC_{50}$ values deduced from **Figure 34**.

**A**

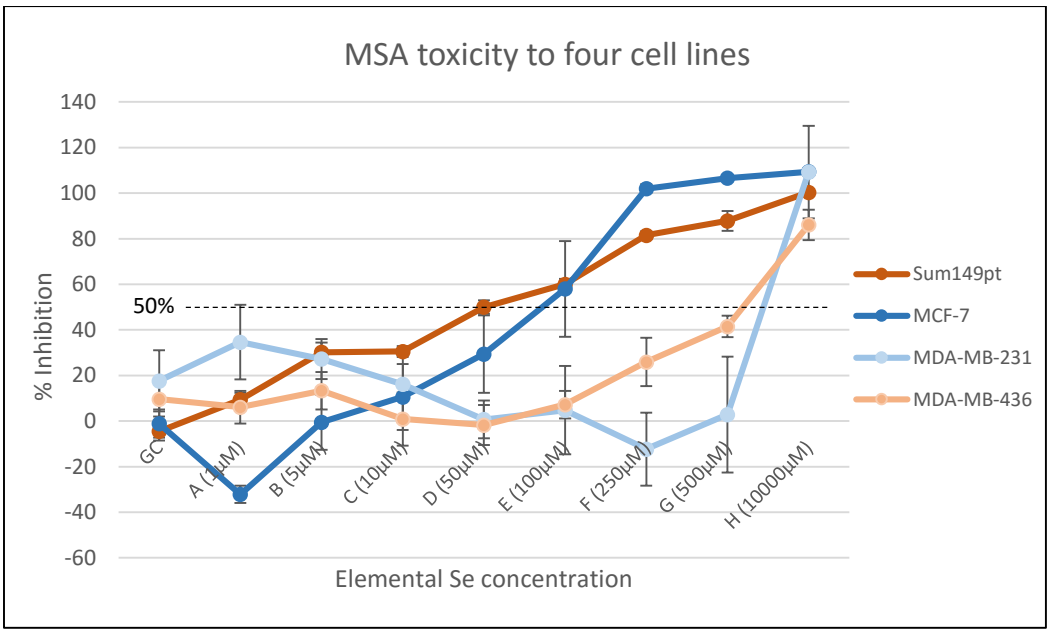


**B**

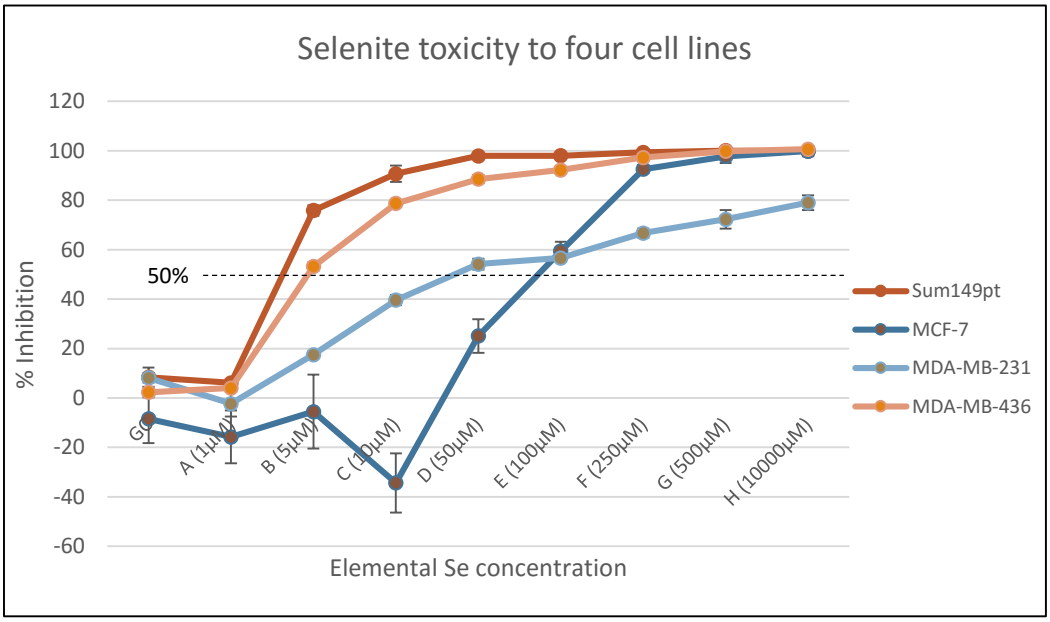


**Figure 34**, MSA and selenite cytotoxicity to four breast cancer cell lines. Line graph of percentage inhibition of cell growth against elemental Se concentration for the cell line**.** Percent inhibition was estimated using an MTT assay followed by 24 hours exposure to a Se compound in a 96-well plate. The data were expressed as mean ± SEM for at least three independent determinations in triplicate for each experimental point (*n*=3).

### 3.8 Cisplatin and Se combined therapy

Based on our MTT and comet assay data, we next investigated the effect of combining Se with chemotherapy on two breast cancer cell lines. Due to time constraints, only one *BRCA1*-mutated and one non-*BRCA1*-mutated cell line were evaluated; MDA-MB-436 and MDA-MB-231, respectively.

MTT experiments were set up with six hours pre-incubation of 2 µM or 10 µM Se as either selenite or MSA, followed by co-incubation with/without 8.33 µM of cisplatin. The 2 and 10 µM Se concentrations were chosen because the lower value is found in the serum of patients who live in high-Se areas such as the mid-west of North America; the latter concentration is considered the transitional Se concentration from protective to the damaging role (El-Bayoumy, 2001). **Figure 35** shows the results of combined treatment on the *BRCA1*-mutated MDA-MB-436 cell line. Both selenite and MSA were more potent in killing these cells at either concentration than cisplatin, and adding cisplatin to either Se compound did not increase the inhibition of cell survival at either 2 µM or 10 µM Se. At 2 µM, MSA had greater cell inhibition compared to selenite, but at 10µM selenite was more potent than MSA towards MDA-MB-436 cells.

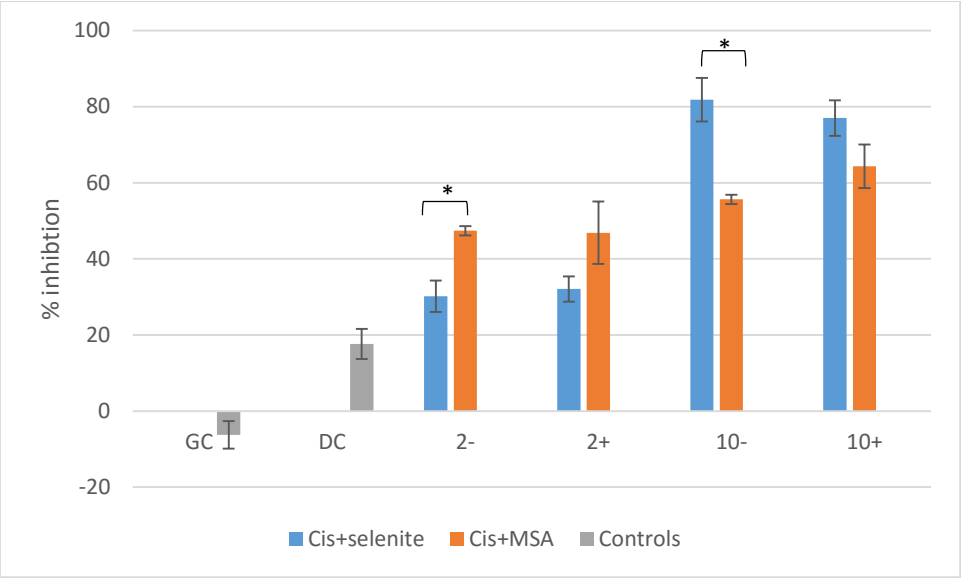


**Figure 35,** Cytotoxicity of 2 µM MSA or selenite with/without 8.33 µM cisplatin on the MDA-MB-436 cell line. MTT assay was used to generate the result. The results were expressed as mean ± SEM. GC= growth control (without Se and cisplatin); DC= drug control (cisplatin only); 2-= 2 µM of elemental Se without cisplatin; 2+= 2 µM of elemental Se with 8.33 µM cisplatin; 10-= 10 µM of elemental Se without cisplatin; 10+= 10 µM of elemental Se with 8.33 µM cisplatin. The results were generated from 3 independent experiments with three replicates (*n*=3). *p-value< 0.05

**Figure 36** shows the results of combined therapy on the non-*BRCA1*-mutated MDA-MB-231 cell line. Similar to the effects seen with MDA-MB-436, combining either Se compound with cisplatin does not have any significant increase in percentage inhibition of cell survival, except for a numerical trend higher with MSA 2 µM and cisplatin (44.2%) compared to MSA alone (29.2%) with a p-value of 0.0282. However, in contrast to the effects on the MDA-MB-436 *BRCA1*-mutated cell line, in this experiment selenite had almost no effect at 2 µM, and was significantly less effective than MSA at all concentrations. In this figure, higher MSA toxicity towards

MDA-MB-231 cell line was noticed compare to the value from **Table 28** for $IC_{50}$ determination.

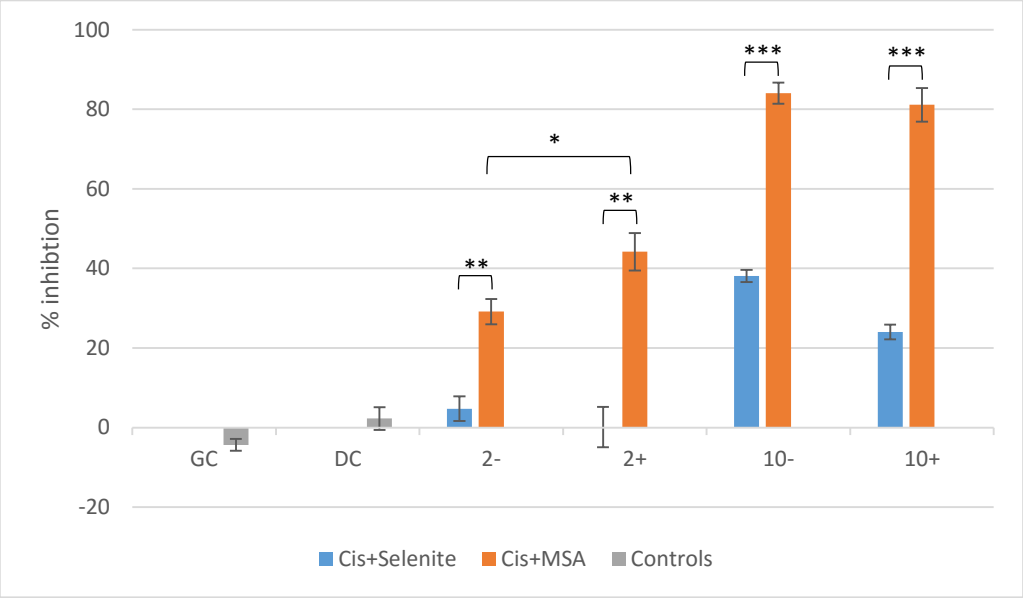


**Figure 36**, Cytotoxicity of 2 µM MSA or selenite with/without cisplatin on MDA-MB-231 cell line. Cytotoxicity was tested with MTT assay. The results were expressed as mean ± SEM. GC= growth control (without Se and cisplatin); DC= drug control (8.33 µM cisplatin only); 2-= 2 µM of elemental Se without cisplatin; 2+= 2 µM of elemental Se with 8.33 µM cisplatin; 10-= 10 µM of elemental Se without cisplatin; 10+= 10µM of elemental Se with 8.33 µM cisplatin. The results were generated with three independent experiment with three replicates (*n*=3). *p< 0.05. **p< 0.01. ***p< 0.001

# Chapter 4:

# Discussion

## 4.1 Validation of Breast Cancer Cell Lines.

The four cell lines used in the present study are two *BRCA1*-mutated, MDA-MB-436 and Sum149pt, and two non-*BRCA1*-mutated MCF-7 and MDA-MB-231 cell lines. The identity of the cell lines was verified from their expected mutations through PCR and DNA sequencing, and also with their epithelial cell morphology which has been inspected under a phase contrast microscope. The current research is a continuation of work from 2014 (Mayall et al., 2014b), mutation validation of the first three cell lines was completed by then. With the MDA-MB-231 cell line, which is the new cell line started this year, the expected mutations on *p53* and *KRAS* have been proven, however, the mutation expected in the *BRAF* gene (c.1391G>T) is absent. The electropherogram showed two equally intensive G and T peaks at this position which suggests the possibility of heterozygous DNA with some alleles carrying the desired mutation. *BRCA1* mutations expected on Sum149pt and MDA-MB-436 cell lines were proven absent on MDA-MB-231 cell line. All four cell lines were proven to be free of mycoplasma contamination via PCR test (**Figure 12** and **Figure 13**).

## 4.2 Differential genotoxicity and cytotoxicity of selenite and MSA towards *in vitro* breast cancer cell lines

Se is an essential trace element for humans which, at low dosage, has

beneficial effects in chemoprotection and cellular oxidative damage repair but high doses can trigger apoptotic pathways, causing cell death or necrosis (Bhabak & Mugesh, 2010; Fischer et al., 2006; Jiang et al., 2002; Seo et al., 2002a). Epidemiological studies suggested that *BRCA1* mutation carriers appear to be more sensitive to relative Se deficiency (Jaworska - Bieniek et al., 2012; Kotsopoulos et al., 2010; Kowalska et al., 2005). However, all the studies that link *BRCA1* mutations and Se to date are focused on DNA repair capacity, not on the potential for differential cytotoxicity of supranutritional doses of Se through killing malignant cells while leaving normal healthy cells unharmed, as exemplified in more recent studies (Cao et al., 2004; Lobb, 2011).

The first aim of this study was to examine the effect of selenite and MSA on commercially-available *BRCA1*- and non-*BRCA1*-mutated cell lines *in vitro*. To the best of our knowledge, this is the first study that links *BRCA1*-mutation and Se with a specific focus on the cytotoxic and genotoxic effect. Se is reported to have both chemoprotective and anti-tumour effects, but the action is dependent on dosage and different chemical forms, with inorganic Se compounds generally considered more genotoxic (Valdiglesias et al., 2010; Wilson et al., 1992). The result of the present study can inform the choice of the chemical form and dose of Se to use in future chemoprotection studies as well as therapeutic trials in women with established *BRCA1*-mutated breast cancer.

The overall results of the comet assay show that selenite is significantly more potent in damaging DNA in *BRCA1*-mutated breast cancer cell lines

than non-*BRCA1*-mutated cells. This is in line with our expectations since it has been demonstrated that selenite is metabolised into $H_2Se$ via a series of reductions, which can generate $O_2^-$ radicals that can react with $H_2O_2$ and undergo Fenton's reaction to damage DNA (Letavayová et al., 2006). Alternatively, the effect of MSA on breast cancer cell lines is significantly less toxic than selenite and appears to have the same level of damage between *BRCA1*-mutated and non-mutated ones. Organic Se such as MSA, enters body mostly as food diet and metabolised into methylselenol which is thought to be the critical metabolite to exert the protective effect on cells (Ip et al., 1991; Ip et al., 2000). This route of Se metabolism that MSA undergoes generates less ROS. Therefore, this is less damaging to cellular DNA (Wilson et al., 1992).

Cells with *BRCA1* mutations are more vulnerable to DNA damage as the machinery for detecting and repairing DNA damage is defective, therefore higher levels of DNA damage are often observed with *BRCA1*-mutated cell lines. It was therefore encouraging to see a report on improving *BRCA1* mutation carriers to the same level as non-carriers with selenite supplementation (Kowalska et al., 2005). Fischer et al. (2006) suggested that Se can increase DNA repair through increasing the association of p53 and BRCA1 proteins, thus activating downstream DNA repair genes. This process occurs via Ref-1 protein, where it acts as a redox regulator for p53 Reduction of p53 can promote its tetramerisation and enhance the DNA-binding ability for triggering downstream repair protein expression. Se is able to activate Ref-1 and therefore promote repair of cells (Fischer et al., 2006). BRCA1 is essential for the protective effect of Se, as complete knock-

out of the *Brca1* gene in mice showed an absence of enhanced DNA repair with Se. This study also showed that Ref-1 and BRCA1 appear to interact with p53 concurrently, and suggest that Ref-1 is a potential regulator for the DNA repair in cells.

Although the DNA-repairing effect of Se was not the focus of the present study, the highly DNA-damaging effect from selenite on *BRCA1*-mutated cells at low dosage (2 μM) conflicts with the findings described by Fischer and Kowalska above. Some of the discrepancies can be explained by the different forms of Se used. Fischer et al. (2006) used 10 μM organic selenomethionine, which is less genotoxic (DNA-damaging) than inorganic selenite, especially at nutritional doses (Valdiglesias et al., 2010). Kowalska used selenite at doses that improved DNA repair capacity while only increasing serum Se to about 90 ng/mL, still well below the recommended optimal range (Rayman, 2012). The likely explanation for why selenite was so genotoxic in our study at 2 μM (~156 ng/mL) when protective in the above-mentioned studies most likely relates to the differential cytotoxicity of Se in malignant compared to normal cells (Cao et al., 2004; Lobb, 2011). The authors above are using Se to look for changes in non-malignant *BRCA1*-mutated cells, whereas this study is using established *BRCA1*-mutated breast cancer cells.

In addition to the level of DNA damage induced, we also examined the cytotoxicity of selenite and MSA. The MTT assay showed that overall the $IC_{50}$ of selenite in *BRCA1*-mutated breast cancer cell lines is ten times lower than in the non-*BRCA1*-mutated cell lines (eg, 4 μM in Sum149pt cell line

and 40 μM in MDA-MB-231, respectively). This result is in agreement with the comet assay data where *BRCA1*-mutated cell lines are much more sensitive to inorganic selenite. However, the same trend was not seen with MSA treatment. In addition, for three of the cell lines tested, the $IC_{50}$ of MSA was ten times higher than for selenite (eg, for Sum149pt, the $IC_{50}$ of selenite is 4 μM and MSA is 50 μM), except with the MCF-7 cell line, where the $IC_{50}$ (80 μM) was identical for both MSA and selenite (**Table 28**).

Many studies to date have shown differential effects of organic and inorganic Se using parallel *in vitro* and *in vivo* models. One study showed a protective effect of MSA on three-week-old female mice inoculated with breast cancer cells, but the same effect was not seen in selenite-treated mice (Chen et al., 2013). In fact, increased metastasis on bone and kidney was observed with selenite as compared to Se-deficient controls. The differential effect of selenite and MSA is mostly due to their metabolic pathways and differences in free radical generation. Smith et al. (2004) discussed the differential pathway that selenite and MSA are involved in within cells. Similar to the above finding, both selenite and MSA have the ability to alter post-translational modifications on p53 via cysteine residues, but the study also found that the two Se compounds can differentially phosphorylate threonine and serine on p53: selenite promotes phosphorylation of p53 on serine 20, 37, and 46 residues, whereas MSA only induces threonine phosphorylation. The three serine residues altered by selenite are known to be responsible for triggering apoptosis by p53. The differential phosphorylation sites on p53 can explain what we see on the cytotoxicity test, that selenite could preferentially activate the apoptotic

branch of p53 and lead to greater cell death.

Two conclusions can be drawn from this part of the study. Firstly, inorganic selenite is significantly more potent in breast cancer cells than MSA. Secondly, *BRCA1*-mutated breast cancer cells are significantly more sensitive to selenite treatment than that non-mutated breast cancer cells studied. The same sensitivity was not observed with organic MSA treatment.

The results of this study can inform future research in two broad directions. Firstly, if Se is used in a chemoprotection trial in the future, then selenite might be best avoided, as it is generally more genotoxic than organic Se compounds. Doses of selenite that achieve serum levels of 2 µM, the lowest examined in this study but often seen in countries with high Se intakes such as the US and Canada, have the potential to increase DNA damage, particularly in individuals who are *BRCA1* mutation carriers. Secondly, however, if the result is viewed from a cancers therapeutics perspective, the sensitivity of *BRCA1*-mutated cancer cells to selenite could potentially augment the effects of chemotherapy and exert target specificity towards tumour cell harbouring *BRCA1* mutations. This potential synergistic effect on cancer treatment leads to the next part of this research where we combined cisplatin chemotherapy with Se.

### 4.3 Combined therapy of cisplatin and Se

In the present study, we chose to use cisplatin to combine with Se and test against three breast cancer cell lines. Cisplatin is a chemotherapy drug which targets fast-proliferating cells by crosslinking the guanine bases on

DNA and interrupting cell division. It is commonly used in various cancer types (Giaccone et al., 2004; Hainsworth et al., 1988; Rose et al., 1999; Silver et al., 2010; Van Cutsem et al., 2006). Two earlier studies have shown *in vitro* and epidemiological evidence that cancer cells with *BRCA1* mutations have a greater response to cisplatin treatment as opposed to wild-type *BRCA1* cells (Bhattacharyya et al., 2000; Silver et al., 2010).

### 4.3.1 No synergism between cisplatin and Se

A few laboratory and clinical studies have combined Se with cisplatin and shown protective effects of Se in reducing toxicities. For example, in 1997 a clinical study supplemented 4000 µg of organic Se in 41 patients with various cancer types treated with 60 to 80 mg/m$^2$ (equivalent to 5 to 6.66 µM) cisplatin, and less nephrotoxicity and bone marrow suppression was observed (Hu et al., 1997). Later, Lobb (2011) examined the cytotoxicity of 2.5 µM and 5 µM MSA with 8.33 µM cisplatin in the THP-1 leukaemia cell line and normal PBMC. The cultured cells were pre-treated for 6 hours with MSA alone followed by co-treatment for 24 hours. They observed increased cytotoxicity of THP-1 cells with combined treatment compare to cisplatin alone, but the same effect was not seen in PBMC. This suggests that MSA along with cisplatin may have target specificity for malignant cells. Furthermore, Zhang et al. (2014) examined the combination effect on two cancer cell lines, MCF-7 and liver hepatocellular cells (HepG2), and one normal kidney cell line, HK-2. The cells were incubated with 10 µM MSA for six hours followed by 24 hours co-incubation with 40 µM cisplatin. Synergistic efficacy was seen in both DNA damage and reducing cell viability in MCF-7 and HepG2 cell lines but the same effect was not seen in

normal HK-2 cells; this again suggests tumour specificity from the combined treatment. Furthermore, the biochemical analysis of HepG2 revealed the down-regulation of anti-apoptotic proteins and up-regulation of pro-apoptotic proteins with combined therapy. Higher levels of p53 phosphorylation and lower phospho-MDM2 (which is responsible for degrading p53) was observed in HepG2 but not HK-2. In conclusion, these three studies provide evidence that organic Se with cisplatin has a synergistic effect on killing tumour cells, but has no effect, or even a protective effect, on normal cells at the doses studied.

In the present study, we did not observe any significant synergy between Se and cisplatin towards the two breast cancer cell lines tested. Here we utilised 8.33 μM of cisplatin, which is considered a therapeutic serum concentration in patients, and 2 and 10 μM of MSA or selenite, with 6 hours pre-incubation of the Se compounds prior to 24 hours co-incubation of Se and cisplatin. In both MDA-MB-231 and MDA-MB-436 cell lines, we saw no significant increase in cell death with combined cisplatin treatment with either Se compound or concentration (**Figure 35** and **Figure 36**).

The differences between the present study and Lobb (2011) include a different way of analysing MTT assay data and also using different cell lines (THP-1 was used, which is an acute monocytic leukaemia cell line). Instead of calculating percentage inhibition with **Equation 6**, they summarised the results directly as the OD reading of each control and treated sample; this may introduce some variation without normalising the reading with solvent control. THP-1 had approximately 20% inhibition of cell survival with

cisplatin-only treatment. In comparison in this study with cisplatin-only treatment, MDA-MB-231 and MDA-MB-436 had approximately 2% and 15% inhibition of cell survival, respectively. The differential result between the present study and Lobb's research may be due to the higher sensitivity of THP-1 cells towards cisplatin which therefore have greater toxicity effect when combined with MSA. Another explanation for us not seeing synergism could be the more sensitive nature of breast cancer cell to Se compare to THP-1 cells. Indeed, the OD reading of Lobb's MTT assay with 2.5 μM MSA on THP-1 cells reduce from 0.65 to 0.52 as extrapolate from the graph; the value is equivalent to 20% of cell inhibition. To compare with our results, MDA-MB-436 and MDA-MB-231 with 2 μM of MSA alone has 47.7% and 29.1% of inhibition rate. This difference suggests that no synergism between cisplatin and Se on breast cancer cell line may be due to higher sensitivity of Se to breast cancer than THP-1 cell line; since the mechanism of inducing synergistic anti-tumour effect between cisplatin and Se is still unclear, high Se sensitivity from breast cancer cells may mask the cytotoxic effect of cisplatin and therefore no synergism between the two compounds.

The discrepancy between this study and Zhang et al. (2014) where synergistic effect between cisplatin and MSA on MCF-7 cells was observed in latter research but not in the present study, can be explained by the different dosage of cisplatin applied. In their study, they incubated the MCF-7 cell line with 40 and 80 μM cisplatin with 5 and 10 μM MSA. The concentration of cisplatin used is 5–10 times higher than in our study. With this higher concentration of cisplatin, the damage is expected to be quantitatively greater, but the cisplatin concentration is not achievable in

clinical use. In the Zhang's paper, 40 μM cisplatin without MSA only reduced cell viability from 100% to 90%. Thus, 8.33 μM cisplatin is likely to have no significant impact on cell survival in their model using the MCF-7 cell line. Indeed, for our non-*BRCA1*-mutated MDA-MB-231 cell line, only 2% inhibition was observed with cisplatin-only treatment. However, in the *BRCA1*-mutated MDA-MB-436 cell line, cisplatin treatment alone created approximately 15% inhibition. This finding is in line with previous research where breast cancer cells with *BRCA1* mutations are more sensitive to cisplatin treatment (Bhattacharyya et al., 2000; Silver et al., 2010). In Zhang's study, 40 μM cisplatin has only slightly higher toxicity than 5 μM MSA in MCF-7 cells, therefore, it is likely that 8.33 μM cisplatin has lower toxicity than 2 μM of MSA in that cell line if we extrapolate the result.

Another interesting result from our study is that both Se treatments, even at 2 μM, appear to have higher cytotoxicity than the therapeutic concentration of cisplatin. MSA was more effective than cisplatin in both the cell lines studied (one *BRCA1*-mutated and one triple-negative, non-*BRCA1*-mutated); selenite showed similar efficacy to MSA in the *BRCA1*-mutated cell line but much lower dose potency in the non-*BRCA1*-mutated cell line.

This finding can lead to future studies evaluating the anti-tumour efficacy of Se with cisplatin and other cytotoxic drugs using *in vivo* mouse xenograft models, which could include *BRCA1*-mutated and triple-negative non-*BRCA1*-mutated tumours. Direct *in vitro* drug incubation can be quite different from drugs administered *in vivo* which undergo hepatic drug metabolism. Different administration routes can also result in different

efficacy. Intravenous administration of cytotoxic drugs is most common, but the optimum administration route for Se compounds in combination with chemotherapy is not yet determined. However the bioavailability of clinically-used Se compounds such a selenite and SeMet is excellent, and clinical trials that have administered Se orally have demonstrated significant benefits in terms of reduced chemotherapy-related toxicity (Hu et al., 1997). It is not known whether administering Se compounds via the subcutaneous (Satoh et al., 1989) or intravenous routes (Siriwardena et al., 2007) will make a difference to the outcomes.

### 4.3.2 Potential chemotherapy drugs with Se

Although the result from cisplatin and Se combined therapy showed no synergy in this study, the effect of Se with other chemotherapy drugs may still show additive effects and some of them have been validated. Li et al. (2009) examined the combination of the organic Se compound methylselenocysteine, and tamoxifen on the MCF-7 cell line with an *in vivo* mouse model. Tamoxifen is a hormonal therapy drug that inhibits tumour growth by blocking the ER and preventing downstream pathways that induce proliferation. Significant tumour growth inhibition was observed in the combined therapy group compared to tamoxifen-only treatment. Immunohistochemistry revealed the significant reduction in ERα and PR protein expression with combined treatment; this is in line with an earlier study where Se was seen to exert its growth inhibition effect via suppressing ER expression (Lee et al., 2005). Later, Park et al. (2015) investigated the *in vitro* effect of Se with docetaxel on breast cancer cell lines. Docetaxel is a chemotherapy drug which targets fast growing cells by binding to cellular

microtubules and preventing depolymerisation. A significant increase in cell apoptosis and growth inhibition in MDA-MB-231 cells was reported with combined treatment than docetaxel alone. However, one drawback of this research is that it did not specify the type of Se used, which makes further interpretation difficult.

A more promising combined therapy study was reported in 2007 whereby the effect of doxorubicin with MSA on MCF-7 cell line was evaluated. Doxorubicin is a chemotherapy drug that inhibits tumour growth via intercalating DNA and forcing the cell to undergo apoptosis. Doxorubicin resistance is a common issue in cancer treatment which requires increased dosage to show an effect; this increases risks of severe side effects. The focus of the study was on restoring sensitivity of the tumour to chemotherapy with assistance from Se. The addition of MSA to doxorubicin significantly increased drug sensitivity and enhanced apoptosis in doxorubicin-resistant MCF-7 cells. Furthermore, they found that cancer cells that were resistant to doxorubicin have increased levels of phosphorylation of Akt kinase which then triggers the downstream cell survival signals and represses pro-apoptotic proteins. Treatment with MSA appears to reverse this effect by reducing the level of phosphorylation on Akt; this result is supported by measuring the level of phosphorylation on GSK3β and FOXO3A which are downstream effectors of activated Akt and are acting as anti-apoptotic proteins when phosphorylated. Therefore, the combined treatment of doxorubicin and MSA can increase drug sensitivity by modulating Akt signalling (Li et al., 2007).

Patients with breast cancer are likely to experience “cocktail treatment” with a combination of chemotherapy drugs. Therefore, even though from this study Se does not synergise with cisplatin, the above-mentioned studies suggest that an addictive anti-cancer effect could be observed by adding Se to other chemotherapy drugs. This hypothesis can be taken further in future research, perhaps most appropriately in murine models where needed before progressing into clinical trials.

### 4.3.3 Unexpected high sensitivity of MDA-MB-231 from MSA

An unexpected finding was the substantial difference in inhibition of survival of MDA-MB-231 cells with MSA in two different experiments, one studying the $IC_{50}$ against all four cell lines studies, and the other evaluating the combination of MSA and selenite with cisplatin. As we observed in **Figure 34** from the earlier Se MTT cytotoxicity assay, MDA-MB-231 is very insensitive to MSA treatment, with an $IC_{50}$ of 800 μM. If we extrapolate data from that MTT assay, the percentage inhibition using either 2 μM or 10 μM MSA is about 20%. In contrast, in the combined therapy experiment, 2 and 10 μM MSA without the addition of cisplatin showed 20% and 80% inhibition respectively. Each data set was formed from three independent experiments, each with triplicate wells for each condition. The possibility of human error such as using incorrect concentrations or type of drug was eliminated because a new dilution of the drug was made between replicate experiments. Technical variables such as incorrect pipetting can also be eliminated from the tight error bars observed in (**Figure 36**).

The discrepancies between the results from the Se cytotoxicity experiment and the combined therapy experiment can be explained by the volatility of MSA. In the earlier MTT assay, we incubated cells with a range of MSA concentrations (0–1000 μM) in a 96-well plate. After 24 hours of MSA incubation, a slight sulfur-like odour was noticed from the incubator. Jüliger et al. (2007) also noticed the “bad smell” after MSA incubation. They trapped and tested the volatile Se metabolites, and detected a massive increase in two Se species, dimethylselenide and dimethyldiselenide. These two Se metabolites are the most biologically-active forms of Se. This observation suggests the potential interference from volatile Se affecting the nearby control wells on the 96-well plates. Indeed, in the earlier MTT assay, lighter formazan colour was observed in the solvent control well which does not have any MSA added. From **Equation 6**, the formula we used to calculate percentage inhibition of cell survival by Se, the OD reading in the solvent control is a reference number for calculation; volatile Se may decrease the reading of control wells which results in a falsely low calculated percentage inhibition. In the Se cytotoxicity assay, the concentration of MSA incubated was very high (up to 1000 μM), which can produce great amounts of volatile Se species that can interfere with solvent controls. In contrast, for the combined therapy assay, we only incubated cells with 2 and 10 μM MSA, so the interference to controls from volatile Se was minimal. In support of this, with similar quantities of initial cell input, the OD reading of the solvent control from the Se cytotoxicity test averaged 0.2, whereas from the combined therapy test the average reading was 0.8. To verify whether volatile Se is affecting results, each concentration of MSA should be incubated separately from any other plates with Se, as volatile Se can affect

other plates in the same incubator. The $IC_{50}$ can then be deduced by compiling the results.

### 4.4 Lord-qPCR vs. comet assay

In this study, we tested the level of DNA damage with Lord-qPCR on two *BRCA1*-mutated and one non-*BRCA1*-mutated breast cancer cell lines after 24 hours incubation with MSA and selenite. To minimise the technical variation, cells intended for analysis in the comet assay and by Lord-qPCR were plated alongside each other with same incubation time and conditions. The results from each assay can, therefore, be directly compared.

For Lord-qPCR, we measured the level of DNA damage on three loci: mitochondria, *p53*, and *B2M* gene. The advantages of Lord-qPCR include the ability to quantify the level of damage as lesions per 10kb, whereas for the comet assay the damage can only be expressed as relative intensity of the comet tail against that from the control sample. Also with the Lord-qPCR method, mitochondrial DNA damage can be measured separately from nuclear DNA damage.

The resulting lesion data from mitochondria appear to be higher than from *p53* which represent nuclear DNA; while these differences were not statistically significant, they raise the possibility that Se may preferentially damage mitochondrial DNA. Support for this comes from a 2010 study investigating the effect of overexpression of a cellular antioxidant enzyme (AE) against selenite-induced ROS. They demonstrated that selenite-induced apoptosis could only be inhibited by overexpression of an AE,

manganese superoxide dismutase (MnSOD), that had a major role in scavenging ROS in mitochondria, while overexpression of other AEs: copper-zinc superoxide dismutase (CuZnSOD), glutathione peroxidase 1(GPxs), and catalase (CAT) that protect from damage in cytosol and lysozymes had no effect (Xiang et al., 2009). The study suggests that selenite-induced superoxide is likely produced inside or on the surface of mitochondria. Furthermore, many studies have suggested that Se induces apoptosis via a mitochondrial-dependent pathway, which again suggests that the ROS generated by selenite is within or close to mitochondria (Jiang et al., 2002; Wang et al., 2008; Zhao et al., 2006). Therefore, the increase in damage in mitochondrial DNA than nuclear DNA from Se in our study is consistent with previous data.

Another support for this comes from the MTT assay which tests cell viability based on mitochondrial enzyme activity, and our results again show greater selenite sensitivity to MSA in three breast cancer cell lines. This again emphasises mitochondrial DNA as potentially the major target for selenite-generated ROS. Furthermore, Lord-qPCR shows greater lesions in the two *BRCA1*-mutated cells lines than the non-mutated one for selenite treatment but these differences were not significant. This trend is observed in both the mitochondrial and *p53* genes. Also, the same trend was detected in MSA-treated *p53* but not mitochondrial DNA. This finding can be explained by the suggestion that selenite generates ROS on the mitochondrial surface, therefore, mitochondrial DNA should be more sensitive to selenite treatment than MSA.

The result from Lord-qPCR is in agreement with the comet assay where *BRCA1*-mutated cells are more sensitive to selenite than non-*BRCA1*-mutated cells. However, greater overall DNA damage in all cell lines with selenite compared to MSA was not seen in the Lord-qPCR results. But, the wide error bars indicate variable replicates which can affect the overall reliability of the Lord-qPCR method. Three reasons could potentially explain the variable replicates. Firstly, different DNA extraction methods used may result in the different quality of DNA extracted. To eliminate this possibility, DNA extracted with conventional phenol-chloroform and a commercial column extraction method were set up in the same qPCR run (data not shown). A difference between the resulting amplified DNA was not detected, suggesting the phenol-chloroform extraction did not lower the quality of DNA in the Lord-qPCR experiment. Secondly, trace amounts of Se carried over from culturing may potentially interfere with the DNA polymerase. However, with repetitive washing steps in the PBS buffer when culturing and the purification procedure in DNA extraction, the chance of having any Se carry-over is minimal. Thirdly, the primer-targeting gene may not be a good representation of nuclear DNA. *p53* gene was chosen in the present study; since it is a tumour suppressor gene, it is likely to harbour mutations that can affect the expression of p53. A BLAT search from the Human Genome Browser also indicates a high quantity of epigenetic tag (H3K27Ac) signatures in the region that the primers target. Although the epigenetic information from ENCODE was extracted from seven cell lines (hESC, GM12878, HSMM, HUVEC, K562, NHEK, NHLF cell lines) that do not include any cell lines from our study, the information still suggests the possibility that this area of the *p53* gene may be hindered with epigenetic

modifications and not prone to damage.

The level of hindering effect from epigenetic tags is hard to determine, but whether *p53* is expressed in the breast cancer cell lines can be examined. When a gene is not expressed, it is tightly wrapped around histone proteins, and DNA in the gene is therefore not prone to radical damage. To eliminate this potential factor as affecting Lord-qPCR, RNA was extracted from one breast cancer cell line followed by cDNA synthesis and PCR to amplify the *p53* gene. *p53* expression was confirmed by sequencing the purified PCR product (155 bp) which indirectly implies the *p53* gene in these cells should be prone to ROS damage with an open conformation. The lesions detected by *B2M* primers are comparable to the ones for *p53,* which strengthened the reliability of the result from *p53* as reflecting nuclear DNA damage.

The most likely explanation for the broad error bars is technical variation. qPCR relies on the versatility and resilience of DNA polymerase and primers to produce reliable and consistent results. It is very sensitive to the quality and quantity of DNA and any inhibitors will reduce amplification. In addition, variation can be introduced during qPCR workflow such as pipetting and poorly-calibrated pipettes.

The lower reproducibility of the Lord-qPCR assay will require future optimisation in primer design and technical improvement. Two differences were noted when comparing the Lord-qPCR method we used to that described in the original paper (Lehle et al., 2013). Firstly, the DNA polymerase we used was HOT FIRE Pol® DNA Polymerase (Solis BioDyne)

as opposed to KAPA2G Fast DNA Polymerase in the original study. Secondly, the fluorescent dye we used is Syto® 82 compared to their use of ResoLight stain. Our reason for changing reagents was to reduce expenditure. The method we used has been optimised to the new polymerase and dye, with proven efficiency from earlier research (Evans & Jacobson, 2015).

On the positive side of Lord-qPCR, it is certainly less labour-intensive than the comet assay. The average time preparing for Lord-qPCR is six hours with mostly long incubations that do not require supervision. Whereas for the comet assay, the total preparation time is ten hours with many complicated reagent preparations and short incubation times with constant labour maintenance.

The Lord-qPCR methodology paper (Lehle et al., 2013) was published in 2014. To date, only five papers have cited this technique. One paper acknowledged the sensitivity of this method for detecting the level of DNA damage, but they also mentioned the downside that it can only account for the polymerase stalling damage, and also different forms of DNA lesions cannot be distinguished (Eurek, 2014).

### 4.5 Future research

The main focus of the study is the cytotoxic and genotoxic effect of MSA and selenite on breast cancer cell line. One avenue for future study is to investigate the chemoprotective effect of protecting normal cell mutate into malignant ones. PBMC cells from a *BRCA1* mutation carrier can be

collected followed by *in vitro* treatment with MSA and selenite with different concentrations. The cytotoxicity and level of genomic and mitochondrial DNA damage can be examined with MTT assay, and developed Lord-qPCR, respectively. With this result in comparison with the present study, whether the Se selectively modulate chemoprotective and cytotoxic effects towards non-malignant and malignant cells can be clarified. The combined result can further lead to a short term Se oral supplementation study and measure the level of DNA damage as the primary end-point. Similar *in vitro* setting with breast cancer cell lines can be done to validate the repairing effect of Se by damaging cultured cells with bleomycin prior Se addition.

The therapeutic potential of Se can be examined further with *in vivo* mouse xenograft model cloned with *BRCA1* or non-*BRCA1*-mutated breast tumour followed by administration of selenite and MSA supplementation at different doses, and record the size of tumour change. The treatment can also include chemotherapy drugs such as cisplatin, doxorubicin, or docetaxel, to investigate the combined therapeutic effect on mouse xenograft.

Despite the Se correlation with *BRCA1* mutations, a further study looking at the effect of Se on triple-negative breast cancer cells and any receptor- (ie, ER, PR and Her-2) dependent proliferating cells can also be done with non-*BRCA1* mutated breast cancer cell lines. The established relationships between receptors and Se can then combined with hormonal drugs such as tamoxifen to examine the tumour-killing effect for developing a more specific clinical treatment.

Biochemical analysis such as western blot can also be performed to monitor the change of protein expression after Se incubation. This can provide an insight to better understanding the chemical pathway which Se targets to. Optimisation of Lord-qPCR method needs to be done in the future for more precise lesion quantification; this can be done by testing a different set of primer and improving technical skill to decrease variation between samples.

# References


Adimoolam, S., & Ford, J. M. (2002). p53 and DNA damage-inducible expression of the xeroderma pigmentosum group C gene. *Proceedings of the National Academy of Sciences, 99*(20), 12985-12990.

Amaral, A. F., Cantor, K. P., Silverman, D. T., & Malats, N. (2010). Selenium and bladder cancer risk: a meta-analysis. *Cancer Epidemiology Biomarkers & Prevention, 19*(9), 2407-2415.

Barile, M. F., & Kruse Jr, P. (1973). Mycoplasma contamination of cell cultures: incidence, source, prevention and problems of elimination *Tissue Culture—Methods and Applications* (pp. 729-735): Academic Press New York.

Bera, S., De Rosa, V., Rachidi, W., & Diamond, A. M. (2013). Does a role for selenium in DNA damage repair explain apparent controversies in its use in chemoprevention? *Mutagenesis, 28*(2), 127-134.

Bernstein, C., Prasad, A. R., Nfonsam, V., Bernstein, H., & Chen, C. (2013). DNA damage, DNA repair and cancer. *New Research Directions in DNA Repair; Chen, C., Ed.; InTech: Rijeka, Croatia*.

Berzelius, J. (1818). Lettre de M. Berzelius à M. Berthollet sur deux métaux nouveaux. *Letter from Mr. Berzelius to Mr. Berthollet on two new metals), Annales de chimie et de physique, series, 2*, 199-206.

Bhabak, K. P., & Mugesh, G. (2010). Functional mimics of glutathione peroxidase: bioinspired synthetic antioxidants. *Acc Chem Res, 43*(11), 1408-1419. doi: 10.1021/ar100059g

Bhattacharyya, A., Ear, U. S., Koller, B. H., Weichselbaum, R. R., & Bishop, D. K. (2000). The breast cancer susceptibility gene BRCA1 is required for subnuclear assembly of Rad51 and survival following treatment with the DNA cross-linking agent cisplatin. *Journal of Biological Chemistry, 275*(31), 23899-23903.

Boulton, S. J. (2006). Cellular functions of the BRCA tumour-suppressor proteins. *Biochem Soc Trans, 34*(Pt 5), 633-645. doi: 10.1042/bst0340633

. Cancer: New registrations and deaths 2012. (2015, 06 October 2015) Retrieved 21 December, 2015, from http://www.health.govt.nz/publication/cancer-new-registrations-and-deaths-2012

Cao, S., Durrani, F. A., & Rustum, Y. M. (2004). Selective modulation of the therapeutic efficacy of anticancer drugs by selenium containing compounds against human tumor xenografts. *Clinical Cancer Research, 10*(7), 2561-2569.

Chandler L. Walker, N.-K. L., Xiao-Ming XU. (2013). PTEN/PI3K and MAPK signaling in protection and pathology following CNS injuries. *Front. Biol., 8*(4), 421-433. doi: 10.1007/s11515-013-1255-1

Chaudiere, J., Courtin, O., & Leclaire, J. (1992). Glutathione oxidase activity of selenocystamine: a mechanistic study. *Archives of biochemistry and biophysics, 296*(1), 328-336.

Chen, Y. C., Prabhu, K. S., Das, A., & Mastro, A. M. (2013). Dietary selenium supplementation modifies breast tumor growth and metastasis. *International journal of cancer, 133*(9), 2054-2064.

Chiba, S., Itoh, Y., Sekine, S., & Yokoyama, S. (2010). Structural basis for the major role of O-phosphoseryl-tRNA kinase in the UGA-specific encoding of selenocysteine. *Mol Cell, 39*(3), 410-420. doi: 10.1016/j.molcel.2010.07.018

Clark, L. C., Combs, G. F., Turnbull, B. W., Slate, E. H., Chalker, D. K., Chow, J., . . . Gross, E. G. (1996). Effects of selenium supplementation for cancer prevention in patients with carcinoma of the skin: a randomized controlled trial. *Jama, 276*(24), 1957-1963.

Clark, S. L., Rodriguez, A. M., Snyder, R. R., Hankins, G. D., & Boehning, D. (2012). Structure-function of the tumor suppressor BRCA1. *Computational and structural biotechnology journal, 1*(1), 1-8.

Clavel, M., Vermorken, J., Cognetti, F., Cappelaere, P., De Mulder, P., Schornagel, J., . . . Clerico, M. (1994). Randomized comparison of cisplatin, methotrexate, bleomycin and vincristine (CABO) versus cisplatin and 5-fluorouracil (CF) versus cisplatin (C) in recurrent or metastatic squamous cell carcinoma of the head and neck A phase III study of the EORTC Head and Neck Cancer Cooperative Group. *Annals of oncology, 5*(6), 521-526.

Combs, G. F., Jr. (2004). Status of selenium in prostate cancer prevention. *Br J Cancer, 91*(2), 195-199.

Commans, S., & Böck, A. (1999). *Selenocysteine inserting tRNAs: an overview* (Vol. 23).

Dejean, L. M., Martinez-Caballero, S., & Kinnally, K. W. (2006). Is MAC the knife that cuts cytochrome c from mitochondria during apoptosis? *Cell Death Differ, 13*(8), 1387-1395. doi: 10.1038/sj.cdd.4401949

Dong, Y., Ganther, H. E., Stewart, C., & Ip, C. (2002). Identification of molecular targets associated with selenium-induced growth inhibition in human breast cells using cDNA microarrays. *Cancer research, 62*(3), 708-714.

Durocher, F., Shattuck-Eidens, D., McClure, M., Labrie, F., Skolnick, M. H., Goldgar, D. E., & Simard, J. (1996). Comparison of BRCA1 Polymorphisms, Rare Sequence Variants and/or Missense Mutations in Unaffected and

Breast/Ovarian Cancer Populations. *Human molecular genetics, 5*(6), 835-842. doi: 10.1093/hmg/5.6.835

El-Bayoumy, K. (2001). The protective role of selenium on genetic damage and on cancer. *Mutation Research/Fundamental and Molecular Mechanisms of Mutagenesis, 475*(1), 123-139.

Elstrodt, F., Hollestelle, A., Nagel, J. H., Gorin, M., Wasielewski, M., van den Ouweland, A., . . . Schutte, M. (2006). BRCA1 mutation analysis of 41 human breast cancer cell lines reveals three new deleterious mutants. *Cancer research, 66*(1), 41-45.

Etminan, M., FitzGerald, J. M., Gleave, M., & Chambers, K. (2005). Intake of Selenium in the Prevention of Prostate Cancer: a Systematic Review and Meta-analysis*. *Cancer Causes & Control, 16*(9), 1125-1131.

Eurek, N. J. (2014). Single Tube, Multiple Enzyme Reaction for Detection of UV and Oxidative Damage in Forensic Physiological Stains.

Evans, S., & Jacobson, G. (2015). Manucript in preparation. [Modified qPCR technique for DNA damage quantification].

Fischer, J. L., Lancia, J. K., Mathur, A., & Smith, M. L. (2006). Selenium protection from DNA damage involves a Ref1/p53/Brca1 protein complex. *Anticancer research, 26*(2A), 899-904.

Ford, D., Easton, D. F., Bishop, D. T., Narod, S. A., & Goldgar, D. E. (1994). Risks of cancer in BRCA1-mutation carriers. Breast Cancer Linkage Consortium. *Lancet, 343*(8899), 692-695.

Giaccone, G., Herbst, R. S., Manegold, C., Scagliotti, G., Rosell, R., Miller, V., . . . Pluzanska, A. (2004). Gefitinib in combination with gemcitabine and cisplatin in advanced non–small-cell lung cancer: A phase III trial—INTACT 1. *Journal of Clinical Oncology, 22*(5), 777-784.

Hainsworth, J. D., Grosh, W. W., Burnett, L. S., Jones, H. W., Wolff, S. N., & Greco, F. A. (1988). Advanced ovarian cancer: long-term results of treatment with intensive cisplatin-based chemotherapy of brief duration. *Annals of internal medicine, 108*(2), 165-170.

Hall, J. M., Lee, M. K., Newman, B., Morrow, J. E., Anderson, L. A., Huey, B., & King, M.-C. (1990). Linkage of early-onset familial breast cancer to chromosome 17q21. *Science, 250*(4988), 1684-1689.

Hartmann, L. C., Sellers, T. A., Schaid, D. J., Frank, T. S., Soderberg, C. L., Sitta, D. L., . . . Jenkins, R. B. (2001). Efficacy of bilateral prophylactic mastectomy in BRCA1 and BRCA2 gene mutation carriers. *J Natl Cancer Inst, 93*(21), 1633-1637.

He, N. W., Shi, X. L., Zhao, Y., Tian, L. M., Wang, D. Y., & Yang, X. B. (2013). Inhibitory Effects and Molecular Mechanisms of Selenium-Containing Tea

Polysaccharides on Human Breast Cancer MCF-7 Cells. *Journal of Agricultural and Food Chemistry, 61*(3), 579-588. doi: 10.1021/jf3036929

Hopert, A., Uphoff, C. C., Wirth, M., Hauser, H., & Drexler, H. G. (1993). Specifity and sensitivity of polymerase chain reaction (PCR) in comparison with other methods for the detection of mycoplasma contamination in cell lines. *Journal of immunological methods, 164*(1), 91-100.

Hu, Y.-J., Chen, Y., Zhang, Y.-Q., Zhou, M.-Z., Song, X.-M., Zhang, B.-Z., . . . Zhao, Y.-B. (1997). The protective role of selenium on the toxicity of cisplatin-contained chemotherapy regimen in cancer patients. *Biological trace element research, 56*(3), 331-341.

Hu, Y. J., & Diamond, A. M. (2003). Role of glutathione peroxidase 1 in breast cancer Loss of heterozygosity and allelic differences in the response to selenium. *Cancer research, 63*(12), 3347-3351.

Ip, C. (1998). Lessons from basic research in selenium and cancer prevention. *The Journal of nutrition, 128*(11), 1845-1854.

Ip, C., Hayes, C., Budnick, R. M., & Ganther, H. E. (1991). Chemical form of selenium, critical metabolites, and cancer prevention. *Cancer research, 51*(2), 595-600.

Ip, C., & Lisk, D. J. (1997). Modulation of phase I and phase II xenobiotic-metabolizing enzymes by selenium-enriched garlic in rats.

Ip, C., Thompson, H. J., Zhu, Z., & Ganther, H. E. (2000). In vitro and in vivo studies of methylseleninic acid: evidence that a monomethylated selenium metabolite is critical for cancer chemoprevention. *Cancer research, 60*(11), 2882-2886.

Jacobs, E. T., Jiang, R., Alberts, D. S., Greenberg, E. R., Gunter, E. W., Karagas, M. R., . . . Schatzkin, A. (2004). Selenium and colorectal adenoma: results of a pooled analysis. *Journal of the National Cancer Institute, 96*(22), 1669-1675.

Jaworska - Bieniek, K., Jakubowska, A., Durda, K., Huzarski, T., Serrano-Fernandez, P., Sukiennicki, G., . . . Lubinski, J. (2012). Selenium (Se) and breast cancer risk. *Hered Cancer Clin Pract, 10*(Suppl 4), A4. doi: 10.1186/1897-4287-10-s4-a4

Jaworska, K., Jakubowska, A., Huzarski, T., Durda, K., Serrano-Fernandez, P., Sukiennicki, G., . . . Gupta, S. (2012). Selenium and genotypes as marker of risk in BRCA1 mutation carriers. *Hereditary cancer in clinical practice, 10*(Suppl 1), A8.

Jiang, C., Ganther, H., & Lu, J. (2000). Monomethyl selenium–specific inhibition of MMP-2 and VEGF expression: Implications for angiogenic switch regulation. *Molecular carcinogenesis, 29*(4), 236-250.

Jiang, C., Wang, Z., Ganther, H., & Lu, J. (2002). Distinct effects of methylseleninic

acid versus selenite on apoptosis, cell cycle, and protein kinase pathways in DU145 human prostate cancer cells. *Mol Cancer Ther, 1*(12), 1059-1066.

Johnsson, A., Björk, H., Schütz, A., & Skärby, T. (1997). Sample handling for determination of free platinum in blood after cisplatin exposure. *Cancer chemotherapy and pharmacology, 41*(3), 248-251.

Johnsson, A., Hoglund, P., Grubb, A., & CavallinStahl, E. (1996). Cisplatin pharmacokinetics and pharmacodynamics in patients with squamous-cell carcinoma of the head/neck or esophagus. *Cancer chemotherapy and pharmacology, 39*(1-2), 25-33. doi: 10.1007/s002800050534

Jüliger, S., Goenaga-Infante, H., Lister, T. A., Fitzgibbon, J., & Joel, S. P. (2007). Chemosensitization of B-cell lymphomas by methylseleninic acid involves nuclear factor-κB inhibition and the rapid generation of other selenium species. *Cancer research, 67*(22), 10984-10992.

Kao, J., Salari, K., Bocanegra, M., Choi, Y.-L., Girard, L., Gandhi, J., . . . Gazdar, A. F. (2009). Molecular profiling of breast cancer cell lines defines relevant tumor models and provides a resource for cancer gene discovery. *PloS one, 4*(7), e6146.

Kent WJ, S. C., Furey TS, Roskin KM, Pringle TH, Zahler AM, Haussler D. (2002). The human genome browser at UCSC. Retrieved 01 Feb https://genome.ucsc.edu/index.html

Kotsopoulos, J., Chen, Z., Vallis, K. A., Poll, A., Ghadirian, P., Kennedy, G., . . . Narod, S. A. (2010). Toenail selenium status and DNA repair capacity among female BRCA1 mutation carriers. *Cancer Causes & Control, 21*(5), 679-687.

Kowalska, E., Narod, S. A., Huzarski, T., Zajaczek, S., Huzarska, J., Gorski, B., & Lubinski, J. (2005). Increased rates of chromosome breakage in BRCA1 carriers are normalized by oral selenium supplementation. *Cancer Epidemiology Biomarkers & Prevention, 14*(5), 1302-1306.

Ledesma, M. C., Jung-Hynes, B., Schmit, T. L., Kumar, R., Mukhtar, H., & Ahmad, N. (2011). Selenium and vitamin E for prostate cancer: post-SELECT (Selenium and Vitamin E Cancer Prevention Trial) status. *Molecular Medicine, 17*(1-2), 134.

Lee, S. O., Nadiminty, N., Wu, X. X., Lou, W., Dong, Y., Ip, C., . . . Gao, A. C. (2005). Selenium disrupts estrogen signaling by altering estrogen receptor expression and ligand binding in human breast cancer cells. *Cancer research, 65*(8), 3487-3492.

Lehle, S., Hildebrand, D. G., Merz, B., Malak, P. N., Becker, M. S., Schmezer, P., . . . Rothfuss, O. (2013). LORD-Q: a long-run real-time PCR-based DNA-damage quantification method for nuclear and mitochondrial genome analysis. *Nucleic acids research*, gkt1349.

Lehmann, B. D., Bauer, J. A., Chen, X., Sanders, M. E., Chakravarthy, A. B., Shyr, Y., & Pietenpol, J. A. (2011). Identification of human triple-negative breast cancer subtypes and preclinical models for selection of targeted therapies. *The Journal of clinical investigation, 121*(7), 2750.

Letavayová, L., Vlčková, V., & Brozmanová, J. (2006). Selenium: from cancer prevention to DNA damage. *Toxicology, 227*(1), 1-14.

Li, S., Zhou, Y., Wang, R., Zhang, H., Dong, Y., & Ip, C. (2007). Selenium sensitizes MCF-7 breast cancer cells to doxorubicin-induced apoptosis through modulation of phospho-Akt and its downstream substrates. *Molecular cancer therapeutics, 6*(3), 1031-1038.

Li, Z., Carrier, L., Belame, A., Thiyagarajah, A., Salvo, V. A., Burow, M. E., & Rowan, B. G. (2009). Combination of methylselenocysteine with tamoxifen inhibits MCF-7 breast cancer xenografts in nude mice through elevated apoptosis and reduced angiogenesis. *Breast cancer research and treatment, 118*(1), 33-43.

Lobb, R. (2011). *Selenium as a Modulator of Efficacy and Toxicity of Chemotherapy and Radiation.* University of Waikato.

Lubinski, J., Jaworska, K., Durda, K., Jakubowska, A., Huzarski, T., Byrski, T., . . . Wasowicz, W. (2011). Selenium and the risk of cancer in BRCA1 carriers. *Hereditary cancer in clinical practice, 9*(Suppl 2), A5.

Lyseng-Williamson, K. A., & Fenton, C. (2005). Docetaxel: a review of its use in metastatic breast cancer. *Drugs, 65*(17), 2513-2531.

Mayall, K., Peters, L., & Jameson, M. (2014a). *In vitro effects of selenium on DNA damage in BRCA1 cell lines.* Master of Science, University of Waikato.

Mayall, K., Peters, L., & Jameson, M. (2014b). *In vitro effects of selenium on DNA damage in BRCA1 cell lines (CP12)*. Paper presented at the 2014 Queenstown Molecular Biology Conference, Queenstown, New Zealand.

McGrath, C. (2014). MCF7 Retrieved 25 Sep, 2014, from http://www.atcc.org/products/all/HTB-22.aspx#history

Miki, Y., Swensen, J., Shattuck-Eidens, D., Futreal, P. A., Harshman, K., Tavtigian, S., . . . Ding, W. (1994). A strong candidate for the breast and ovarian cancer susceptibility gene BRCA1. *Science, 266*(5182), 66-71.

Moghadaszadeh, B., & Beggs, A. H. (2006). *Selenoproteins and Their Impact on Human Health Through Diverse Physiological Pathways* (Vol. 21).

Nasr, M. A., Fedele, M. J., Esser, K., & Diamond, A. M. (2004). GPx-1 modulates Akt and P70< sup> S6K</sup> phosphorylation and Gadd45 levels in MCF-7 cells. *Free Radical Biology and Medicine, 37*(2), 187-195.

Oelen, W. (2011). Selenium. In SeBlackRed.jpg (Ed.).

Oldfield, J. E. (2006). Selenium: a historical perspective *Selenium* (pp. 1-6): Springer.

Ostling, O., & Johanson, K. (1984). Microelectrophoretic study of radiation-induced DNA damages in individual mammalian cells. *Biochemical and biophysical research communications, 123*(1), 291-298.

Park, S. O., Yoo, Y. B., Kim, Y. H., Baek, K. J., Yang, J.-H., Choi, P. C., . . . Park, K. S. (2015). Effects of combination therapy of docetaxel with selenium on the human breast cancer cell lines MDA-MB-231 and MCF-7. *Annals of surgical treatment and research, 88*(2), 55-62.

Pinsent, J. (1954). The need for selenite and molybdate in the formation of formic dehydrogenase by members of the coli-aerogenes group of bacteria. *Biochemical Journal, 57*(1), 10.

Price, J. E., Polyzos, A., Zhang, R. D., & Daniels, L. M. (1990). Tumorigenicity and metastasis of human breast carcinoma cell lines in nude mice. *Cancer research, 50*(3), 717-721.

Proia, T. A., Keller, P. J., Gupta, P. B., Klebba, I., Jones, A. D., Sedic, M., . . . Schnitt, S. (2011). Genetic predisposition directs breast cancer phenotype by dictating progenitor cell fate. *Cell stem cell, 8*(2), 149-163.

Rayman, M. P. (2005). Selenium in cancer prevention: a review of the evidence and mechanism of action. *Proceedings of the Nutrition Society, 64*(04), 527-542.

Rayman, M. P. (2008). Food-chain selenium and human health: emphasis on intake. *British Journal of Nutrition, 100*(2), 254-268.

Rayman, M. P. (2009). Selenoproteins and human health: insights from epidemiological data. *Biochimica et Biophysica Acta (BBA)-General Subjects, 1790*(11), 1533-1540.

Rayman, M. P. (2012). Selenium and human health. *The Lancet, 379*(9822), 1256-1268.

Robinson, M., & Thomson, C. (1987). Status of the food supply and residents of New Zealand.

Rose, P. G., Bundy, B. N., Watkins, E. B., Thigpen, J. T., Deppe, G., Maiman, M. A., . . . Insalaco, S. (1999). Concurrent cisplatin-based radiotherapy and chemotherapy for locally advanced cervical cancer. *New England Journal of Medicine, 340*(15), 1144-1153.

Rosenberg, B., Van Camp, L., & Krigas, T. (1965). Inhibition of cell division in Escherichia coli by electrolysis products from a platinum electrode. *Nature, 205*(4972), 698-699.

Rothfuss, O., Gasser, T., & Patenge, N. (2010). Analysis of differential DNA damage in the mitochondrial genome employing a semi-long run real-time PCR approach. *Nucleic acids research, 38*(4), e24-e24.

Sanmartín, C., Plano, D., Sharma, A. K., & Palop, J. A. (2012). Selenium compounds, apoptosis and other types of cell death: an overview for cancer therapy.

*International journal of molecular sciences, 13*(8), 9649-9672.

Satoh, M., Naganuma, A., & Imura, N. (1989). Optimum schedule of selenium administration to reduce lethal and renal toxicities of cis-diamminedichloroplatinum in mice. *Journal of pharmacobio-dynamics, 12*(4), 246-253.

Schrauzer, G., White, D., & Schneider, C. J. (1977). Cancer mortality correlation studies-III: statistical associations with dietary selenium intakes. *Bioinorganic chemistry, 7*(1), 23-34.

Seko, Y., Saito, Y., Kitahara, J., & Imura, N. (1989). Active oxygen generation by the reaction of selenite with reduced glutathione in vitro *Selenium in biology and medicine* (pp. 70-73): Springer.

. Selenium Dietary Supplement Fact Sheet. (2013) Retrieved 27 Aug 2014, from http://ods.od.nih.gov/factsheets/Selenium-HealthProfessional/#en6

Seo, Y. R., Kelley, M. R., & Smith, M. L. (2002a). Selenomethionine regulation of p53 by a ref1-dependent redox mechanism. *Proceedings of the National Academy of Sciences, 99*(22), 14548-14553.

Seo, Y. R., Sweeney, C., & Smith, M. L. (2002b). Selenomethionine induction of DNA repair response in human fibroblasts. *Oncogene, 21*(23), 3663-3669.

Sheridan, C., Kishimoto, H., Fuchs, R. K., Mehrotra, S., Bhat-Nakshatri, P., Turner, C. H., . . . Nakshatri, H. (2006). CD44+/CD24-breast cancer cells exhibit enhanced invasive properties: an early step necessary for metastasis. *Breast Cancer Res, 8*(5), R59.

Siegel, R., Naishadham, D., & Jemal, A. (2012). Cancer statistics, 2012. *CA: a cancer journal for clinicians, 62*(1), 10-29.

Silver, D. P., Richardson, A. L., Eklund, A. C., Wang, Z. C., Szallasi, Z., Li, Q., . . . Buraimoh, A. (2010). Efficacy of neoadjuvant Cisplatin in triple-negative breast cancer. *Journal of Clinical Oncology, 28*(7), 1145-1153.

Siriwardena, A. K., Mason, J. M., Balachandra, S., Bagul, A., Galloway, S., Formela, L., . . . Jamdar, S. (2007). Randomised, double blind, placebo controlled trial of intravenous antioxidant (n-acetylcysteine, selenium, vitamin C) therapy in severe acute pancreatitis. *Gut, 56*(10), 1439-1444.

Smith, M. L., Lancia, J. K., Mercer, T. I., & Ip, C. (2004). Selenium compounds regulate p53 by common and distinctive mechanisms. *Anticancer research, 24*(3A), 1401-1408.

Thomson, C. D. (2004). Selenium and iodine intakes and status in New Zealand and Australia. *British Journal of Nutrition, 91*(05), 661-672.

Uphoff, C., & Drexler, H. (2011). Detecting Mycoplasma Contamination in Cell Cultures by Polymerase Chain Reaction. In I. A. Cree (Ed.), *Cancer Cell Culture* (Vol. 731, pp. 93-103): Humana Press.

Uphoff, C. C., & Drexler, H. G. (2002). Comparative PCR analysis for detection of mycoplasma infections in continuous cell lines. *In Vitro Cellular & Developmental Biology-Animal, 38*(2), 79-85.

Valdiglesias, V., Pásaro, E., Méndez, J., & Laffon, B. (2010). In vitro evaluation of selenium genotoxic, cytotoxic, and protective effects: a review. *Archives of toxicology, 84*(5), 337-351.

Van Cutsem, E., Moiseyenko, V. M., Tjulandin, S., Majlis, A., Constenla, M., Boni, C., . . . Voznyi, E. (2006). Phase III study of docetaxel and cisplatin plus fluorouracil compared with cisplatin and fluorouracil as first-line therapy for advanced gastric cancer: a report of the V325 Study Group. *Journal of Clinical Oncology, 24*(31), 4991-4997.

Vinceti, M., Wei, E. T., Malagoli, C., Bergomi, M., & Vivoli, G. (2001). Adverse health effects of selenium in humans. *Rev Environ Health, 16*(4), 233-251.

Wang, D.-Y., Fulthorpe, R., Liss, S. N., & Edwards, E. A. (2004). Identification of estrogen-responsive genes by complementary deoxyribonucleic acid microarray and characterization of a novel early estrogen-induced gene: EEIG1. *Molecular Endocrinology, 18*(2), 402-411.

Wang, D., & Lippard, S. J. (2005). Cellular processing of platinum anticancer drugs. *Nature reviews Drug discovery, 4*(4), 307-320.

Wang, Z., Hu, H., Li, G., Lee, H.-J., Jiang, C., Kim, S.-H., & Lü, J. (2008). Methylseleninic acid inhibits microvascular endothelial G1 cell cycle progression and decreases tumor microvessel density. *International journal of cancer, 122*(1), 15-24. doi: 10.1002/ijc.23077

Wang, Z., Jiang, C., & Lü, J. (2002). Induction of caspase-mediated apoptosis and cell-cycle G1 arrest by selenium metabolite methylselenol. *Molecular carcinogenesis, 34*(3), 113-120.

Wilson, A. C., Thompson, H. J., Schedin, P. J., Gibson, N. W., & Ganther, H. E. (1992). Effect of methylated forms of selenium on cell viability and the induction of DNA strand breakage. *Biochemical pharmacology, 43*(5), 1137-1141.

Xiang, N., Zhao, R., & Zhong, W. (2009). Sodium selenite induces apoptosis by generation of superoxide via the mitochondrial-dependent pathway in human prostate cancer cells. *Cancer chemotherapy and pharmacology, 63*(2), 351-362.

Yoon, S.-O., Kim, M.-M., & Chung, A.-S. (2001). Inhibitory effect of selenite on invasion of HT1080 tumor cells. *Journal of Biological Chemistry, 276*(23), 20085-20092.

Zeng, H., Davis, C. D., & Finley, J. W. (2003). Effect of selenium-enriched broccoli diet on differential gene expression in min mouse liver< sup> 1, 2</sup>. *The Journal of nutritional biochemistry, 14*(4), 227-231.

Zhang, Y., Zheng, S., Zheng, J.-S., Wong, K.-H., Huang, Z., Ngai, S.-M., . . . Chen, T. (2014). Synergistic induction of apoptosis by methylseleninic acid and cisplatin, the role of ROS-ERK/AKT-p53 pathway. *Molecular pharmaceutics, 11*(4), 1282-1293.

Zhao, R., Domann, F. E., & Zhong, W. (2006). Apoptosis induced by selenomethionine and methioninase is superoxide mediated and p53 dependent in human prostate cancer cells. *Molecular cancer therapeutics, 5*(12), 3275-3284.

Zhuo, H., Smith, A. H., & Steinmaus, C. (2004). Selenium and lung cancer: a quantitative analysis of heterogeneity in the current epidemiological literature. *Cancer Epidemiology Biomarkers & Prevention, 13*(5), 771-778.

# Appendix One:

# Recipes for experimental solutions

## 1. General solutions

**10x Phosphate buffer saline (PBS), pH 7.4**

40 g NaCl (1.37 M)

1 g KCl (27 mM)

5.75 g $Na_2HPO_4$ (81 mM)

1 g $KH_2PO_4$ (14.7 mM)

Dissolve all the ingredients above in 500 mL mQ water

Adjust pH to 7.4 with concentrated HCl

Autoclave

**1x PBS**

100 mL 10x PBS pH7.4

900 mL mQ water

Autoclave

**1 M Sodium selenite**

Dissolve 0.76 g of sodium selenite in 2 mL of 1xPBS

Filter sterilise with 0.2 µM of filter

Store in -20°C

**1 M Methylseleninic acid (MSA)**

Dissolve 0.41 g of MSA in 2 mL of 1xPBS

Filter sterilise with 0.2 µM of filter

Store in -20°C

## 2. DNA extraction

**1 M Tris-Cl, pH 8.0**

Dissolve 60.5 g Tris base in 500 mL mQ $H_2O$

Adjust pH to 8.0 with concentrated HCl

Autoclave

**0.5 M EDTA, pH 8.0**

Dissolve 93.05 g of $Na_2EDTA \cdot 2H_2O$ in 500 mL of mQ water

Adjust pH to 8.0 with 10 M sodium hydroxide

Autoclave

**Tris-EDTA (TE buffer), pH 8.0**

0.5 M EDTA 2 mL

1 M Tris 10 mL

Fill the volume to 1 L with mQ $H_2O$

Autoclave

**3 M Sodium Acetate, pH 4.8**

Dissolve 40.8g of sodium acetate$\cdot 3H_2O$ in 100 mL of $H_2O$

Adjust pH to 4.8 with 3M acetic acid

Autoclave

**5 M NaCl**

Dissolve 29.2 g of NaCl in 100 mL of $H_2O$

Autoclave

**Sodium dodecyl sulphate (SDS) 10%**

Dissolve 2.5 g of SDS to 25 mL of mQ $H_2O$

Leave solution in an 80°C oven to dissolve overnight

**Proteinase K, 10 mg/mL**

10 mg Proteinase K

0.5 M EDTA 2 µL

1 M Tris 10 µL

Make up to 1 mL with mQ $H_2O$

Store at -20°C

**DNA digestion buffer**

0.5 M EDTA 1 mL

1 M Tris 0.5 mL

5 M NaCl 1 mL

10% SDS 2.5 mL

Fill up the volume to 50 mL with mQ water

## 3. Gel electrophoresis

**50x Tris-acetate EDTA (TAE) buffer**

242 g Tris base dissolved in 800 mL mQ water

100 mL 0.5 M EDTA

57.1 mL Glacial acetic acid

Fill up the volume to 1 L with mQ water

**1x TAE gel running buffer**

20 mL 50x TAE buffer

980 mL mQ water

**1% agarose gel**

Dissolve 0.4 g of agarose in 40 mL of 1xTAE buffer

**2% agarose gel**

Dissolve 0.8 g of agarose in 40 mL of 1xTAE buffer

## 4. Comet assay

**1% normal melting point agarose (NMPA)**

250 mg of NMPA to 25 mL of 1xPBS.

Microwave for 60 seconds with low power (700 W) to melt.

**0.5% low melting point agarose (LMPA)**

125 mg of LMPA to 25 mL of 1xPBS

Microwave at low power for 30 seconds (700 W) to melt.

**Cell lysis stock solution, pH 10**

Dissolve 146.1g of NaCl (2.5 mM), 37.2 g disodium EDTA (100 mM), 1.2 g Tris (10 mM), 12 g NaOH, and 1 g SDS in 890 mL of mQ water.

**0.5% Triton-X 100**

250 µL Triton-x 100

Fill up to 50 mL with 1xPBS

**Cell lysis working solution**

72.81 mL lysis stock solution

2.19 mL 0.5% Triton-X 100

**Electrophoresis buffer for Comet assay**

- Stock solution 1:

Dissolve 80 g of NaOH (10 M) in 200 mL of mQ water.

- Stock solution 2:

Dissolve 14.89 g of disodium EDTA (200 mM) in 200 mL mQ water

Adjust pH to 10 with NaOH.

- Working solution

30 mL Stock 1 solution

5 mL Stock 2 solution

Mix and fill up volume to 1 L with mQ water

**Neutralisation buffer**

Dissolve 48.5 g of Tris (0.4M) in 1 L of mQ water

Adjust pH to 7.5 with HCl

**SYBR® Gold fluorescent stain**

1.3 µL 1000x SYBR® Gold

1289.7 µL mQ water

## 5. MTT assay

**MTT 3-(4,5-dimethylthiazol-2-yl)-2,5-diphenyltetrazolium bromide, 5 mg/mL**

Dissolve 0.05 g of MTT with 10 mL of 1xPBS

Filter sterilise

Store in -20°C

**MTT assay solubilising solution**

Dissolve 10 g of SDS in 23 mL of mQ $H_2O$ and add

25 mL Dimethylformamide (DMF)

1 mL Glacial acetic acid

1 mL 1M HCl

Leave solution in 80°C 20 minutes prior to use to dissolve SDS

# Appendix Two:

# Melt curve from Lord-qPCR

The following figures show the raw melt curve analysis of primers targeting *p53* (shown as an example in **Figure 24**), mitochondrial DNA, and *B2M* genes with MDA-MB-436 DNA.

## 2.1 MDA-MB-436 DNA with Ko6 primers

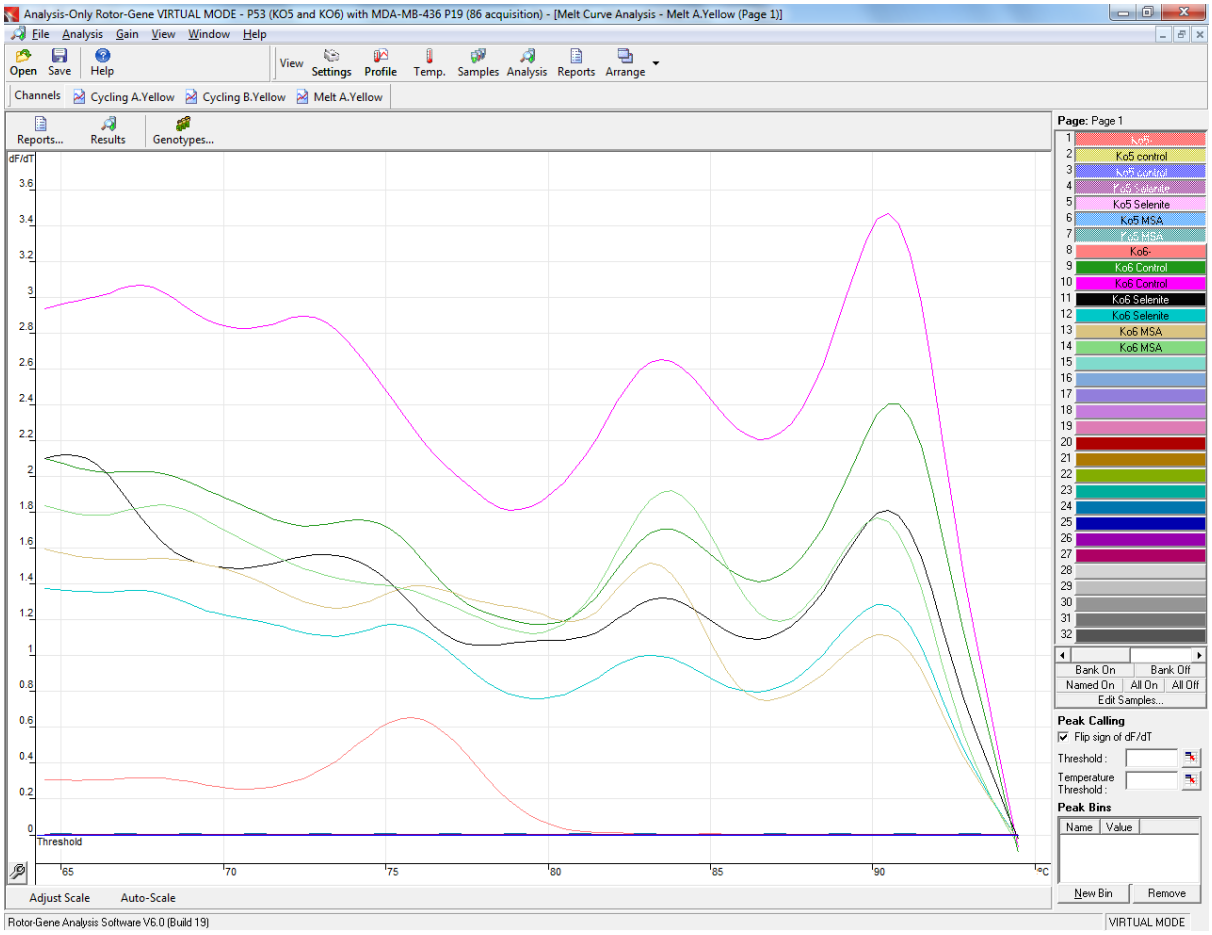


**Figure 37**, Melt curve from Lord-qPCR reaction of MDA-MB-436 with Ko6 p53 primer. The single sharp peak at 90°C indicates only one product was amplified with Ko8 primers. Melting point at high temperature suggests the single amplicon has a larger sequence which requires a higher temperature to denature.

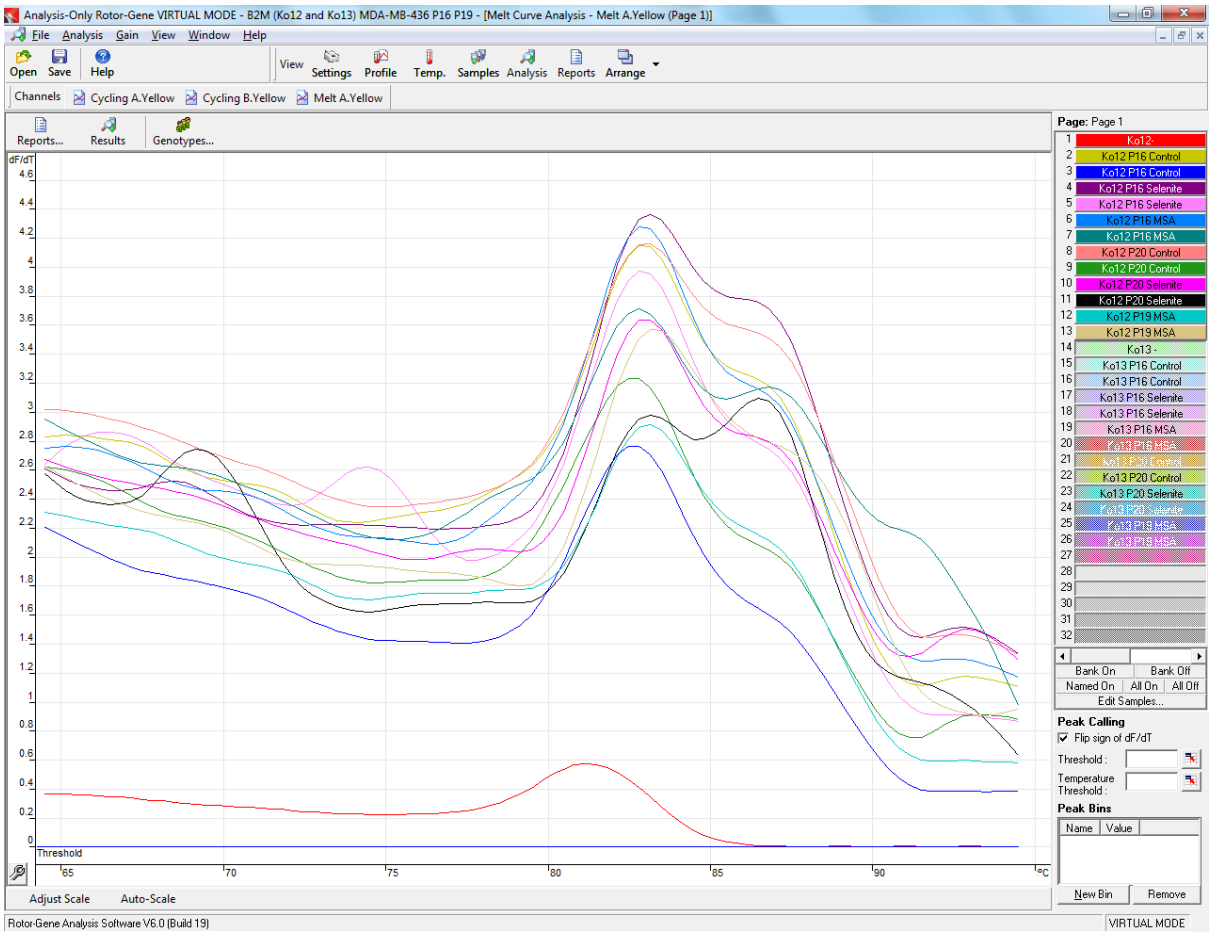


**Figure 38**, Melt curve from Lord-qPCR reaction of MDA-MB-436 with Ko12 B2M primer. The single sharp peak at 82°C indicates only one product was amplified with Ko8 primers. Melting point at high temperature suggests the single amplicon has larger sequence which requires higher temperature to denature

# Appendix Three:

# Electropherogram of sequenced top PCR band Figure 28

The sequencing result of top purified PCR band from lane three **Figure 28**. The overall low quality of sequence explains the mismatching when aligned with the *p53* genomic sequence.

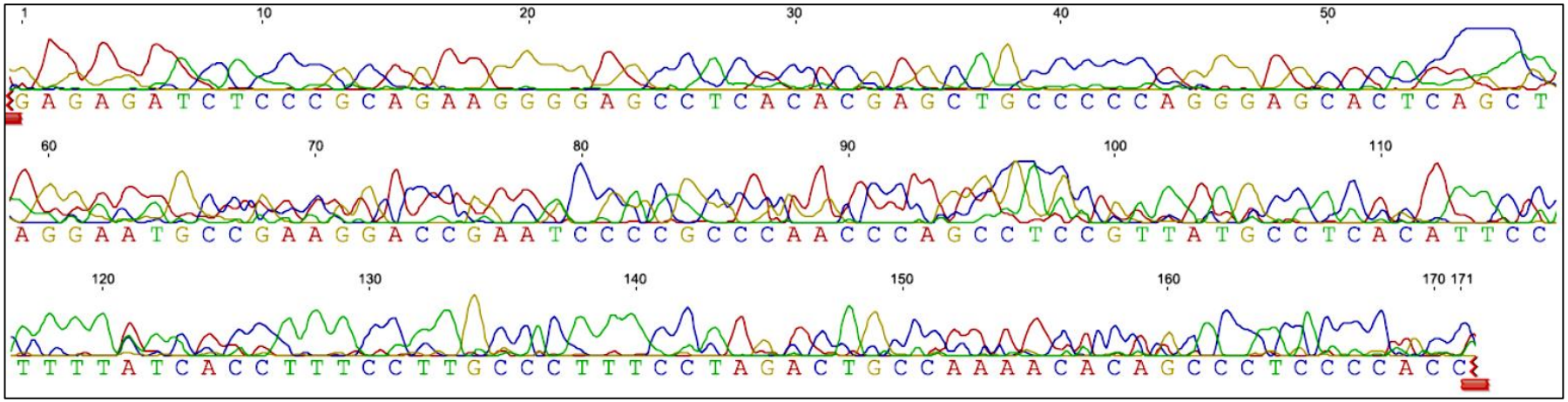


**Figure 39,** Electropherogram of purified *p53* using Ko9F primer. The resulting sequencing is derived from the top PCR band (238 bp) that was gel purified from lane three of **Figure 28**. Percentage sequence with high quality (HQ %): 2.5%. Low-quality sequence begins at position 54 with misreading from A to C.

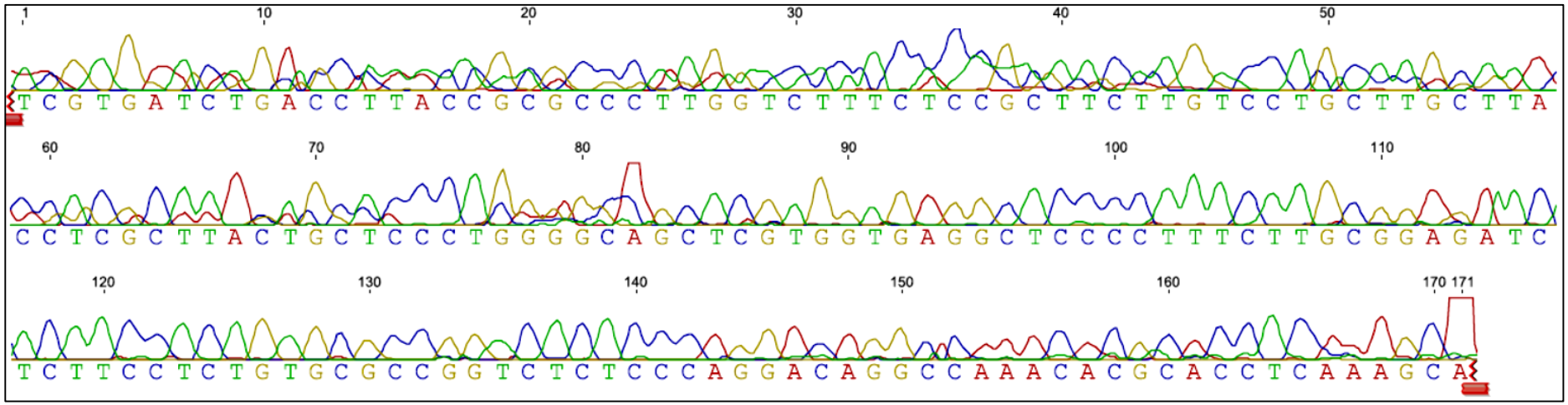


**Figure 40**, Electropherogram of the *p53* top band from lane three of **Figure 28**. Sequencing results from Ko9R. HQ%: 25.2%

# Appendix Four:

# Raw data for experimental results

All the experimental raw data were organised in the CD disc attached, please see the disc for more detail.